INVESTIGATION ON PROPERTIES OF CEMENTITIOUS MATERIALS REINFORCED BY GRAPHENE

by

Zhou Fan

B.S. Engineering, Hunan University, 2010

Submitted to the Graduate Faculty of

The Swanson School of Engineering in partial fulfillment

of the requirements for the degree of

Master of Science in Civil Engineering

University of Pittsburgh

2014

UNIVERSITY OF PITTSBURGH

SWANSON SCHOOL OF ENGINEERING

This thesis was presented

by

Zhou Fan

It was defended on

March 26, 2014

and approved by

Jeen-Shang Lin, ScD, Associate Professor,
Department of Civil and Environmental Engineering

John Brigham, PhD, Assistant Professor,
Department of Civil and Environmental Engineering

Thesis Advisor: Qiang Yu, PhD, Assistant Professor,
Department of Civil and Environmental Engineering

INVESTIGATION ON PROPERTIES OF CEMENTITIOUS MATERIALS REINFORCED BY GRAPHENE

Zhou Fan, M.S.

University of Pittsburgh, 2014

Graphene nanoplatelet has been found to be able to improve the mechanical and electrical properties of concrete so that it can make the concrete to be a "smart material". However, its effects on some other properties of graphene additive concrete, e.g., frost and corrosion resistance, remain unknown. Therefore, it cannot be directly applied in the construction practice without further investigation. The purpose of this research is to study the frost resistance and corrosion resistance of graphene additive mortar as well as the corresponding compressive strength enhancement induced by the addition of graphene. Here the tests are performed on 5 groups of mortar specimens with the same mix proportion. One group of them were cast by normal mortar, while each of the other four groups was enriched by an equal amount of C grade graphene particles (GC), C grade oxidative graphene particles (GOC), M grade graphene particles (GM) and M grade oxidative graphene particles (GOM), respectively. The dimension of the C grade graphene nanoplatelets is smaller than that of M grade graphene nanosheets. After 28 days curing, compressive strength test, Young's modulus and Poisson ratio measurement test, water absorption test, 300 cycles freezing and thawing test and 5-month corrosion test were performed. The results exhibit that the performance of the GOM group is the best among all of the experimental groups. The enhancement of the compressive strength of the GOM group is 13.2% compared to the normal mortar. The corrosion and frost resistance of cement are both slightly improved by adding the M grade oxidative graphene particles. In order to study the

corresponding mechanism from the microstructure of concrete, atomic force microscopy, Raman spectroscopy and scanning electron microscopy were implemented in this research. The results of this study indicate that the oxidative graphene nanoplatelets can effectively reduce the porosity of the cementitious material and therefore increase its strength as well as the corrosion and the frost resistance.

TABLE OF CONTENTS

LIST OF TABLES

LIST OF FIGURES

ACKNOWLEDGEMENTS

First, I would like to thank my advisor Dr. Yu for providing me the opportunity to do the research and supporting me throughout my graduate studies. I could not finish this thesis without his instruction and education.

I would also like to acknowledge my committee members, Dr. John Brigham and Dr. Jeen-Shang Lin. Thank you for your precious time and instructive advice.

Many thanks to the Post Doctorial Associate of our group, Dr. Qiong Liu. Thank you for helping me design the experiments, guiding me to perform the tests and giving me suggestions.

I would like to extend my gratitude and appreciation to Dr. Susheng Tan and Tong Teng, the PhD student of Dr. Yu, for helping me with the microscopic experiments.

Furthermore, I want to acknowledge Dr. Julie M. Vandenbossche and her graduate students Nicole Dufalla, Zichang Li and Feng Mu. Thank you for providing me the experimental apparatus and equipment to make my experiments possible.

Finally, I would like to take this opportunity to express my thanks to my parents and my wife Wenjie Huang for their continuous support throughout my graduate studies.

1.0 INTRODUCTION

1.1 GENERAL

Concrete, with its low price, simple production process, high compressive strength and excellent durability, is one of major civil engineering materials and has been deeply studied and widely used. However, with the applications of new technologies, demands are more and more intense on the innovative concrete, which is stronger and smarter. It means that people want concrete to be able to provide strength for structure, as well as to integrate other functional applications, such as self-monitoring. Thus, carbon fiber additive concrete comes forth.

Adding carbon fibers can improve the electric conductivity of concrete for various applications such as electromagnetic interference shielding, lateral guidance in automatic highways, traffic monitoring, weighing in motion, deicing and self-monitoring (Hou et al. 2006). With the development of nano materials, carbon nano-fibers were gradually being studied, such as carbon nanotubes and graphene nanoplatelets. During recent decades, using carbon nanotubes to improve the performance of concrete has been attracting increasing interests. However, the research about graphene additive concrete is still in its infancy.

Graphene is a two-dimensional carbon molecule in which the structure is quite similar to graphite. "Graphene" refers to a single layer of graphite, and in some cases means a few layers of graphite as well. Because of its unique structure, the surface area of graphene nanoplatelets is

greatly increased to make itself an ideal nano material which can be used to reduce the electric resistivity of concrete.

Furthermore, it has been noted that enriched by graphene nano-material merely 0.01 % to 1 % of the weight of the Portland cement, the concrete compressive strength could be improved from 5% to 40%, depending on the particle dimension of the additive materials and the different treatment methods that have been used in the experiments. Thus, this technology could have a wide application in civil engineering.

However, except the current studies on the compressive strength, tensile strength and the flexural strength of this new type of "cement", some other important material properties of this "smart material" still need to be investigated, e.g., the frost and corrosion resistance.

In practice, the concrete structure is subject to alternating hot and cold external environment during each calendar year, especially in high latitude regions. The annual temperature difference in some areas can reach 100 °C. Under such extreme conditions, frost resistance of concrete is particularly important. Similarly, the structures are expected to be contacted by water, such as ground water, acid rain and sea water, and therefore under attack by the corrosive chemicals in the water. If the application of a new additive resulted in weakening of concrete frost or corrosion resistance, then the engineering application of this new material is significantly limited. Thus it is of great importance to study the frost and corrosion resistance of graphene additive concrete.

Therefore, the main purpose of this research is to study the frost resistance and corrosion resistance of cementitious materials which are reinforced by graphene nanoplatelets, with an aim of promoting the pace of using this technique in practice and filling the gaps of the studies in this area. In addition, this study will try to explore the mechanism of how mechanical properties of

Portland cement can be enhanced by graphene, which has not yet been fully explained. In detail, this study sets up a series of tests on graphene additive Portland cement to study its concrete compressive strength, Young's model, Poisson's ratio, frost resistance and corrosion resistance. The processes, results and related discussions of these tests will be introduced in following chapters.

1.2 THESIS OUTLINE

The outline of the thesis is organized as follows.

Chapter 2 presents a literature review of the current studies about graphene additive cementitious materials.

Chapter 3 describes the experimental program of this research.

Chapter 4 reports the experimental results and presents the discussions based on the experiments.

Chapter 5 shows the microscope observation results.

Chapter 6 presents the conclusions, summaries and recommendations of this research.

2.0 LITERATURE REVIEW

2.1 CEMENT ENHANCED BY C-NANOTUBES

The carbon nanotubes are the one-dimensional molecules which can be treated as sheets of graphite rolled up and capped at one end or both ends by half of a fullerene. There are two forms of carbon nanotubes: multiwall and single-walled. The multiwall carbon nanotubes consist of nested tubes, whereas the single-walled carbon nanotubes only consist of one-layer tubes. The diameter of the single-walled carbon nanotubes is only about 1 nm; however, the length of it can be 1000 nm long or even longer. Recent researches indicate that the carbon nanotubes can be added into composite material as nanofibers to enhance the strength of the material as well as improve other properties. (Brown et al. 2010)

In 2012, a research about cement paste reinforced by multiwall carbon nanotubes was presented by Kumar et al. (2012). In this research, the authors mixed 0.5, 0.75, and 1.0 percent carbon nanotubes (CNTs) with Portland cement to study the strength gain in the cement composite material. The specimens were tested on compression strength at 7, 28, 60 90 and 180 days of curing. The results show that the compressive and tensile strengths were increased by 15% and 36%, respectively, with 0.5% CNT content. The authors also indicated that the strength enhancement mainly occurred during the 7 days and 28 days of curing. However, the rate of change of compressive and tensile strength with respect to curing age between CNT specimens

and control specimens was seen to be very similar. Thus, the authors claimed that the strength enhancement is primarily because of cement hydration, rather than the reaction between CNTs and cement compounds.

In the same year, Abu Al-Rub et al. (2012) presented research about the effect of functionalized CNTs and carbon nanofibers (CNFs) on the mechanical properties of cement composites. The concentrations of treated and untreated CNFs and CNTs were 0.1% and 0.2% by weight of cement. The treated CNFs and CNTs were oxidized in a solution of sulfuric acid and nitric acid and washed clean before being added into the cement paste. The results showed that, compare to the plain cement, the average enhancements on ductility, flexural strength, Young's modulus and toughness modulus were 73%, 60%, 25% and 170%, respectively. The authors also suggested that the reasonable value of the concentration of graphene by weight is around 0.1%.

Besides, Konsta-Gdoutos et al. (2010) presented research to study the effects of ultrasonic energy and surfactant concentration on the dispersion of multiwall CNTs for cement based material reinforcement. The authors concluded that, for proper dispersion, the application of ultrasonic energy is necessary and the ratio of surfactant to CNTs is suggested to be 4.0.

2.2 CEMENT ENHANCED BY GRAPHENE

In 2013, Alkhateb et al. (2013) showed a series methods to investigate the properties of cementitious material reinforced by graphene nanoplatelets. In this research, the authors presented a general framework for using a systematic approach to study the cementitious materials. These research approaches include molecular dynamics simulations (MD) as well as

observation via atomic force microscopy (AFM), scanning electron microscopy (SEM), X-Ray diffraction (XRD) and resonant ultrasound spectroscopy.

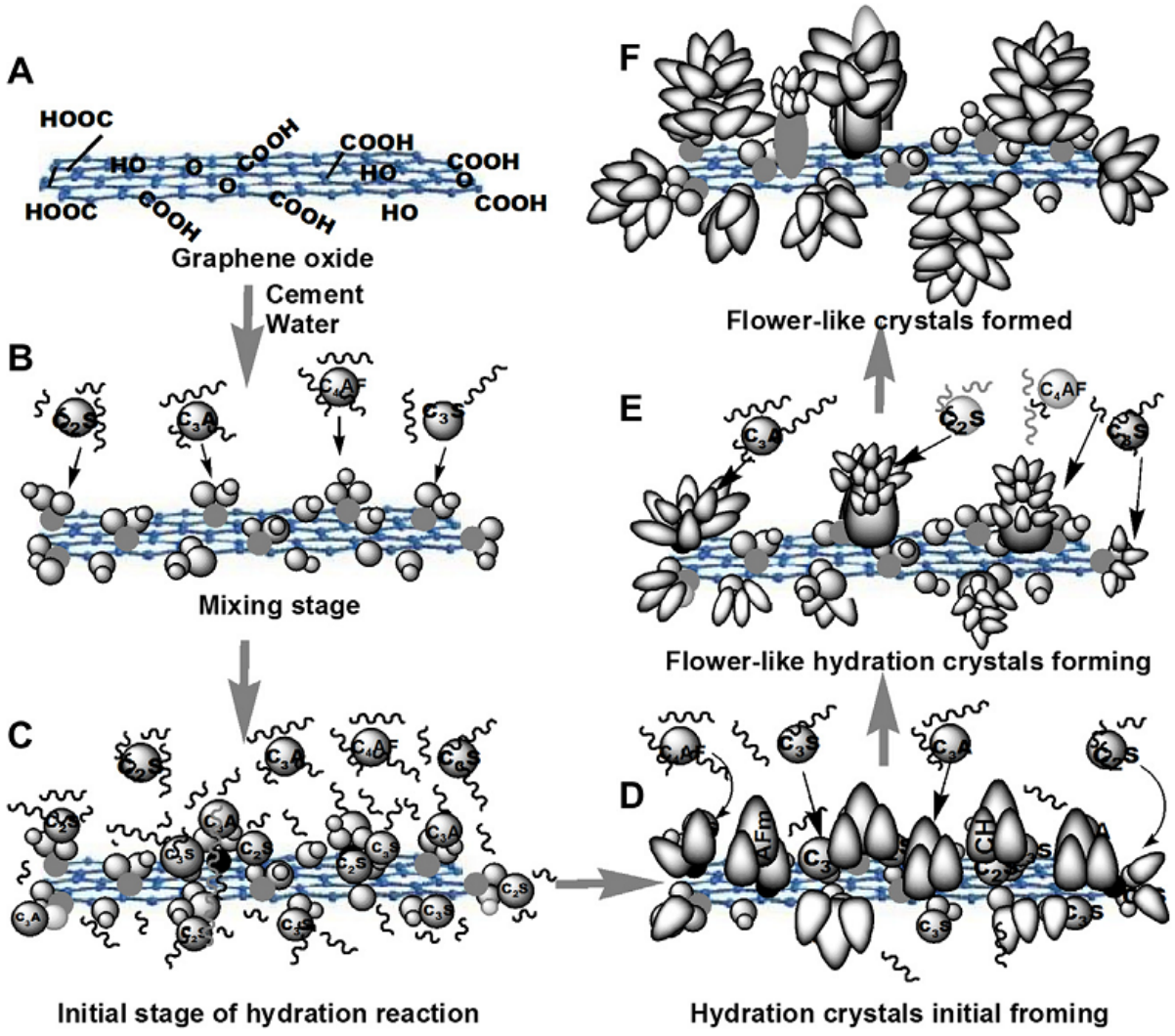

Figure 2-1. Schematic diagram of regulation mechanism of GO on cement hydration crystals (Lv et al. 2013)

Lv et al. (2013) presented research about the effect of graphene oxide nanosheets (GO) in cement composites. The graphene nanoplatelet used in this research is relatively small (<30 μm). The functionalized graphene is treated by 98% H_2SO_4 and $NaNO_3$. The experimental results showed that, when the content of GO was 0.03%, the cement composites exhibited striking increase in tensile strength (78.6%), flexural strength (60.7%) and compressive strength (38.9%),

compared to those of normal cement composites. Based on the XRD tests and SEM, the authors speculated that tricalcium silicate C_3S (Ca_3SiO_5), dicalcium silicate C_2S (Ca_2SiO_4) and tricalcium aluminate C_3A ($Ca_3Al_2O_6$), which are the major ingredients of unhydrous cement, react preferentially with functional groups (-OH, -COOH and $-SO_3H$) on the surface of GO. The mechanism for GO cement hydration is shown in Figure 2-1.

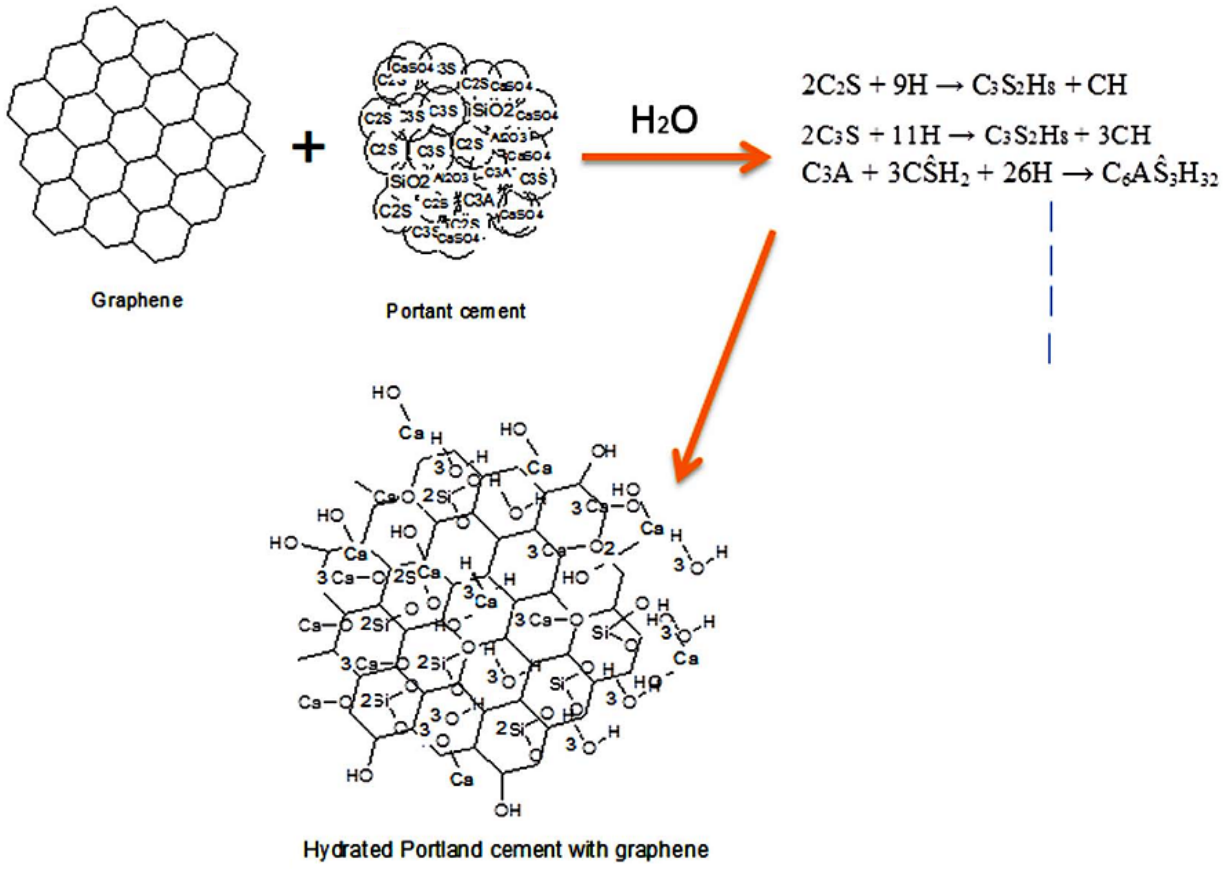

Figure 2-2. Schematic diagram of reaction between graphene and cement (Sedaghat et al. 2013)

Sedaghat et al. (2013) and his team also put forward their theory about the mechanism of the improvement of material properties caused by GO. The authors claimed that graphene reacts with portant cement in the hydration process (Figure 2-2). By measuring thermal diffusivity, the authors indicated that the reaction between graphene and cement can improve concrete heat

dissipation during the hydration process. This led to thermal cracking decrease in specimens so that graphene could improve the strength of the cementitious materials.

2.3 CARBON NANO-COMPOSITE OXIDATION

The oxidation process can add functional groups on the surface of the carbon molecules in order to change its properties of interaction with cement. Thus, the oxidation is also called functionalization. Current literature suggests that the oxidation process is achieved by using high concentration acid to react with graphene particles. In some cases, catalysts are needed.

In Abu Al-Rub's research (Abu Al-Rub et al. 2012), the oxidation procedure was performed as follow: 0.9 g CNTs and CNFs was added into 300ml acid solution. The sulfuric to nitric acid ratio of this solution is 2:1. All the substrate was refluxed for 1 h at 85 °C and continuously stirred with a magnetic stirrer. The solution was diluted in 4 L distilled water and then filtered through a polytetrafluorethylene membrane.

Figure 2-3. Process of oxidation (Alkhateb et al. 2012)

As shown in Figure 2-3, the oxidation method used by Alkhateb et al. (2013) is similar with the method proposed by Rosca et al. (2005). 3 g of graphene and 300 ml of nitric acid were mixed in a 500-mL glass flask and dispersed in the ultrasound disperser for 15 min. The total reacting time is 24 hours and then the mixture is purified by filtration using distilled water.

Another oxidation method presented by Lv et al. (2013) is relatively complicated than the 2 methods mentioned previously. As described by the authors, 5g graphite, 30g 98% H_2SO_4 and 2 g $NaNO_3$ was added into a three-necked round-bottomed flask placed in an ice bath (<5 °C) under stirring. 6g $KMnO_4$ was gently added to the flask. The flask was maintained at 5 °C for 1 hour until the color of the solution had turned green. Then it was heated and kept to 35 °C for 12 hours. Then 100 mL deionized water was slowly added in and was heated to 90 °C. Then 300 mL deionized water and 30g hydrogen peroxide were slowly added in. After the color of the solution changed from brown to bright yellow, the mixture was filtered to neutral pH.

2.4 FREEZING & THAWING TESTS

The slow freezing method and the fast freezing method are two main concrete frost resistance test methods. Existing international standards include ASTM C666-97 and ASTM C672-2003 (United States), BS 5075 (British), CSA A23.2-94 (Canada), NS 3473-92 and NS 4320-86 (Norway) and TC117-2FDC (Sweden) etc. In slow-freezing method, loss of compressive strength is generally used as a criterion. However, according to the fact that concrete damage in freezing tests is caused by the internal tension cracking, the specimens are sensitive to distribution of the tension cracks. It means the results of the compressive strength test are unpredictable because of the randomness of the internal tension cracks. Thus, the results of slow-

freezing method are unrepeatable for the other researchers. Furthermore, due to the long test cycle, heavy workload, the experimental error and other shortcomings, the slow-freezing method is seldom used now and the fast-freezing method wins the popularity. In addition to the compressive strength loss, the mass loss ratio is now used as a criterion in the fast-freezing as well as the slow-freezing methods. It is worth mention here that there is a certain error of this evaluation criterion, and therefore, in most cases, it is used in conjunction with the relative dynamic modulus loss to evaluate the frost resistance. (Zhang et al. 2008)

Figure 2-4. Freezing and thawing machine (Hamoush et al. 2012)

At present, there is no research using freezing and thawing test to evaluate the properties of the cementitious material reinforced by graphene nanoplatelets. In order to fully understand the freezing and thawing test, some researches about freezing and thawing tests were reviewed. Shang and Yi (2013) presented a research about the durability of air-entrained concrete by freezing and thawing test. Their freezing and thawing cycles consisted of alternately lowering the temperature of the specimens from 6 °C to -15 °C and raising it from -15 °C to 6 °C. The

specimen size was 100 mm × 100 mm× 400 mm. The dynamic modulus of elasticity and weight loss of the specimens were measured before the freezing cycles. Hamoush et al. (2011) also used freezing and thawing test to evaluate the durability of high strength concrete. The freezing and thawing cycles were performed using the specialized machine which is shown in Figure 2-4. Their experiments were performed according to ASTM C-666 procedure-A. The dynamic modulus of elasticity, dynamic modulus of rigidity, Poisson's ratio, flexural strength and durability factors were investigated after each number of cycles.

2.5 CORROSION TESTS

Schneider and Chen (1997) presented research about the chemomechanical effect and the mechanochemical effect on high-performance concrete. In this research, the specimens were subjected to flexural loads with a level of 30% of their initial strengths, while immersed into a 5% ammonium sulfate solution, a 10% ammonium nitrate solution, or a saturated calcium hydroxide solution.

In 2004, Schneider and Chen presented another experiment used ammonium nitrate solution to corrode high-performance concrete. The concentrations of ammonium nitrate in the solution are 10%, 5%, 1% and 0.1%. The authors also mentioned that during the test the solutions were replaced as needed to maintain the solution concentration.

2.6 ATOMIC FORCE MICROSCOPY

AFM is a perfect technique to study nanomaterials because it can provide high resolution topography of microstructure, combine advantages of digital three-dimensional morphological information in atmosphere, and have no vacuum requirement. (Yang et al. 2003)

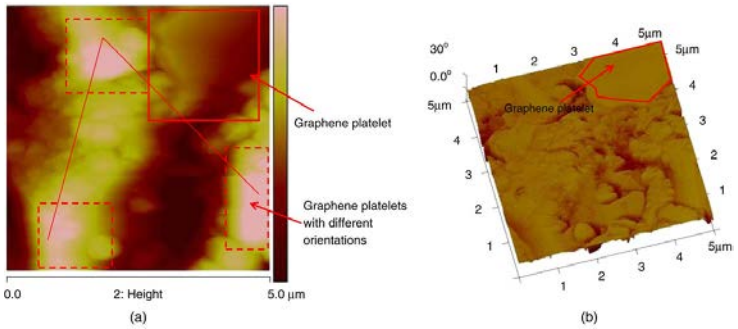

Figure 2-5. Hydrated Portland cement with pristine graphene nanoplatelets (Alkhateb et al. 2013)

Alkhateb et al. (2013) indicated that AFM can be used for graphene nanoplatelet cement observation. In the paper, the authors exhibited some images of AFM obtained by them, e.g., Figure 2-5. The authors claimed that, in Figure 2-5a, a graphene platelet at the top-right corner is identified, and the 3D phase image in Figure 2-5b confirms the graphene platelet is clearly correlated with the hi-stiffness phase topography.

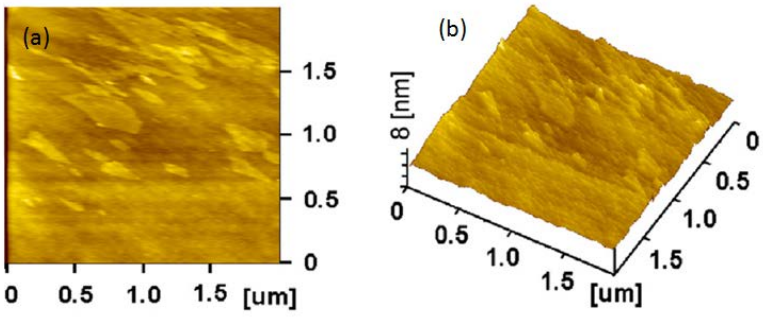

Figure 2-6. AFM images of the smallest lamellae of GO (Lv et al. 2013)

Lv et al. (2013) also indicated that the AFM technique can be used to probe the products of graphene oxidation and help to examine the obtaining of GO nanosheets suspension solution. As shown in figures, the images indicated that single irregular lamella of GO is observed with a size of 80 ~ 260 nm (Figure 2-6 a), and a thickness less than 8 nm (Figure 2-6 b).

2.7 RAMAN SPECTROSCOPY

In 1928, Sir C.V. Raman was awarded the Nobel Prize for discovering an effect which relies on the fact that when light interacts with matter, the incoming wavelength shifted as vibrational transitions are excited. This effect then is known as the Raman Effect (Zoubir, 2012). In the last eighty years, the Raman Effect has been maturely developed to be applied in practice. Nowadays, the Raman spectroscopy is an ideal tool to identify the molecules of interested materials.

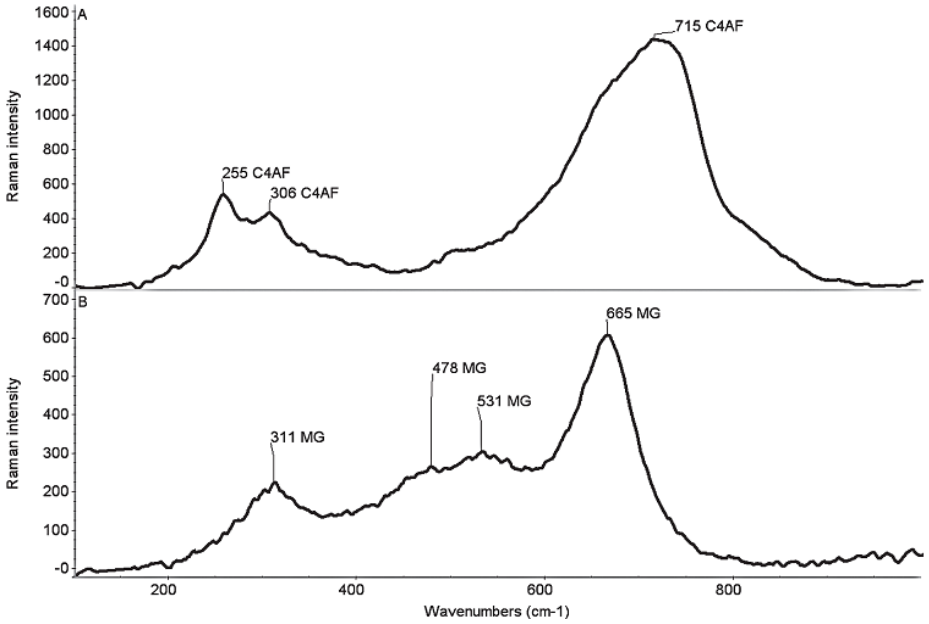

Figure 2-7. Raman spectra of dark particles of original concrete (Pešková et al. 2011)

Pešková et al. (2011) presented research to study fired concrete by using Raman spectroscopy. The specimens were placed in furnace at 1200 °C for 160 minutes. The mixture of dicalcium silicate and gehlenite was found on the surface of heated concrete. Figure 2-7 showed the Raman spectra of dark particles of original concrete.

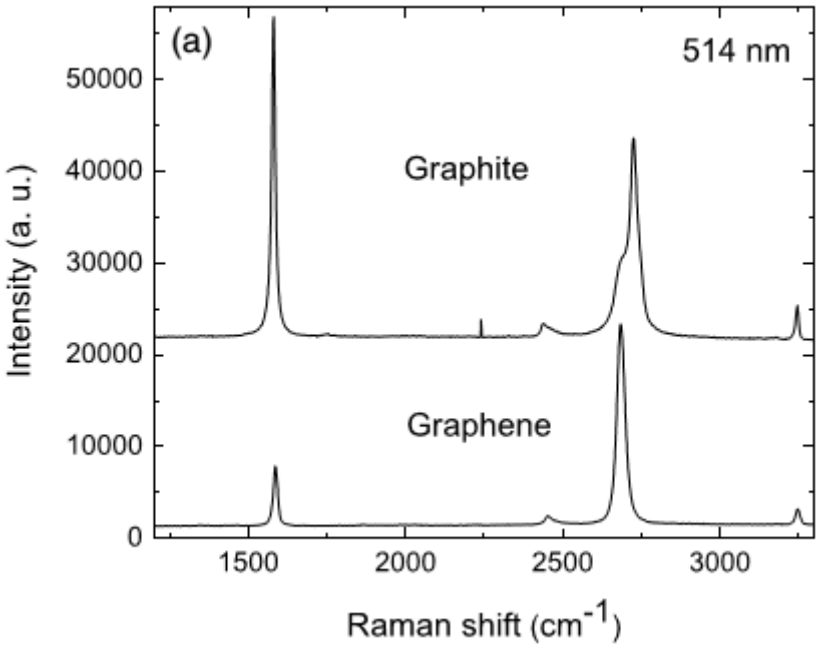

Figure 2-8. Comparison of Raman spectra between graphite and graphene (Ferrari et al. 2006)

Ferrari et al. (2006) used Raman spectroscope to study graphene and graphite. The Raman spectrum is shown in Figure 2-8. The authors concluded that graphene's electronic structure was uniquely captured in its Raman spectrum so that an unambiguous, high-throughput and nondestructive identification of graphene was provided via the Raman spectroscopy technique.

Scanning electron microscopy is another powerful "weapon" to study the microstructure of cementitious materials. The scanning electron microscope is particularly suitable for samples with rough surface because of its far depth of field, high resolution and strong magnification

ability. Furthermore, comparing to AFM, scanning electron microscopy does not need to physically contact the specimen. In general, SEM has wider application than AFM in the researches on cementitious materials.

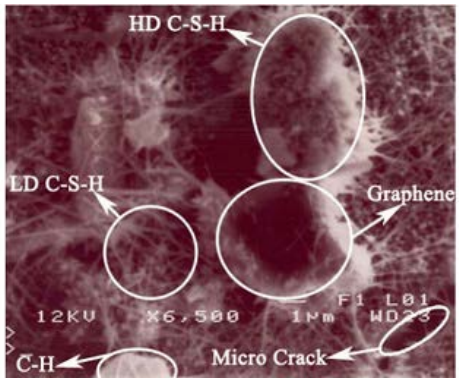

Figure 2-9. SEM image of cement mixed with pristine graphene (Alkhateb et al. 2006)

Alkhateb et al. (2013) used SEM in their research to observe graphene in the cement. As shown in Figure 2-9, SEM has identified a graphene platelet in the exfoliated pristine graphene-cement specimens.

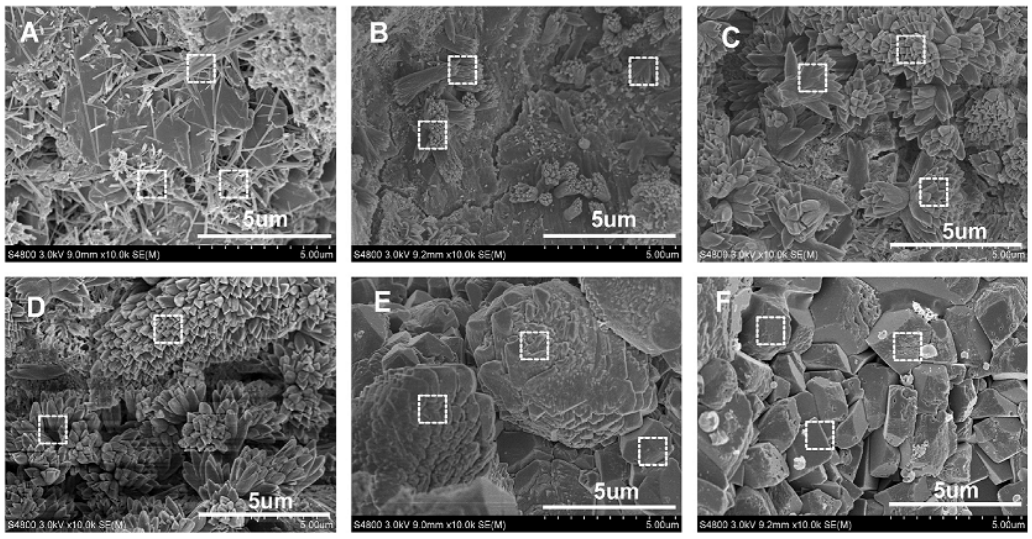

Figure 2-10. (A) no GO; (B) GO 0.01%; (C) 0.02%; (D) 0.03%; (E) 0.04%; and (F) 0.05% (Lv et al. 2013)

Lv et al. (2013) also performed the SEM observation in their study. Figure 2-10 shows the C-S-H crystal flower growing status of different specimens which were cast with different graphene concentration.

3.0 EXPERIMENTAL PROGRAM

In this chapter the details of the experimental program including experiment design, specimen preparation, and experiment procedure, are reported.

3.1 EXPERIMENT DESIGN

A series of tests were performed in order to study the effects of normal graphene and oxidized graphene on the cementitious material as well as the influence of different particle size on the material. They included compression strength test, the Young's modulus and the Poisson's ratio measurement, corrosion test and freezing & thawing test. For each type of test, the specimens were divided into four experimental groups and one control group. In the four experimental groups, the specimens were cast with the additive of C grade graphene particles (GC), C grade oxidative graphene particles (GOC), M grade graphene particles (GM) and M grade oxidative graphene particles (GOM), respectively. The specimens in the control group were cast by normal mortar (N). The details of the graphene powder used will be given in the following section.

Because of the limitations of test conditions, equipment and materials, all of the graphene specimens of the experimental groups were cast with the same graphene concentration which is determined in the trail test. Thus, factor of graphene concentration is not concerned in the experimental program.

3.2 SPECIMEN PREPARATION

3.2.1 Graphene oxidation

In the Graphene oxidation, predetermined quantities of raw graphene (5g) and nitric acid (68% 300ml) were added into a round-bottomed glass flask, and the graphene was dispersed for 30 minutes in an ultrasonic bath. Next, the reaction flask equipped with a reflux condenser and thermometer was mounted in the preheated oil bath with the temperature at 110~120 °C (230~250 °F) for 24 hours. Then, the sample was filtered on a membrane filter and washed to a neutral pH level. The experiment set-up is shown in Figure 3-1.

Figure 3-1. Graphene oxidation set-up

Because the obtained oxidative graphene coagulates after drying, it was preserved in deionized water. This led directly to the problem that the quantity of the oxidative graphene could not be measured. To solve this problem, this oxidation experiment was repeated several times to determine the weight reduction of the oxidative graphene during the process. Thus, the amount of the obtained oxidative graphene could be roughly controlled by the amount of the raw graphene added at the beginning. Before casting the specimen, the amount of oxidative graphene still had to be measured for mix design. The measurement method is described in the following section.

3.2.2 Materials and casting procedure

All specimens had a water/cement ratio of 0.53. The graphene content of the GC and GM experimental groups were designed to be 0.1% (graphene/cement) which was determined in section 3.3.1. The oxidative graphene content of the GOC and GOM experimental groups were also designed to be 0.1% (graphene/cement). The mix design used for all the specimens is shown in Table 3-1.

The GC (xGnP® Graphene Nanoplatelets Grade C) and GM (xGnP® Graphene Nanoplatelets Grade M) were procured from XG Sciences, Inc. Grade C particles typically consist of aggregates of sub-micron platelets that have a particle diameter of less than two microns and a typical particle thickness of a few nanometers. The average surface areas of Grade C particles are 500 m^2/g. Grade M particles have an average thickness of approximately 6 to 8 nanometers and a typical surface area of 150 m^2/g. The average particle diameter of Grade M is 15 microns. (XG Sciences, 2013) The other specific characteristics of GC and GM are documented in Appendix B1.

For the GC and GM experimental groups, the graphene particles were dispersed in a cup for 30 minutes with water reducer. The water reducer was necessary because graphene particles could not be dispersed well in the water without water reducer. The graphene particles aggregate quickly after being removed from the dispersing sink. The mass ratio of graphene to water reducer is 1:5, which was determined based on trial tests.

Table 3-1. Mix design for tests

	Graphene Content	Mix Percentage		
		Cement	Sand	Water
N	0%	30.22%	53.33%	16.44%
GC	0.10%			
GM				
GOC				
GOM				

The GOC and GOM were obtained by the method mentioned in section 3.2.1. The GC and GM used for oxidation are the same as the GC and GM which were added in the GC and GM experimental groups. In the oxidation process, 10g GC and 10g GM were used for the oxidation process. Before the specimen casting, a small amount of oxidative graphene with water were taken out from the preserving container. This small amount of oxidative graphene with water was weighed and then dried off to determine the graphene/water ratio which would be used to calculate the actual oxidative graphene content. All the results are shown in Table 3-2. For GOM and GOC, all of the mixtures were also dispersed for 30 min in an ultrasonic bath. It is worth mentioning here that water reducer was not added in with GOC and GOM because the oxidative graphene particles can be dispersed well in the water without additional additive.

Table 3-2. Oxidative graphene content

	Divided Mixture		Total Mixture	
	Total	Graphene	Total	Graphene
GOC	3.5769	0.0825	400	9.2258g
GOM	3.6382	0.0554	568	8.6491g

Then the specimens are ready to be cast. The dispersed graphene particles were added into the water. Note: the total water content follows the mix design. The cement and sand were premixed in the mixer, and then water and graphene were added in. The used cement is Type I Portland cement. The fineness modulus of the used sand is 2.557. The sand sieve data is documented in Appendix B3. The mixture was mixed in the mixer for 20 minutes and manual mixed during the procedure to disintegrate some agglomerations. After casting the material in the mould, the samples were vibrated for 5 minutes. Before de-molding, all the specimens sat for 24 hours with polyethylene film covering on the surface to prevent moisture loss. Every specimen was cured in the moisture chamber (23°C, 100% humidity) for 28 days before the further use. The composition of all the specimens is shown in Table 3-3.

Table 3-3. Specimen composition

Name	Weight(g)				
	Graphene	Water Reducer	Cement	Sand	Water
N	0	0	9227.6	16284	5020.9
GC	9.2276	50			
GM	9.2276	50			
GOC	9.2258	0			
GOM	8.6491				

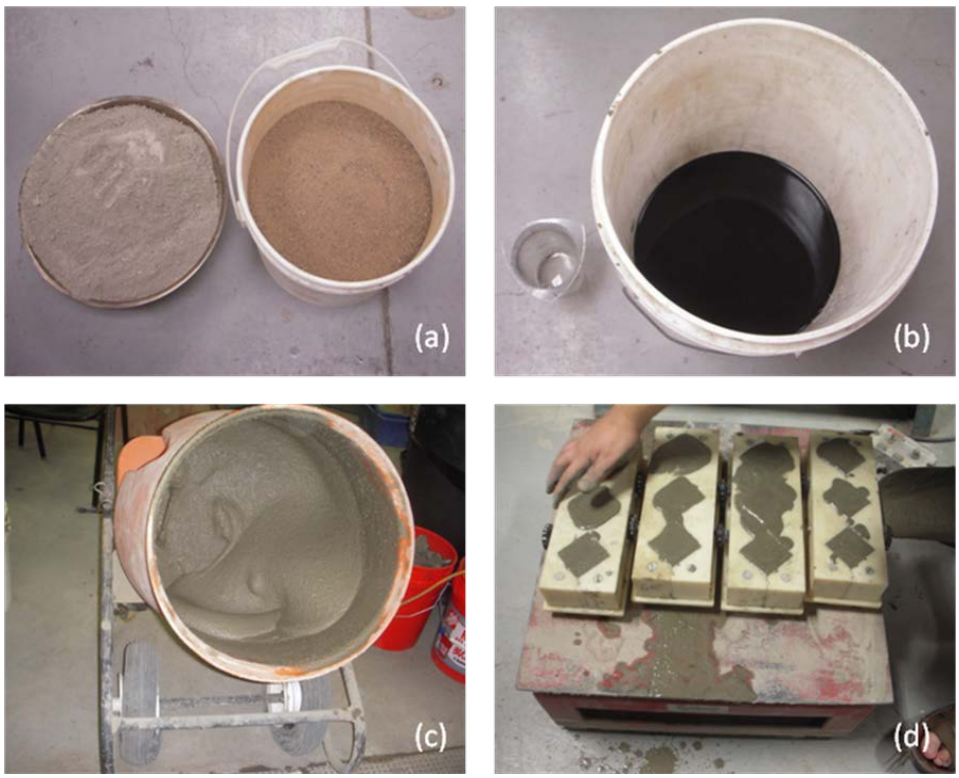

Figure 3-2. Casting procedure (a) cement and sand; (b) graphene with water; (c) mixer; and (d) specimen vibration

A total of 5 batches were cast, labelled as N, GM, GC, GOM and GOC based on graphene particle used. Each batch has 3 cylinders, 12 cubes and 3 beams. Other specimen information is shown in Table 3-4.

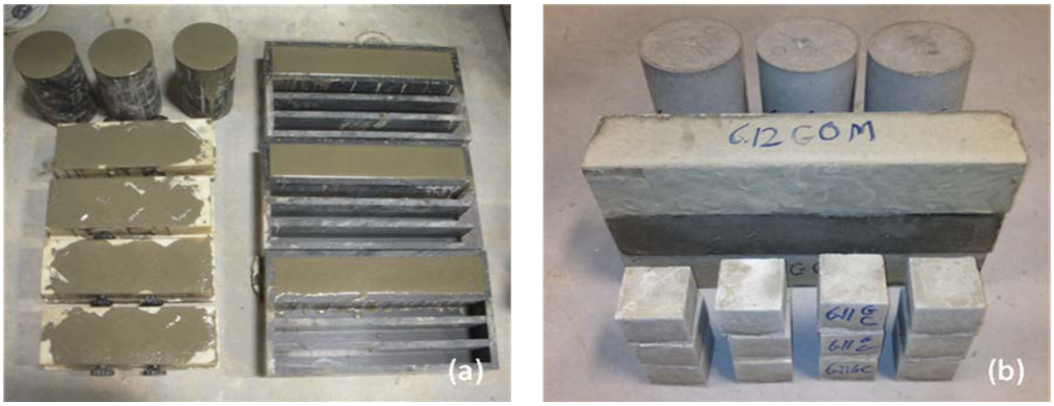

Figure 3-3. Specimens (1 batch): (a) fresh cast specimens and (b) 28-day cured specimens

Table 3-4. Specimen casting information

Name	Specimen Volume(Liter)			Whole Volume	Batch Volume	Batch Weight
	1.640	0.125	1.715			
	Cylinder	Cube	Beam			
N	3	12	3	11.57 L^3	12.72 L^3	30.53 kg
GC						
GM						
GOC						
GOM						

3.3 TESTING

3.3.1 Trial tests

3.3.1.1 Compressive strength trial

In order to determine the graphene content in the experiments, a series of trial tests were performed before the formal experiments. Several specimens were cast and tested for compressive strength by using the TEST MARK CM4000 compression machine. All of the specimens have the same mix proportion as mentioned in section 3.2.2, except the graphene content. There are 7 groups of specimens with different graphene content for GC and GM. The graphene content of these 7 groups of specimens are 0%, 0.1%, 0.2%, 0.4%, 1%, 2% and 4%, respectively. The specimens are 5cm ×5cm × 5cm in size. Each group has 5 specimens except the 1% and 4% graphene content groups. Because of the material availability, here only one specimen was cast for the 1% and 4% groups. The tests results are shown in Table 3-5.

The results reveal that, for the GC specimens, the strength enhancements of all the graphene additive specimens are about 10% higher than normal mortar. The strength enhancement is relatively higher when graphene content is 0.2% and 1%. Among the GM specimens, ones containing the 0.2% graphene content have the highest compressive strength. When the graphene content is 2% and 4%, the strength of the specimens is less than the normal mortar specimens. Considering the material availability and the trial tests results, the 0.1% graphene content is chosen for the formal experiments.

Table 3-5. Compressive strength trial test results

Name		Graphene Content						
		0%	0.1%	0.2%	0.4%	1%	2%	4%
GM	Specimen1	22400	22380	23810	21250	22760	20740	21240
	Specimen2	22270	22320	25090	22390		20410	
	Specimen3	20510	21760	23460	24550		20120	
	Average	21726.67	22153.33	24120	22730	22760	20423.33	21240
	Strength Comparison		1.96%	11.02%	4.62%	4.76%	-6.00%	-2.24%
GC	Specimen1	22400	25140	26000	23410	24980	24100	24620
	Specimen2	22270	24430	23480	23610		24850	
	Specimen3	20510	24260	25350	24320		23680	
	Average	21726.67	24610	24943.33	23780	24980	24210	24620
	Strength Comparison		13.27%	14.81%	9.45%	14.97%	11.43%	13.32%

3.3.1.2 Water absorption trial test

The water absorption trial tests of some specimens were also performed before the formal experiments. After compressive tests, some broken specimens were smashed into small pieces to make sure internal cracks did not exist. All the loosened particles were also eliminated from the specimen surfaces. Before being put in the drying chamber for 48 hours, all of the samples were

submerged in the water for 24 hours and then were wiped to surface dry condition and then weighed and marked. After drying, the specimens were weighed again, and the results are shown in the Table 3-5.

Table 3-6. Water absorption strength trial test results

Graphene Content	N	GC	GM	GOC	GOM
0%	12.70%				
0.1%		12.80%	13.20%	12.80%	12.70%
0.2%		12.30%	12.10%		
0.4%		12.40%	12.70%		

Concerning the results, the water absorption ability of all the samples showed no significant difference. The detailed test results could be found in Appendix A1.

3.3.2 Compressive strength test and Young's modulus & Poisson's ratio measurement

3.3.2.1 Introduction

Compressive strength, Young's modulus and Poisson's ratio are the basic parameters for cementitious materials. In structural engineering, cementitious materials are always designed to work under compression, and therefore the compressive strength is the key factor for a new cementitious material. In addition, the Young's modulus and Poisson's ratio are necessary in describing the mechanical property and prediction of the material behavior during the service. Thus, this test was designed to compare the difference on the three material properties between normal mortar and graphene reinforced mortar.

Here the specimens are cast in the shape of cylinders according to ASTM Standards. The size is 10.16cm in radius and 20.23cm in height. Each group has three specimens, and all the

specimen were cast by the method which is described in the section 3.2.2 and were cured for 28 days.

3.3.2.2 Apparatus

The apparatus for this test are the Concrete Elastic Modulus Meter and the TEST MARK CM4000 compression machine which are shown in Figure 3-4 (a) and (b).

Figure 3-4. Apparatus for compressive strength test and Young's Modulus & Poisson's Ratio measurement: (a) Concrete Elastic Modulus Meter, (b) TEST MARK CM4000 compression machine

3.3.2.3 Test setup and procedure

The Concrete Elastic Modulus Meter is fixed on the specimen surface. The loading rate of the TEST MARK was set to 440 lbs/s based on the ASTM standard.

Before the formal test, a trial-test was carried out on one specimen of the N group to determinate the probable compressive strength. The test process for other specimens is divided

into three sequential steps. The first step is to preload to 10% of the compressive strength which is estimated by the trial-test. All the loads were removed once the 10% of the compressive strength was reached. The purpose of this step is to make sure the compression platforms have full contact with the specimen. The second step is load to 40% of the compressive strength. All the loads were removed once 40% of the compressive strength was reached. During this step, the longitudinal and transverse dial gage readings were recorded as well as the corresponding compressive force which is obtained from the loading machine. The Elastic Modulus Meter was un-mounted from the specimen after this step. In the last step, the specimens were reloaded until they were failed. The highest compressive forces were recorded for the compressive strength calculation.

The stress was calculated as follows:

$$S = \frac{P}{A}$$

where: S is stress; P is applied load; and A is cross-sectional area of the cylindrical specimen.

The strain was calculated as follows:

$$\varepsilon = gI / L_o$$

where: ε is strain; g is the longitudinal dial gage reading; L_o is the length of the tested area; and I is the reduction coefficient. Here, I=0.5.

The Young's modulus was calculated as follows:

$$E = \frac{S_2 - S_1}{\varepsilon_2 - 0.000050} \quad \text{(ASTM C469)}$$

where: E is chord modulus of elasticity, MPa; S_2 is stress corresponding to 40% of ultimate load; S_1 is stress corresponding to a longitudinal strain, ε_1, of 50 millionths, MPa; and ε_2 is longitudinal strain produced by stress S_2.

The Poisson's ratio was calculated as follows:

$$\mu = \frac{\varepsilon_{t2} - \varepsilon_{t1}}{\varepsilon_2 - 0.000050} \qquad \text{(ASTM C469)}$$

where: μ is Poisson's ratio; ε_{t2} is transverse strain at midheight of the specimen produced by stress S_2; ε_{t1} is transverse strain at midheight of the specimen produced by stress S_1; and ε_2 is longitudinal strain produced by stress S_2.

3.3.3 Water absorption test

3.3.3.1 Introduction

The water absorption ability could generally reflect the porosity of the specimens. The porosity of cementitious material is closely related with compressive strength, corrosion resistance, frost-resistance and other material properties.

3.3.3.2 Apparatus

The water absorption test does not require sophisticated instrumentation. Only some containers are needed for soaking the specimens. Besides, the drying chamber is needed to dry the specimens.

3.3.3.3 Test setup and procedure

All the specimens were obtained from the compressive test which was presented in section 3.3.2. The test setup and procedure is the same as the test which was mentioned in section 3.3.1.2.

3.3.4 Freezing and thawing test

3.3.4.1 Introduction

The freezing and thawing test is carried out here to investigate the frost resistance of the graphene reinforced material. The parameters which were monitored during the process are the specimen length and weight. The test procedure, test setup and test instruments were designed based on the ASTM C666/C666M with some slight modifications according to the restrictions on experimental equipment and materials. This test is still considered to be valuable and objective because the conclusions and discussions of this test are based on comparing the differences between the experimental groups and the control group.

The specimens are cast in the shape of beams with size = 7cm × 7cm × 35cm. Every group has three specimens, and all the specimens were cast by the method which was described in the section 3.2.2 and were cured in the moisture chamber for 28 days.

3.3.4.2 Apparatus

As shown in Figure 3-5, the equipment for the freezing and thawing test includes a 150cm (L) × 75cm (W) × 30cm (H) water container, a GE 7.0 cubic ft. chest freezer and an electronic thermometer. An electronic scale and an electronic slide caliper with calibrated precision were also used for this test.

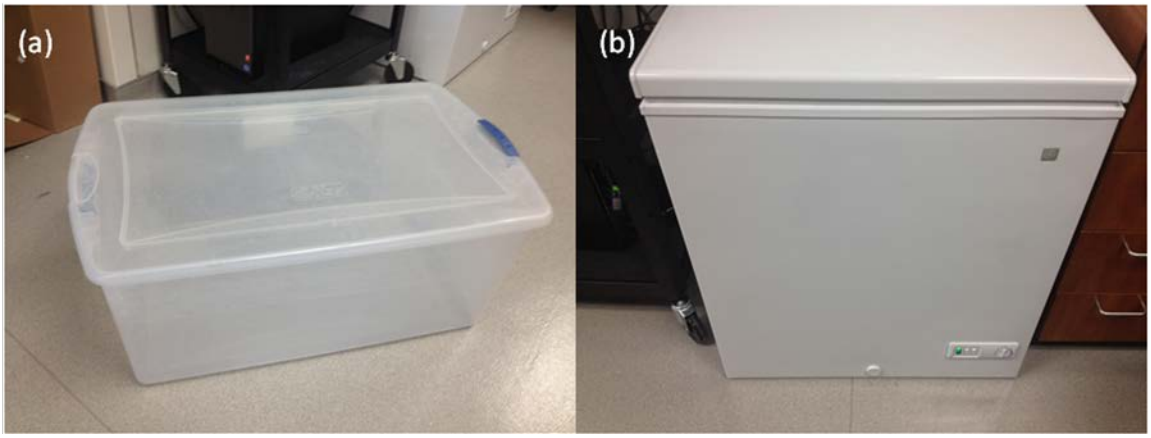

Figure 3-5. Apparatus for freezing and thawing test: (a) water container and (b) chest freezer

3.3.4.3 Test setup and procedure

After cured in the moisture chamber for 28 days, the specimens were taken out and drilled with a hole (1cm in depth, 0.2cm in radius) at the center of each end (Figure 3-6). The prepared stainless steel rods that were around 2cm in length were inserted into the holes and fixed with epoxy resin. The specimen configuration is shown in Figure 3-7.

Figure 3-6. Stainless steel rods embedded in the end

The freezing and thawing test includes 300 cycles. Each cycle contains two phases: freezing phase and thawing phase. For every cycle, the freezing phase was performed before the thawing phase. All of the specimens were weighed and measured before the test cycles begin. For every 26 cycles, each specimen was wiped to surface dry to weigh and measure for length with the electronic scale and the electronic slide caliper, except the last cycle which has only 14 cycles. The specimens were weighed and measured for 13 times and all the experimental data was recorded with the dates.

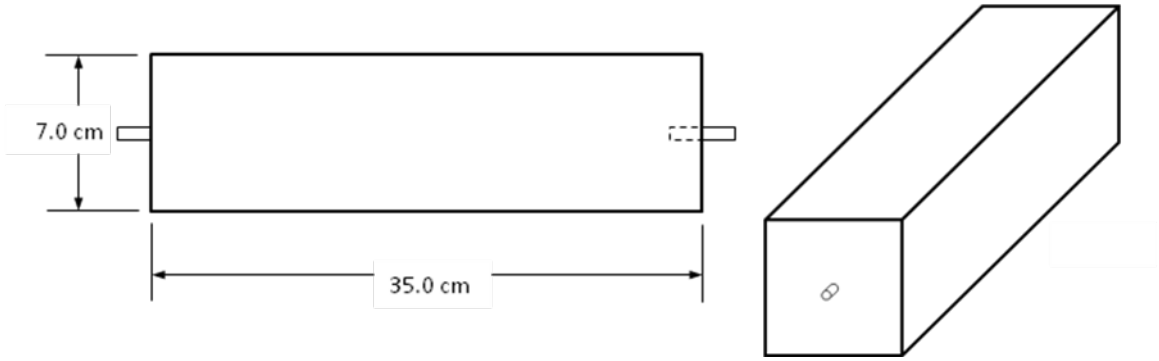

Figure 3-7. Specimen configuration

In freezing phase, the specimens were standing straight up in the chest freezer. In order to make sure all of the specimens contact with the cold air, some wood battens were placed on the bottom of the freezer, as shown in Figure 3-8. Because the temperature in the freezer is not uniform from the top to the bottom, the specimens were placed on each end by turns. Thus, a "×" symbol was marked on one end of every specimen (Figure 3-8). For the purpose of improving the stability of the temperature in the freezer, several bottles of water were placed in the freezer 3 days before the test. These bottles of water were frozen into ice in two days and were preserved in the freezer during the whole test. Their significant heat capacity could help to achieve constant temperature during the freezing. Based on several trial tests in which the temperature in the

freezer was measured by the electronic thermometer, the temperature of the specimens in the freezer would reach 18±1 °F in two hours. As a result, the specimens were placed in the freezer for 5 hours during the freezing phase.

Figure 3-8. Freezing phase setup

In the thawing phase, the specimens were laid down in the water container which was filled with saturated calcium hydroxide solution. The three specimens of the same group were laid in one stack and were separated by 3 wood blocks, as shown in Figure 3-9. The wood blocks were placed to make sure all of the specimens were fully contact with the solution in the container. In the thawing process, all of the specimens were immersed in the solution for 2 hours. The temperature of the solution is varied from 20 °F to 32°F.

Figure 3-9. Thawing phase setup

In the thawing phase, the specimens were laid down in the water container which was filled with saturated calcium hydroxide solution. The three specimens of the same group were laid in one stack and were separated by 3 wood blocks, as shown in Figure 3-9. The wood blocks were placed to make sure all of the specimens were fully contact with the solution in the container. In the thawing process, all of the specimens were immersed in the solution for 2 hours. The temperature of the solution is varied from 20 °F to 32°F.

The weight change in percent was calculated as follows:

$$W_c = \frac{w_2 - w_1}{w_1} \times 100$$

where: W_c is weight change of the test specimen after C cycles of freezing and thawing, %; w_1 is weight of test specimen at 0 cycles; and w_2 is weight of test specimen at C cycles.

The weight change in percent was calculated as follows:

$$L_c = \frac{l_2 - l_1}{l_1} \times 100$$

where: L_c is weight change of the test specimen after C cycles of freezing and thawing, %; l_1 is measured length between 2 stainless steel rods of test specimen at 0 cycles; and l_2 is measured length between 2 stainless steel rods of test specimen at C cycles.

3.3.5 Corrosion test

3.3.5.1 Introduction

In practice, the corrosion is one of the most common reasons for the destruction of concrete structures, especially for reinforced concrete structures. The reinforcing steel bar inside the concrete is susceptible to corrosion effect which lowers its strength level. However, the concrete protective layer can effectively reduce the probability of corrosion of the internal steel bar. Therefore, the corrosion resistance of concrete in reinforced concrete structures is particularly important. This test is designed to investigate the corrosion resistance difference between normal mortar and cementitious material reinforced by graphene.

The test method in this research is designed based on the study of Schneider and Chen (2004). The specimens are cast in the shape of cube with size of 5cm × 5cm × 5cm. Each group has 3 specimens. All of the specimens were cast by the method mention in Section 3.3.2.

3.3.5.2 Apparatus

As shown in Figure 3-10, the equipment used in this test includes a small water container which has dimensions of 50cm (L) × 30cm (W) × 20cm (H) and the TEST MARK loading machine. The chemical agents include ammonium nitrate, sodium hydroxide, phenolphthalein and formaldehyde. All of these chemical agents were procured from Fisher Science Inc. To do the

acid-base neutralization titration and adding the solute, a burette and several beakers were also needed.

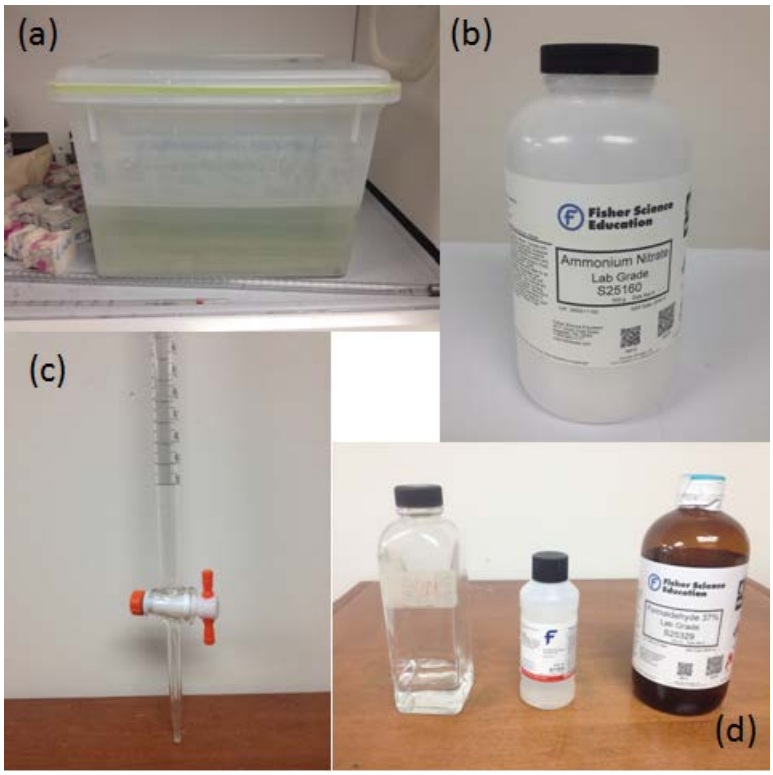

Figure 3-10. Agents for corrosion test: (a) 15% ammonium nitrate solution; (b) ammonium nitrate; (c) burette; and (d) sodium hydroxide solution, phenolphthalein and formaldehyde (from left to right)

3.3.5.3 Test setup and procedure

The highest ammonium nitrate concentration of the corrosion solution is 10% in Schneider and Chen's (2004) research. Based on this, the concentration of ammonium nitrate in this study was set to 15%. All of the specimens were directly immersed in 15% ammonium nitrate solution after 28 days curing. The specimens were taken out from the solution to do compression test after corrosion for 1 month, 3 months and 5 months.

The stress of specimen was calculated as follows:

$$S = \frac{P}{A}$$

where: S is stress; P is applied load; and A is cross-sectional area of the cube specimen.

To maintain the concentration of ammonium nitrate of the solution, the concentration was tested by acid-base neutralization titration and the ammonium nitrate was added into the solution if the observed concentration is too low. The acid-base neutralization titrations were performed as the following steps:

1. Make 2.5 mol/L NaOH solution standby for the further step.
2. Take 25 mL NH_4NO_3 solution from the specimen container and keep in a beaker.
3. Add 17 mL formaldehyde into the beaker.
4. Add 2 drops of phenolphthalein into the beaker.
5. Use burette to add the NaOH solution into the beaker till the solution change to red. Swirl the beaker after every few drops to mix well.
6. Read the Burette and calculate the concentration.

The titration records and the records of adding solute can be found in Appendix A2

4.0 EXPERIMENTAL RESULTS AND DISCUSSION

This chapter reports the experimental records and results of the tests which are described in chapter 3. The discussions of these results are also reported in this chapter.

4.1 COMPRESSIVE STRENGTH TEST AND YOUNG'S MODULUS & POISSON'S RATIO MEASUREMENT

4.1.1 Results

The compressive strength, Young's modulus and Poisson ratio test records, calculations and results are reported in the following sections. All of the results are calculated based on the ASTM C39 (Compressive Strength of Cylindrical Concrete Specimens) and ASTM C469 (Static Modulus of Elasticity and Poisson's Ratio of Concrete in Compression). The following tables and figures are the test result summaries. The test records and calculations are shown in Appendix A3.

Table 4-1. Compressive strength results

Compressive Strength (Mpa)				
Name	Average	Min	Max	%
N	34.59	31.37	37.53	
GM	38.55	37.64	39.55	11.5%
GC	41.48	38.93	43.17	19.9%
GOM	39.14	37.94	41.39	13.2%
GOC	38.10	37.05	38.86	10.2%

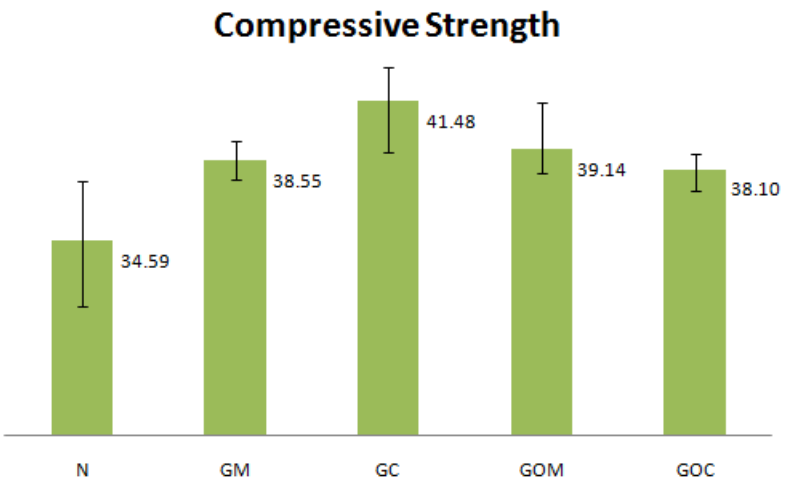

Figure 4-1. Compressive strength results

Table 4-2. Young's modulus results

Young's Modulus (Gpa)				
Name	Average	Min	Max	%
N	17.00	16.97	17.02	
GM	16.51	16.06	16.88	-2.9%
GC	17.68	17.20	17.97	4.0%
GOM	16.98	16.86	17.11	-0.1%
GOC	17.39	17.33	17.44	2.3%

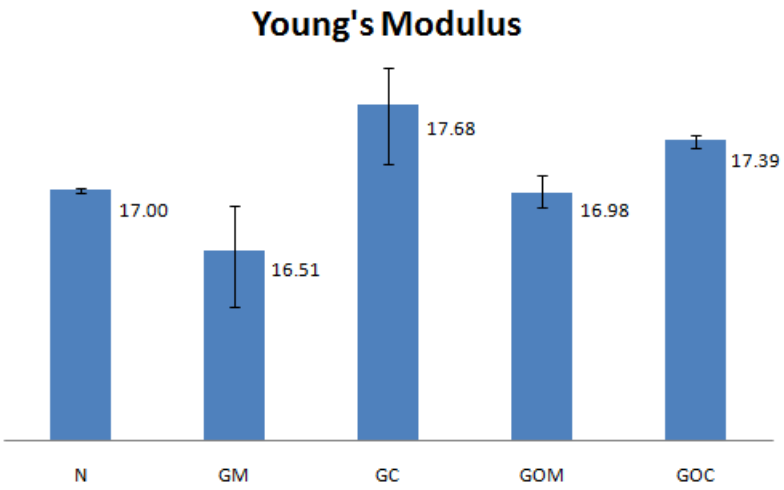

Figure 4-2. Young's modulus results

Table 4-3. Poisson's ratio results

Poisson ratio				
Name	Average	Min	Max	%
N	0.1595	0.1543	0.1646	
GM	0.1626	0.1615	0.1646	2.0%
GC	0.1682	0.1572	0.1753	5.5%
GOM	0.1555	0.1446	0.1677	-2.5%
GOC	0.1761	0.1750	0.1772	10.4%

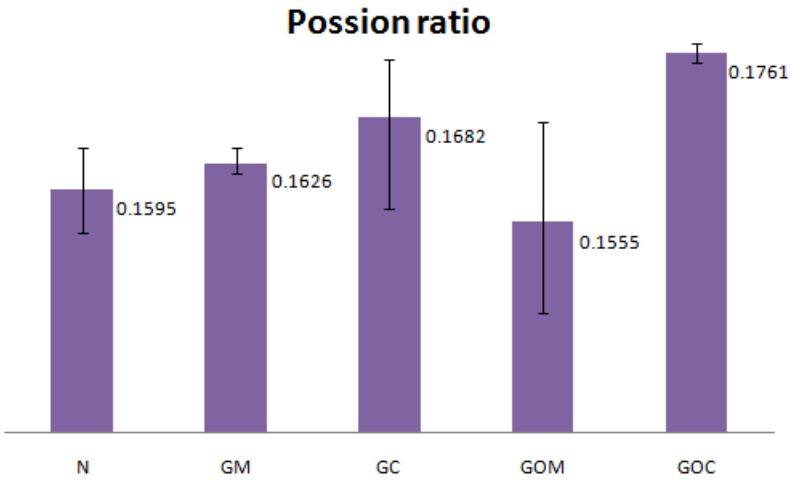

Figure 4-3. Poisson's ratio results

4.1.2 Discussion

During the casting process of the trail tests and the formal tests, the graphene particles exhibit the remarkable capacity to influence the liquidity and workability of cement paste. The graphene particle additive mortar is more viscous than the normal mortar. This could be considered evidence that the graphene nanoplatelets consumed the water in the cement composite because of their high surface area.

The results of the compression strength test reveal that the strength increase of the GC experimental group, about 20% compared to the control group, is higher than the other experimental groups (Figure 4-1 and Table 4-1). In addition, the compressive strength of the GOM group is 13.2% higher than that of the control group. The compressive strength increase of the GM and GOC experimental groups are all about 10% compared to the control group.

As shown in Figure 4-2 and Table 4-2, the Young's modulus' results also show a similar pattern. From the results, the Young's modulus of all the specimens are both 17.0±1.0 Gpa. Thus, to some extent, the Young's modulus of the experimental groups can be regarded as not having big differences. It is worth noting that, compared to the normal mortar group, the Young's modulus of GC group is the highest in the experimental groups. As calculated in Table 4-2, the Young's modulus of the GC group is 4% higher than the N group.

In the results of Poisson's ratio (Figure 4-3 and Table 4-3), the GOC group shows the highest value (10.4% compared to the normal cement). In addition, the variation range of value of three specimens of GOC group is smallest.

4.2 WATER ABSORPTION TEST

4.2.1 Results

The results of water absorption test could be found in Table 4-4 and Figure 4-4.

Table 4-4. Water absorption results

Name	Soaked Weight (g)	48 hrs Dry Weight (g)	Water Content
N	73.1	64.8	12.8%
	91.4	81.1	12.7%
	66.9	59.2	13.0%
	72.6	64.5	12.6%
	Average		**12.8%**
GM	90.9	80.4	13.1%
	91.5	80.8	13.2%
	81.7	72.1	13.3%
	49.7	43.8	13.5%
	Average		**13.3%**
GC	72.3	64.3	12.4%
	106.1	95.5	11.1%
	66.3	59.1	12.2%
	88.9	79.4	12.0%
	Average		**11.9%**
GOM	81.3	72.1	12.8%
	79.9	70.6	13.2%
	62.1	55.0	12.9%
	37.2	32.9	12.9%
	Average		**12.9%**
GOC	97.6	86.6	12.7%
	97.2	86.2	12.8%
	72.5	63.9	13.5%
	79.1	70.0	13.0%
	Average		**13.0%**

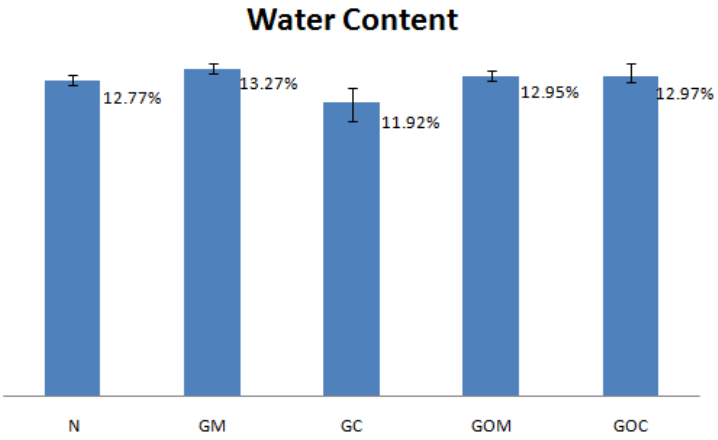

Figure 4-4. Water absorption results

4.2.2 Discussion

As shown in Figure 4-4 and Table 4-4, the water content of GC groups is 11.92%, which is the lowest value of all the experimental groups. The water content percent of other experimental groups are both around 13%, and the GM group has the highest water content (13.27%). This result reveals that, the porosity of the specimen is reduced because the presence of the C grade graphene nanoplatelets. By comparing the GC with the GM experimental groups, it is found that the grade C graphene is more effective than the grade M graphene on reducing the porosity. Furthermore, the comparison between GM and GC experimental group is not affected by water reducer, because the water reducer content is same in the GC group and GM group.

4.3 FREEZING AND THAWING TEST

4.3.1 Results

The test results summary is shown in the following figures. The detailed test records and calculations of each specimen can be found in Appendix A4.

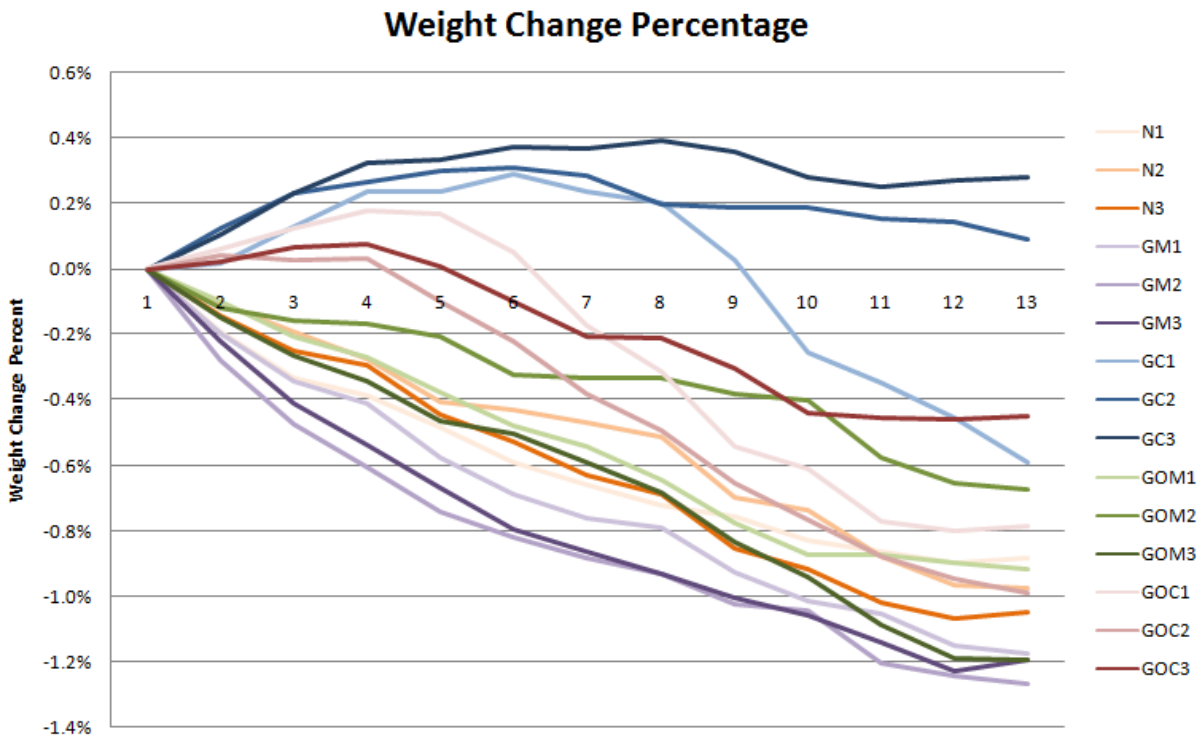

Figure 4-5. Weight change percentage of all the specimens

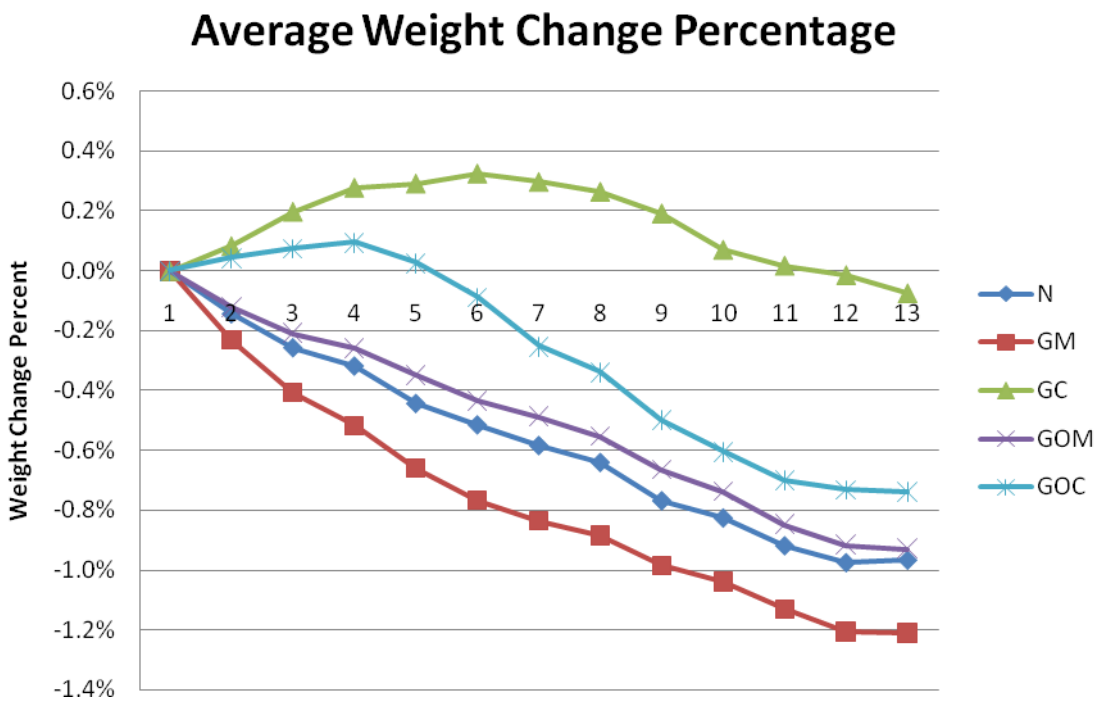

Figure 4-6. Average weight change percentage all the groups

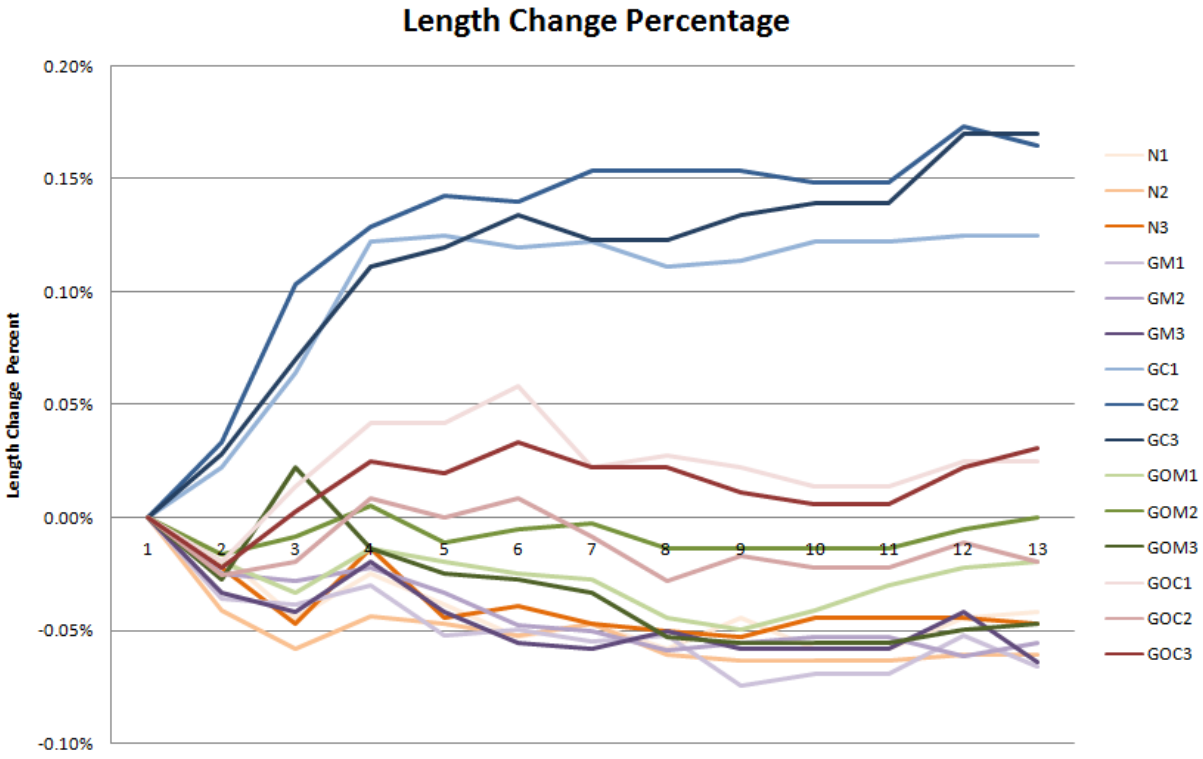

Figure 4-7. Length change percentage of all the specimens

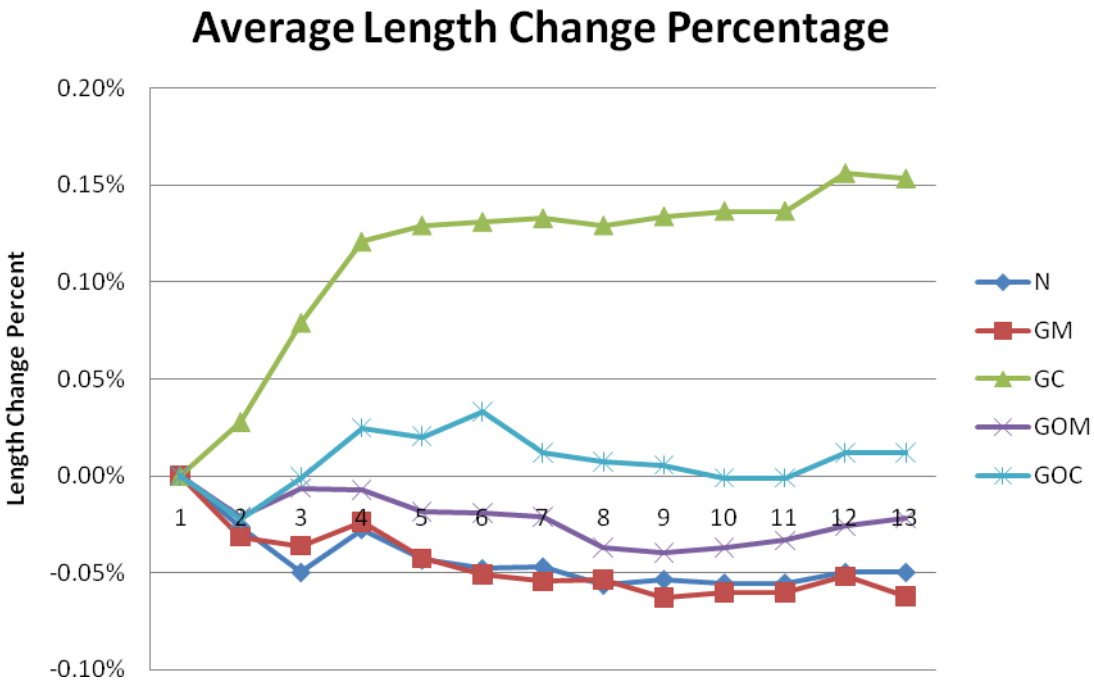

Figure 4-8. Average length change percentage of all the groups

4.3.2 Discussion

In this test, the weight change is monitored during the freezing and thawing cycles. For the GC group, the specimens' weight increased at the first 130 cycles and decreased at the last 170 cycles. The GOC group also shows the similar weight change record; however, the weight growing phase of the GOC group (100 cycles) is shorter than this of GC group. Besides that, the extent of weight growth of the GOC group is less than GC group.

Except the GC and the GOC group, the weight of the GOM, GM groups and the control group are both decreased from the beginning. Among these three groups, the weight decrease of the GOM group is the smallest.

The behaviors of the specimens' length were similar with the specimens' weight. The percentages of length change of all the specimens are within 0.07%, except for the GC group, for which the length increase reached 0.15% at the last cycles. The behaviors of increase are found both in the GC and the GOC groups. But the amplitude of length increase of the GOC group is less compared to the GC group. The largest length change of the GC group is 0.61 mm, while the other specimens are around 0.2 mm.

On the other hand, the GOM group shows the lowest length change during the freezing and thawing cycles. The average length change of the GOM group is within -0.04%. The calculated results of weight and length change percentages can be found in Appendix A3.

The weight increase in the freezing and thawing test is considered as an abnormal behavior. During the freezing and thawing cycles, the calcium hydroxide cannot cause the weight gain because the concentration of calcium hydroxide inside the specimens is much higher than that in the solution. The concentration of calcium hydroxide inside the specimens is high because the calcium hydroxide is the main product of cement hydration. Therefore, the only possibility for the weight gain of the GC and GOC groups is that water is preserved inside the specimens. In the weight measurement, all of the specimens were only wiped to surface dry. Thus, the weight of water inside the specimens was included in the results. Furthermore, the spalling of specimens was rarely observed during the freezing and thawing cycles. Therefore, the GC group showed the weight increase at the first 130 cycles.

It is also possible that the water preserving ability of the GC and GOC groups increased because the internal tension cracks emerged. This conjecture is confirmed by the results of length change. The length increase is generally considered as a sign of developing of tension cracks. Actually, the ASTM standard says that if the expansions of the length exceed 0.1%, it means the

specimen failed to meet the requirement of the frost resistance. Thus, the performance of the GC group in the freezing and thawing test is the worst.

Nevertheless, compared to the other groups, the GOM group showed the best performance in the freezing and thawing cycles. The weight loss of the GOM group is lower than the GM and N groups; the length change percentage of it is the smallest among all the groups.

4.4 CORROSION TEST

4.4.1 Results

The test results summary is shown in Table 4-5 and Figure 4-9. The detailed test records and calculations can be found in Appendix A5.

Table 4-5. The average compressive strength test records of the N group

Stress(psi)	N	GC	GM	GOC	GOM
28 Days	6263.33	6827.50	6122.50	6234.17	6592.50
Corrosion for 1 month	6546.67	6677.50	6315.83	6403.33	6166.25
Corrosion for 3 months	5629.17	5538.33	5275.83	5555.00	5951.25
Corrosion for 5 months	4885.00	5429.17	4410.83	4723.33	4950.00

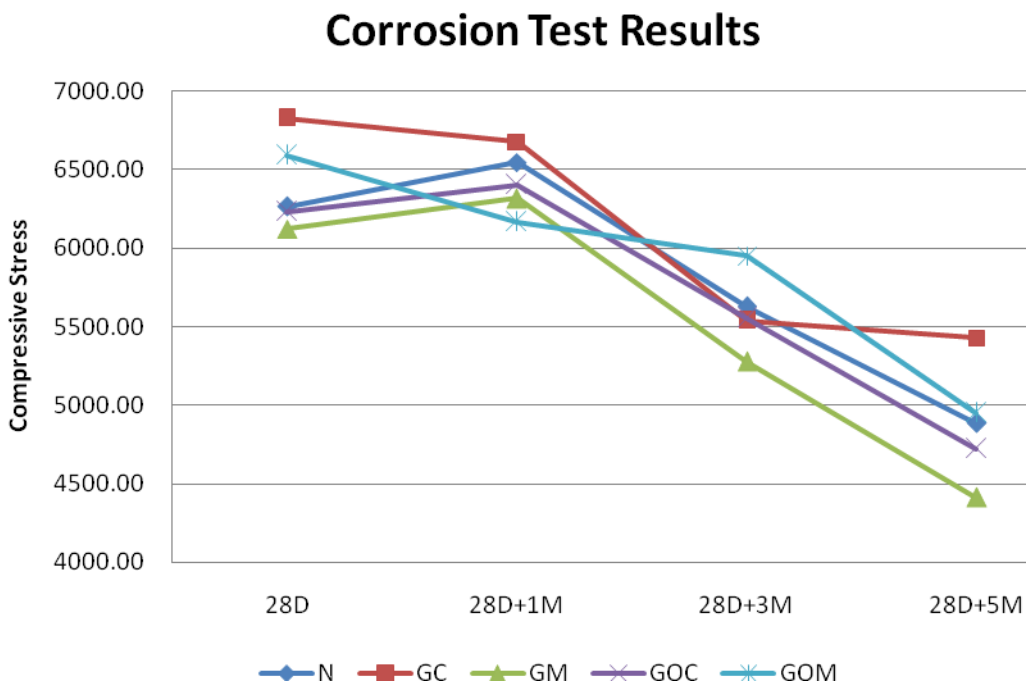

Figure 4-9. Average relative length of all the groups

4.4.2 Discussion

Through observation, no obvious corrosion signs were found in the specimen surface in the first month of the corrosion test. In the third month of corrosion test, some crystalline substance was found on the surface of the specimens. In the last two month, some tiny cracks appeared on the specimen surface. The broken specimens of every compression test were tested by phenolphthalein. The alkaline substance which can turn phenolphthalein to red was reduced during the testing period. As shown in Figure 4-10, the depth of the ammonium nitrate attack was increased as time went on. In the first month, the attack depth was about 0.3 cm. and it increased to 1.5~2.5 cm after 3-months of corrosion. Finally, the ammonium nitrate almost penetrated the whole specimen.

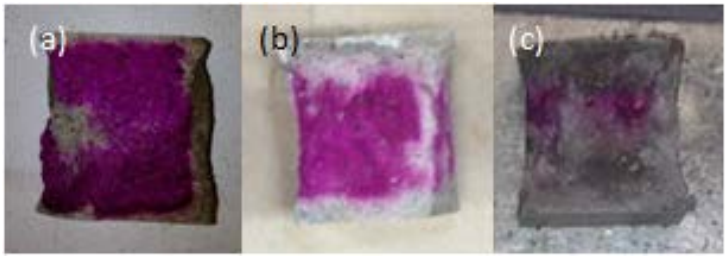

Figure 4-10. Specimens tested by phenolphthalein: (a) corrosion for 1 month; (b) 3 months; and (c) 5 months

The corrosion test result shows that the compressive strength of all the specimens is weakened after 5-month corrosion. In the first month, the strength of the GC and GOM groups dropped down while strength of the other groups rose up. In the second month and the third month, the strength of all the specimens dropped down; furthermore, the dropping rate of the GC group was the highest, and that of the GOM group was the lowest among all the other groups. However, in the last two months, the strength dropping rate of the GC group was much lower than the other groups. The results of the final compression test show that the compressive strength of the GC and GOM groups is higher than the control group, while that of the GOC and GM groups is lower than the control group.

The conclusion made by Lv et al. (2013) in their research may be used to explain the specimen behavior in the corrosion test.

It is generally known that the mainly hydrates of hardened Portland cement are C-S-H ($3CaO{\cdot}2SiO_2{\cdot}4H_2O$), calcium hydroxide ($Ca(OH)_2$), ettringite ($6CaO{\cdot}Al_2O_3{\cdot}3SO_3{\cdot}32H_2O$) and calcium aluminum sulfate hydrate ($4CaO{\cdot}Al_2O_3{\cdot}SO_3{\cdot}12H_2O$). Chen and Lei (2003) indicated that NH_4NO_3 reacts with $Ca(OH)_2$ and CaO of hydrates of Portland cement so that to damage the composite structure of harden Portland cement. The reaction formulas are shown as follow:

$$Ca(OH)_2 + NH_4NO_3 \rightarrow Ca(NO_3)_2 + NH_3\uparrow + H_2O$$

$$CaO + NH_4NO_3 \rightarrow Ca(NO_3)_2 + NH_3\uparrow + H_2O$$

Lv et al. suggested that the graphene reacts with Portland cement. They also indicated that ettringite is less prevalent in the hydrates because of the reaction between graphene and cement. Lv et al. also concluded that the reaction between graphene and Portland cement is an endothermic reaction which can reduce the thermal cracks during the hydration process, enhancing the strength of the specimen.

Based on this, the reasonable speculation is: the ettringite in the GC group's specimens is less than the other specimens because the GC group shows the highest compressive strength in section 4.1.1. Therefore, the strength dropping rate of the GC group is slightly faster than the other groups in the first three months. Another conjecture is GC can accelerate the hydration process during the 28-day curing. Thus strength of GC group dropped down at the beginning of the corrosion; while the strength of the other groups slightly grew up because of the continuous hydration.

Chen and Lei (2003) also indicate that the reaction product $Ca(NO_3)_2$ can continuously react with $Ca(OH)_2$, producing $Ca(NO_3)_2 \cdot H_2O$ which is a large crystal. The growth of this crystal inside the microcracks and cavities of hardened Portland cement can cause expansion stress so that to further damage the cement. Therefore, the GC group which has fewer microcracks resisted the corrosion better than the other groups, so that the GC group exhibited the highest compressive strength at the end.

5.0 MICROSCOPIC PROBE

This chapter shows the microscope observations of the cementitious material samples. The microscopic approaches include atomic force microscope (AFM) observation, Raman spectroscopy test and scanning electron microscope (SEM) observation. This chapter also discusses the results of these probe methods.

5.1 SPECIMEN PREPARATION

5.1.1 Specimen casting

The specimens for microscopic observation were both cut from broken pieces of the compression test, as describes in section 3.3.2. The broken pieces were cut into small blocks with dimensions: 10mm (L) × 5mm (W) × 5mm (T). Each sample was polished by the 150 grade sand paper to smoothen the surface. Every group has one sample. All of the polished samples were cast in the plastic rings with epoxy resin and then were dried in the drying chamber for 24 hours. As shown in Figure 5-1, three samples were cast in the same ring so that to reduce the polishing workload in the next step.

Figure 5-1. Microscope observation samples

5.1.2 Specimen polishing

After drying, all of the specimens were polished by the 300, 600 and 1200 grade abrasive paper in turns. The cast epoxy and the outside ring were polished together. At the final step, each specimen was polished with polishing machine to make sure there were no tiny scratches on the specimens' surface. The polishing paste and disk that were used in this step were procured from Struers, Inc. (Figure 5-2)

Figure 5-2. Polishing paste and disks

5.2 ATOMIC FORCE MICROSCOPE OBSERVATION

5.2.1 Test instrumentation and setup

The device used for this test is the Veeco Manifold Multimode V& Dimension V scanning probe microscopy (Figure 5-3). By combining the Multimode V SPM and the Dimension V SPM with several advanced application modules, the manifold SPM combination offers atomic force microscopy observation. (PINSE, 2014) The tapping mode was used in the test and the scan rate is set to 0.5 Hz. The samples used in this test were prepared by the method that mentioned in section 5.1.

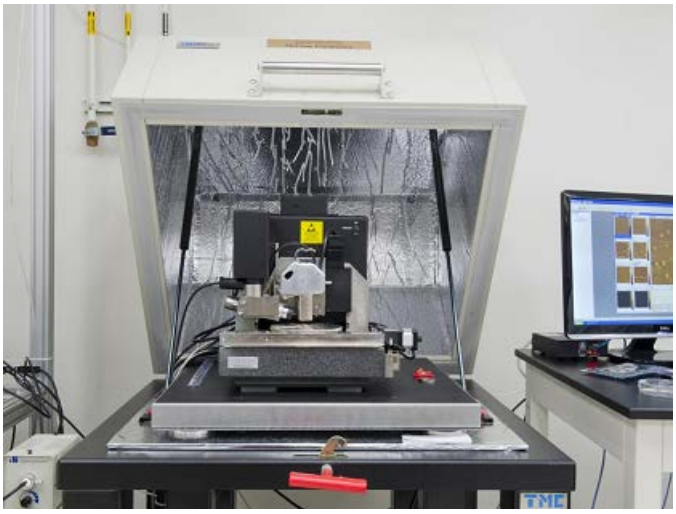

Figure 5-3. Atomic force microscope (PINSE, 2014)

5.2.2 Results and discussion

The images obtained by the AFM of all the samples are shown in Figure 5-4~8. The scan areas of N, GC and GM samples are 2.0 μm. The scan areas of GOC and GOM samples are 300 nm.

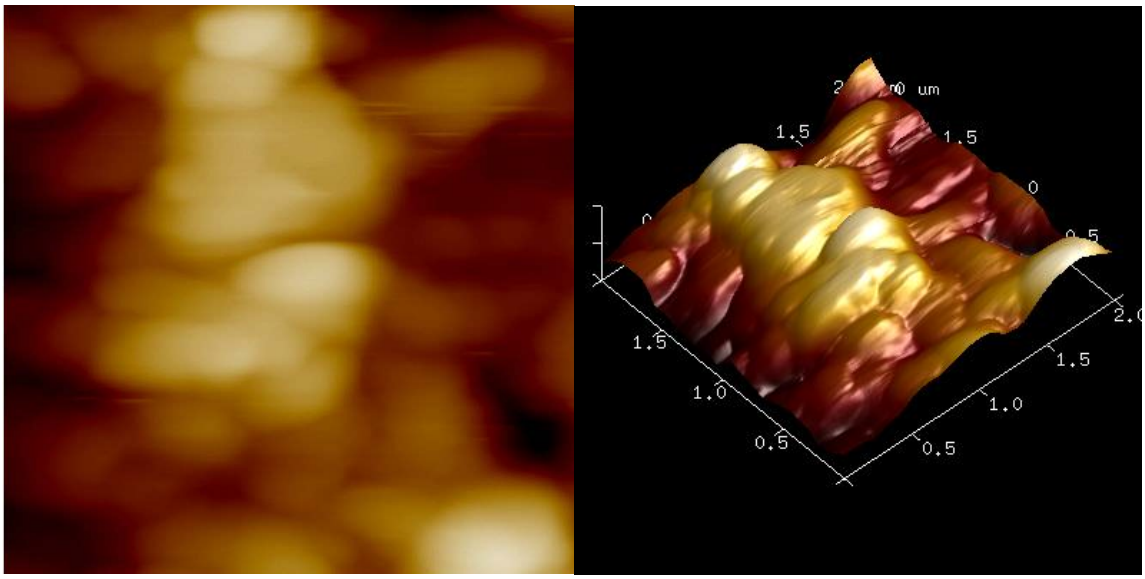

Figure 5-4. The N sample's image obtained by AFM

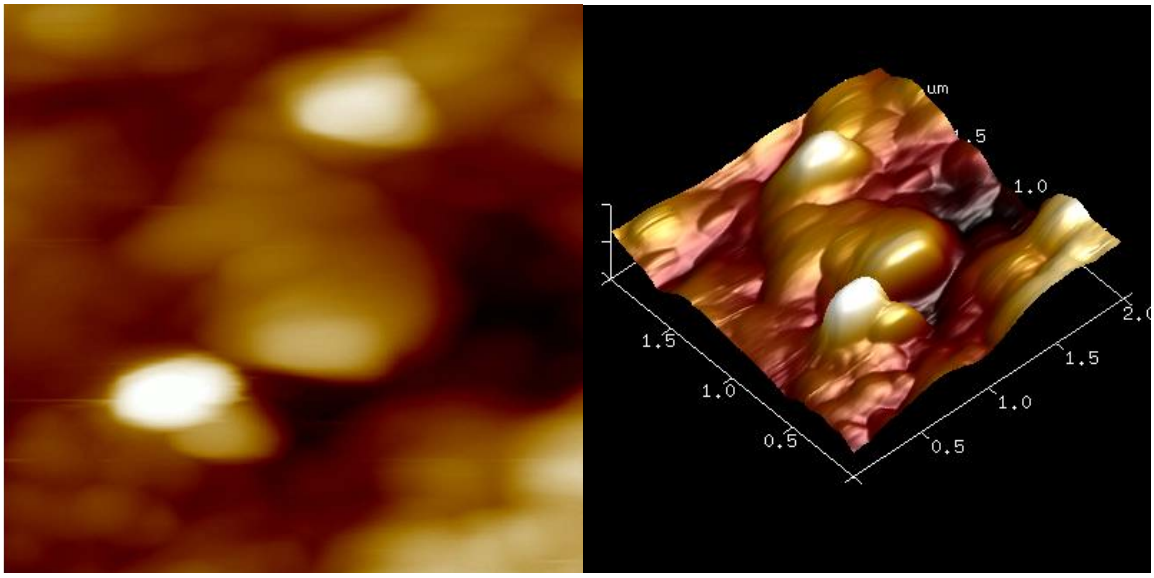

Figure 5-5. The GM sample's image obtained by AFM

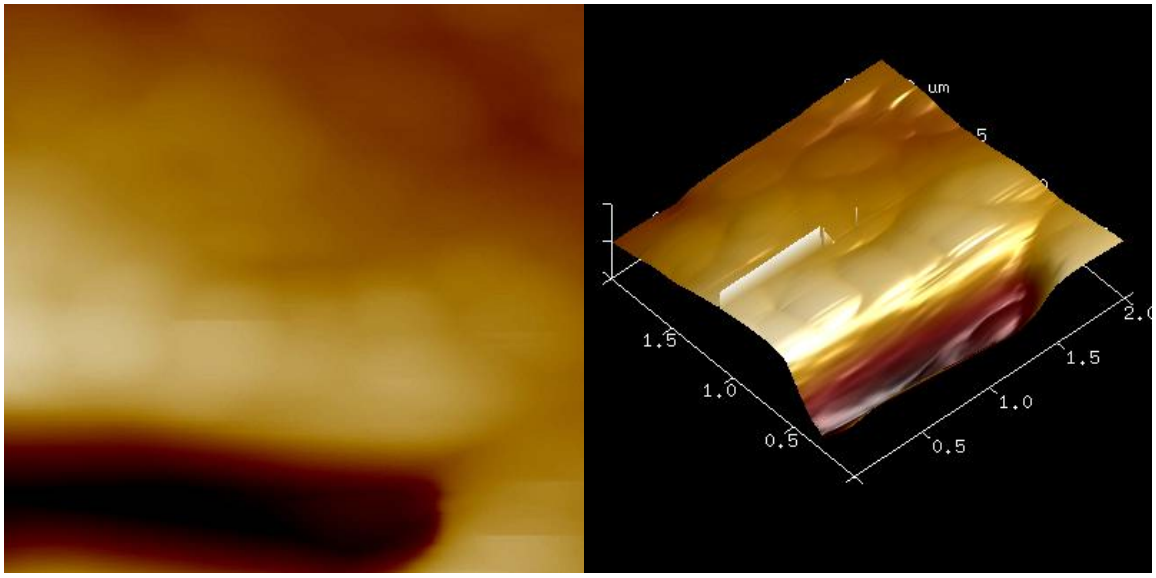

Figure 5-6. The GC sample's image obtained by AFM

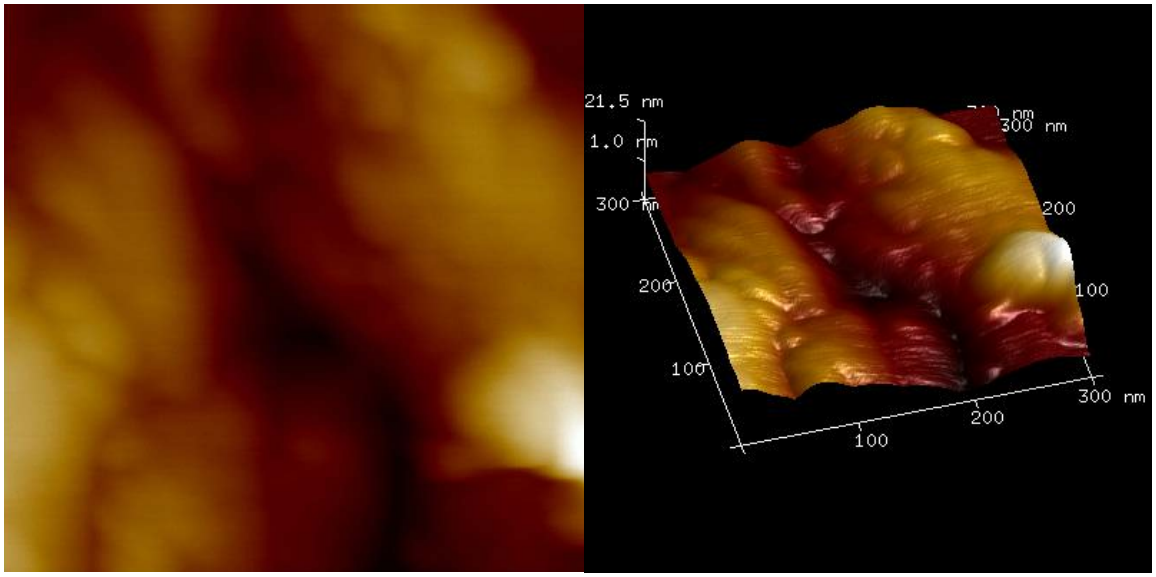

Figure 5-7. The GOM sample's image obtained by AFM

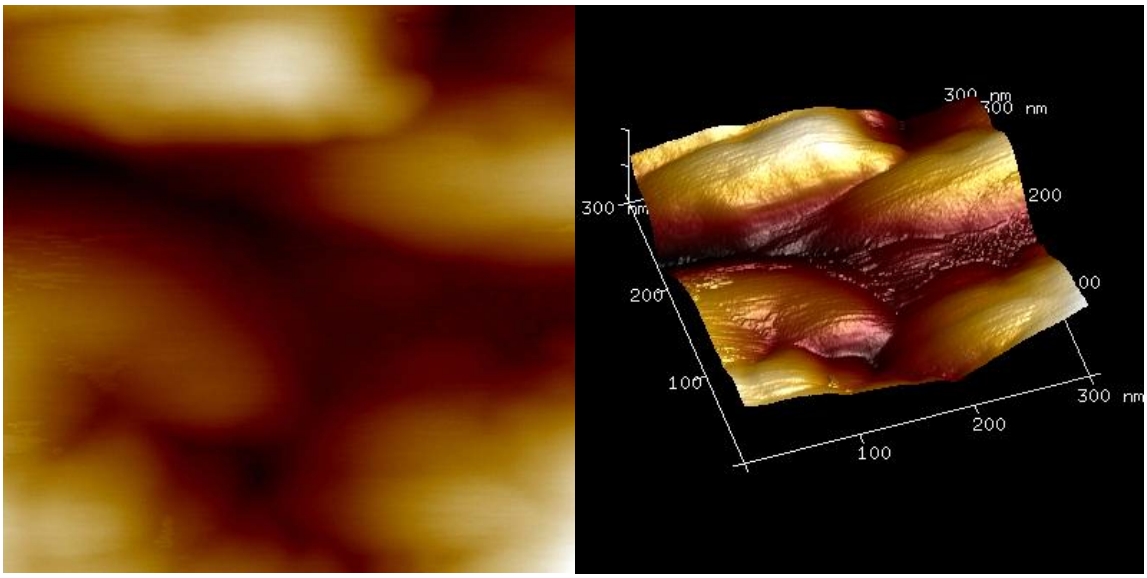

Figure 5-8. The GOC sample's image obtained by AFM

These images were obtained from AFM by scanning the interested points on the specimen surface. The interested points were black particles or with other features that graphene was possibly embedded.

Based on the research of Alkhateb (Alkhateb et al. 2013), the variation in the C-S-H distribution and packing could be disturbed because of the presence of the graphene nanoplatelets. More specifically, the surface of graphene should be smoother than that of C-S-H. However, from the results of this test, the surfaces of all the samples are both exhibit a relatively coarse topography, except the images of GC sample. Even though the topography in the image is relatively flat and smooth as shown in Figure 5-6, the conclusion cannot be determined that graphene is embedded in the observed surfaces. Therefore, before the AFM observations, other approaches should be performed to roughly locate the graphene particles.

5.3 RAMAN SPECTROSCOPY TEST

5.3.1 Test instrumentation

As shown in Figure 5-9, the Renishaw inVia Raman microscope is used in this test.

Figure 5-9. Renishaw inVia Raman microscope (PINSE, 2014)

5.3.2 Results and discussion

In this test, the pristine GM and the sample of GM was tested. Figure 5-10 shows the results of pristine GM. The peak waves of Raman shift are presented around 1600 cm^{-1} and 2600 cm^{-1}. This result is similar to the Raman spectroscopy of GM which is provided by XG Sciences, Inc. Because the particularity of graphene Raman spectrum, the location of the graphene can be determined by the following steps. First, use optical microscope to roughly locate a point that may be graphene particles on the sample's surface. Secondly, induce the red laser to precisely locate the interested point on the sample. Next, perform Raman spectrum scan and analyze the

results. If the results exhibit peak waves around 1600 cm^{-1} and 2600 cm^{-1} (Figure 5-11), it means this point should be graphene. Finally, record the optical microscope image (Figure 5-12) with the Raman spectroscopy results. Some Raman spectroscopy images obtained in this test can be found in Appendix B2.

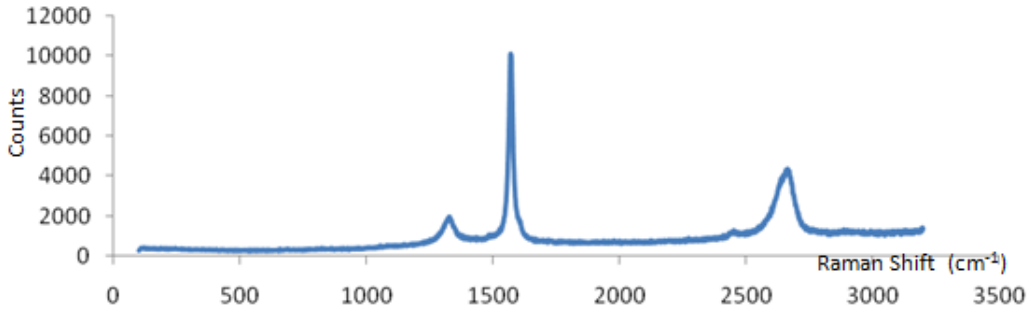

Figure 5-10. Raman spectroscopy observation results of GM

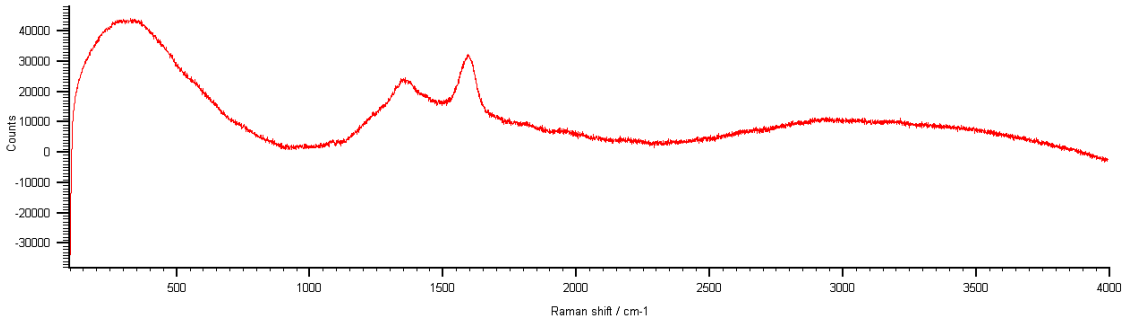

Figure 5-11. Raman spectroscopy results of GC cement sample

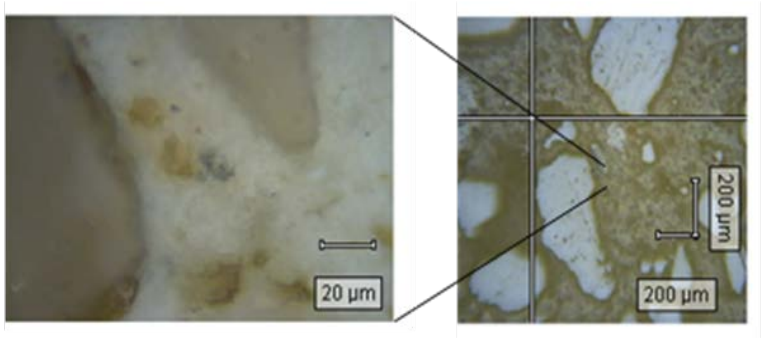

Figure 5-12. Optical microscope image of GC cement sample

After locating the graphene particles on the surface, other microscope observation is possible to find the graphene and to study the interface between graphene and cement paste. For example, when perform AFM, the graphene location can be found by the integrated optical microscope of AFM, then be scanned. Figure 5-13 is an image obtained by AFM after Raman spectroscopy location. The scan area is the same with the area exhibits in Figure 5-12. From this AFM image, a graphene platelet at the low-right corner is identified.

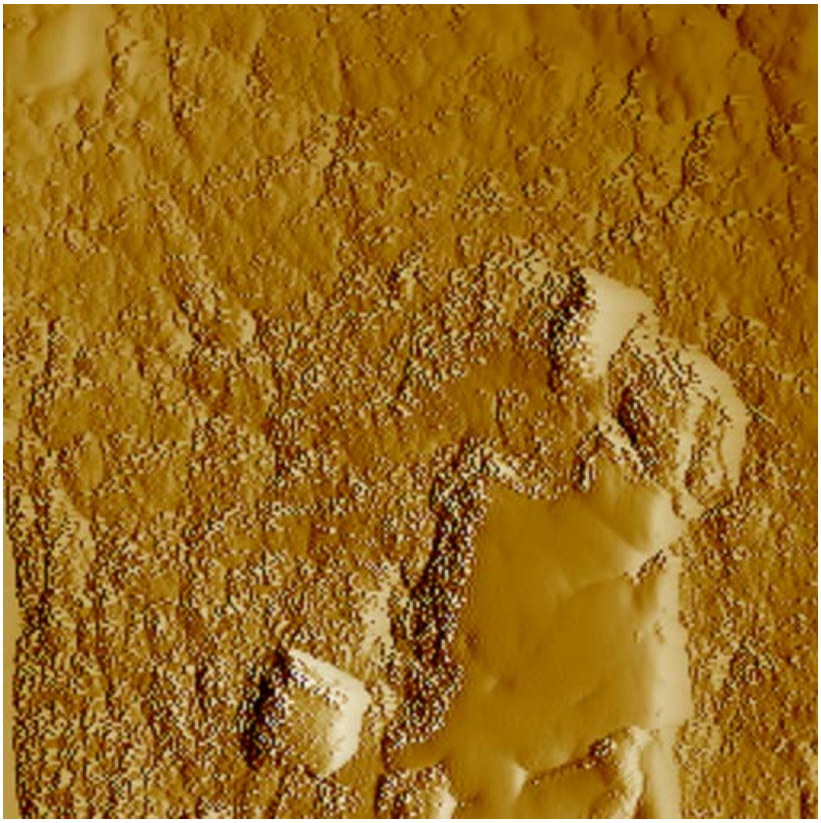

Figure 5-13. AFM images of GC simple after Raman spectroscopy location

5.4 SCANNING ELECTRON MICROSCOPE OBSERVATION

5.4.1 Test instrumentation

The low vacuum scanning electron microscope (SEM) was used in this test (JEOL JSM-6510LV/LGS), shown in Figure 5-14.

Figure 5-14. JEOL JSM-6510LV/LGS scanning electron microscope (PINSE, 2014)

5.4.2 Results and discussion

Figure 5-15 is an image of the GC samples obtained by SEM. The suspected GC is shown at the top-centre. Around this particle, some crystalline substances were found, which is speculated to be C-S-H. The magnified image of this area is shown in Figure 5-16. This crystalline structure is similar with the crystalline flower that is mentioned by Lv et al. (2013).

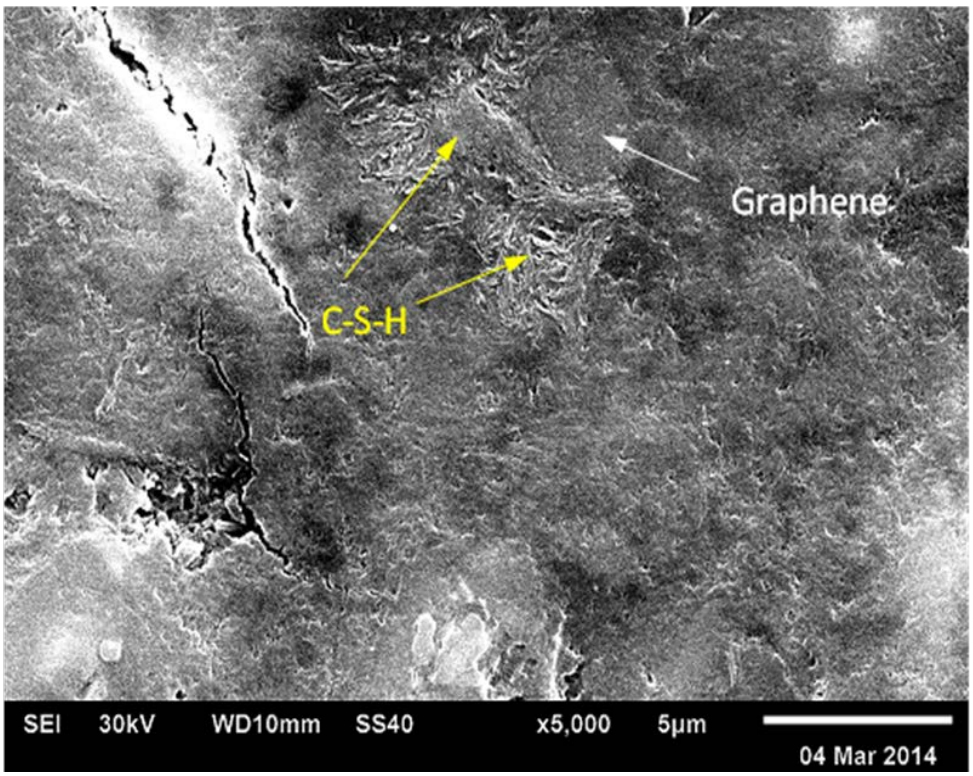

Figure 5-15. SEM images of GC sample

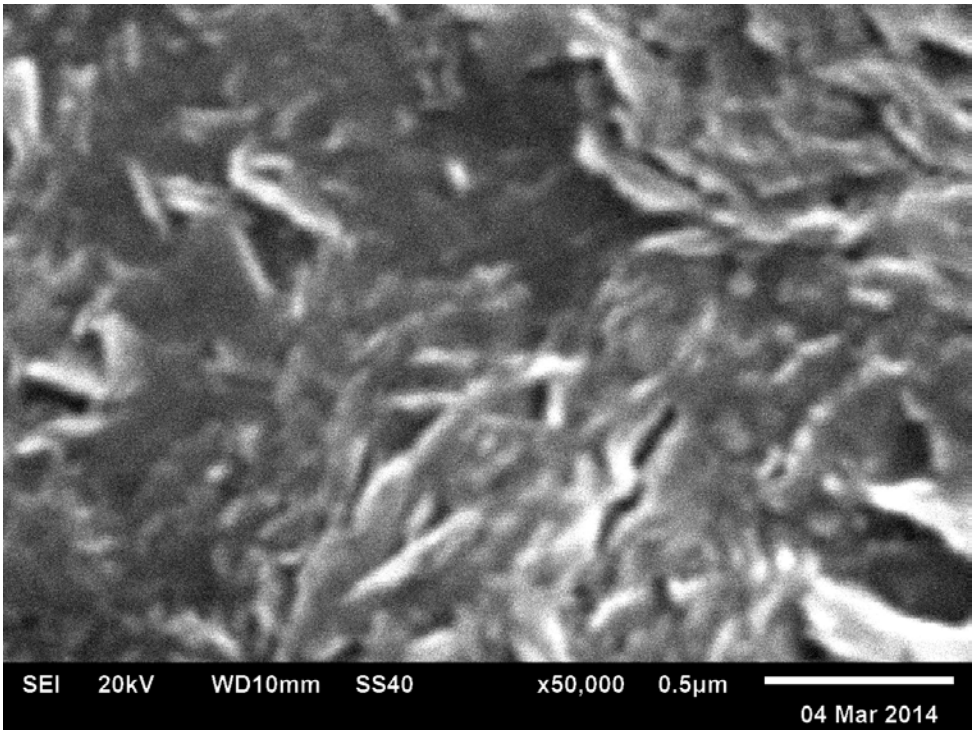

Figure 5-16. SEM images of GC sample

6.0 SUMMARY, CONCLUSIONS, AND RECOMMENDATIONS

6.1 SUMMARY

This research presented a series of experiments to investigate the properties of cementitious material which is reinforced by graphene nanoplatelets. All the specimens were casted and cured based on the ASTM C192/C192M "Standard Practice for Making and Curing Concrete Test Specimens in the Laboratory". The curing time of all of the specimens was 28 days.

In the compressive strength and Young's modulus & Poisson's ratio test, a total of fifteen specimens were tested based on ASTM C469/C469M "Standard Test Method for Static Modulus of Elasticity and Poisson's Ratio of Concrete in Compression". The broken pieces were used to determine water absorption by measuring soaked weight and dry weight.

The freezing and thawing tests were also performed in this research. Every specimen was experienced 300 freezing thawing cycles. The mass weight loss and specimen length were measured each 26 cycles. The test procedure and condition were designed and modified based upon ASTM C666/C66M "Standard Test Method for Resistance of Concrete to Rapid Freezing and Thawing".

A total of 60 specimens were tested in corrosion experiment. After curing for 28 days, every specimen is placed in 15% ammonium nitrate solution for 5 months. The first 15

specimens were tested for 28-days compressive strength. Each 15 specimens were tested at 1 month, 3 months and 5 months corrosion period.

To explore the mechanism of mechanical properties enhancement caused by graphene, the atomic force microscopy, Raman spectroscopy and scanning electron microscopy observation were performed.

6.2 CONCLUSIONS

Based on the literature review and the test results, the conclusions are made as follows:

1. The GC, GOM, GM and GOC can improve the compressive strength of cementitious materials. The compressive strength of them is 19.9%, 13.2%, 11.5% and 10.2% higher than the normal mortar, respectively.
2. The GC can effectively improve the water preserving ability of cementitious materials and thus it will weaken the frost resistance of harden Portland cement, whereas the GOM can slightly improve the frost resistance of cementitious materials.
3. The corrosion resistance of cementitious materials within 5 months can be boosted by the GC and GOM, while this can be weakened by the GM. From the current experimental data, the GC and GOM are more likely to raise long-term acid corrosion resistance of concrete.
4. Nitric acid oxidation of graphene nanoplatelets on improving the cementitious material strength is not as good as expected. However, the oxidation treatment is necessary because it can mitigate the detrimental effect of plain graphene particles on frost resistance of cementitious materials.

5. The performance of the GOM group is best among all the experimental groups, by comprehensive consideration of all the experimental results
6. The Raman spectroscopy observation is powerful when locating graphene nanoplatelets in the cement surface. It can help the researchers to locate the graphene in AFM observation to make the images obtained in AFM are more credible rather than only judging the existing of graphene by topography.

6.3 RECOMMENDATIONS

This research is presented with limited experimental conditions and materials. It can be improved in several aspects. In addition, the mechanism of improvement of cementitious material caused by graphene is still unclear. Thus, the further studies are needed. There are some recommendations for the future studies:

1. The small size graphene nanoplatelet exhibits more effective capacity to improve the compressive strength of the cementitious materials than the big one. To reach higher compressive strength, the small size graphene is recommended, such as the graphene platelets used by Sedaghat et al. (2013). Its dimension is only 110 × 110 × 0.12 nm (Angstrom Materials, N008-100-N). In addition, it is better to set more experimental groups with different graphene platelet sizes.
2. Continue research on how to improve the frost resistance of C grade graphene additive cement, such as adding air entraining agent in to the mix proportion design.
3. Try other oxidation treatment method of graphene particles, such as the method presented by Lv et al. (2013).

4. Adopt freezing thawing chamber for the freezing and thawing test. It can improve the stability of the freezing and thawing cycles so to reduce the experiment error. Furthermore, employ relative dynamic modulus loss as a criterion to evaluate the frost resistance.
5. Add more types of corrosive solution in the corrosion test to perform contrast experiments and advisably elongate the corrosion period.
6. Perform nano indentation tests by using AFM to measure the micro modulus of the specimens. The researching area should be focused at the interface between the graphene platelet and C-S-H.
7. Molecular dynamics simulation is helpful to research the mechanism of enhancement of cementitious materials by graphene nanoplatelets.

APPENDIX A

A.1 TRIAL WATER ABSORPTION RESULTS RECORD

Table A-1. Test results of water absorption trial test: N

	Soaked Weight	48 hrs Dry Weight	Water Content
N	120.4	107.3	12.2%
	135.5	119.8	13.1%
	96.8	85.8	12.8%
	Average		12.7%

Table A-2. Test results of water absorption trial test: 0.1% GC

	Soaked Weight	48 hrs Dry Weight	Water Content
0.1% GC	90.0	79.5	13.2%
	75.4	67.0	12.5%
	81.0	71.9	12.7%
	92.0	81.5	12.9%
	Average		12.8%

Table A-3. Test results of water absorption trial test: 0.1% GM

	Soaked Weight	48 hrs Dry Weight	Water Content
0.1% GM	68.1	60.1	13.3%
	85.8	75.8	13.2%
	70.6	62.4	13.1%
	85.5	75.6	13.1%
	Average		13.2%

Table A-4. Test results of water absorption trial test: 0.1% GOC

	Soaked Weight	48 hrs Dry Weight	Water Content
0.1% GOC	92.1	81.8	12.6%
	75.2	66.7	12.7%
	75.5	66.7	13.2%
	Average		12.8%

Table A-5. Test results of water absorption trial test: 0.1% GOM

	Soaked Weight	48 hrs Dry Weight	Water Content
0.1% GOM	92.4	82.8	11.6%
	84.3	74.0	13.9%
	98.2	87.4	12.4%
	77.1	68.3	12.9%
	Average		12.7%

Table A-6. Test results of water absorption trial test: 0.2% GC

	Soaked Weight	48 hrs Dry Weight	Water Content
0.2% GC	55.6	49.4	12.6%
	109.2	97.1	12.5%
	93.2	83.3	11.9%
	Average		12.3%

Table A-7. Test results of water absorption trial test: 0.2% GM

	Soaked Weight	48 hrs Dry Weight	Water Content
0.2% GM	81.6	73.2	11.5%
	99.4	87.1	14.1%
	93.4	83.8	11.5%
	90.1	80.8	11.5%
	Average		12.1%

Table A-8. Test results of water absorption trial test: 0.4% GC

	Soaked Weight	48 hrs Dry Weight	Water Content
0.4% GC	103.4	92.5	11.8%
	97.9	86.3	13.4%
	90.3	80.3	12.5%
	61.5	55.0	11.8%
	Average		12.4%

Table A-9. Test results of water absorption trial test: 0.4% GM

	Soaked Weight	48 hrs Dry Weight	Water Content
0.4% GM	83.7	74.9	11.7%
	95.1	84.7	12.3%
	90.7	80.0	13.4%
	63.9	56.4	13.3%
	Average		12.7%

A.2 TITRATION RECORDS

Table A-10. Titration records before the first compression test

	Date	Quantity of used NaOH solution(mL)	Concentration
28 Days + 1 Month	Jul. 15	19.2	15.36%
	Jul. 16	16.3	13.04%
	Jul. 17	16.3	13.04%
	Jul. 17	**Add**	**196g**
	Jul. 18	17.7	14.16%
	Jul. 19	17.1	13.68%
	Jul. 22	16.6	13.28%
	Jul. 22	**Add**	**172g**
	Jul. 24	16.6	13.28%
	Jul. 26	15.8	12.64%
	Jul. 26	**Add**	**236g**
	Jul. 31	16.1	12.88%
	Jul. 31	**Add**	**212g**
	Aug. 09	16.9	13.52%
	Aug. 13	15.6	12.48%

Table A-11. Titration records before the second compression test

	Date	Quantity of used NaOH solution(mL)	Concentration
28 Days + 3 Months	Aug. 15	15.3	12.24%
	Aug. 15	**Add**	**276g**
	Aug. 28	15.5	12.40%
	Aug. 28	**Add**	**260g**
	Sept. 09	16.8	13.44%
	Sept. 16	15.8	12.64%
	Sept. 23	15.1	12.08%
	Sept. 23	**Add**	**292g**
	Sept. 30	17.6	14.08%
	Oct. 07	16.8	13.44%
	Oct. 14	16.1	12.88%
	Oct. 14	**Add**	**212g**

Table A-12. Titration records before the last compression test

	Date	Quantity of used NaOH solution(mL)	Concentration
28 Days + 5 Months	Oct. 21	17.8	14.24%
	Oct. 28	17.2	13.76%
	Nov. 04	16.7	13.36%
	Nov. 11	16.2	12.96%
	Nov. 11	**Add**	**204g**
	Nov. 18	18.1	14.48%
	Nov. 25	17.4	13.92%
	Dec. 02	16.9	13.52%
	Dec. 09	16.7	13.36%
	Dec. 14	16.3	13.04%
	Dec. 14	**Add**	**196g**

A.3 TESTS RECORDS OF COMPRESSIVE STRENGTH TEST AND YOUNG'S MODULUS & POISSON'S RATIO MEASUREMENT

Table A-13. Compressive strength records and calculations of the N group

	F(lbs)	Area(mm²)	Strength(MPa)
N1	57220	8107.32	31.37
N2	68440	8107.32	37.53
N3	63580	8107.32	34.86
		Average	34.59

Table A-14. Young's modulus records and calculations of the N group

	0.005	0.005 Force	End	End Force	Stress	Strain	E
N1	-	-	-	-	-	-	-
N2	0.0125	2680	0.1390	22000	10.59	0.000622539	17015.81
N3	0.0050	1080	0.1620	25000	13.12	0.000772638	16974.52
						Average	16995.16

Table A-15. Poisson's ratio records and calculations of the N group

	Force	Long. DSPL	Tran. DSPL	Poisson's's ratio	Average
N1					0.15394
N2	2680	0.0125	0.0030	0.2400	
	4980	0.0254	0.0050	0.1969	
	6980	0.0381	0.0070	0.1837	
	8910	0.0508	0.0090	0.1772	
	13040	0.0762	0.0130	0.1706	
	22000	0.1397	0.0230	0.1646	
N3	1080	0.0050	0.0000	0.0000	
	3440	0.0200	0.0020	0.1000	
	6880	0.0400	0.0060	0.1500	
	10200	0.0600	0.0090	0.1500	
	16600	0.1000	0.0160	0.1600	
	25000	0.1620	0.0250	0.1543	

Table A-16. Compressive strength records and calculations of the GM group

	F(lbs)	Area(mm²)	Strength(MPa)
GM1	72130	8107.32	39.55
GM2	68650	8107.32	37.64
GM3	70130	8107.32	38.45
		Average	38.55

Table A-17. Young's modulus records and calculations of the GM group

	0.005	0.005 Force	End	End Force	Stress	Strain	E
GM1	0.0400	6690	0.1670	25000	10.04	0.000625	16062.78
GM2	0.0200	3770	0.1640	25200	11.75	0.000708661	16580.42
GM3	0.0050	1470	0.1610	25100	12.96	0.000767717	16876.22
						Average	16506.47

Table A-18. Poisson's ratio records and calculations of the GM group

	Force	Long. DSPL	Tran. DSPL	Poisson's ratio	Average
GM1	0	0.0000	0.0000	0.0000	0.16260
	0	0.0000	0.0000	0.0000	
	6690	0.0400	0.0070	0.1750	
	9890	0.0600	0.0100	0.1667	
	16050	0.1000	0.0170	0.1700	
	25000	0.1670	0.0270	0.1617	
GM2	0	0.0000	0.0000	0.0000	
	3770	0.0200	0.0030	0.1500	
	6960	0.0400	0.0070	0.1750	
	10300	0.0600	0.0100	0.1667	
	16590	0.1000	0.0160	0.1600	
	25000	0.1640	0.0270	0.1646	
GM3	1470	0.0050	0.0010	0.2000	
	3780	0.0200	0.0030	0.1500	
	7160	0.0400	0.0040	0.1000	
	10030	0.0600	0.0090	0.1500	
	16780	0.1000	0.0160	0.1600	
	25100	0.1610	0.0260	0.1615	

Table A-19. Compressive strength records and calculations of the GC group

	F(lbs)	Area(mm²)	Strength(MPa)
GC1	78730	8107.32	43.17
GC2	71000	8107.32	38.93
GC3	77230	8107.32	42.34
		Average	41.48

Table A-20. Young's modulus records and calculations of the GC group

	0.005	0.005 Force	End	End Force	Stress	Strain	E
GC1	0.0050	1220	0.1590	25000	13.04	0.000757874	17203.91
GC2	0.0050	1460	0.1510	25010	12.91	0.000718504	17971.07
GC3	0.0050	1400	0.1540	25300	13.10	0.000733268	17870.95
						Average	17681.98

Table A-21. Poisson's ratio records and calculations of the GC group

	Force	Long. DSPL	Tran. DSPL	Poisson's ratio	Average
GC1	1220	0.0050	0.0000	0.0000	0.16825
	3610	0.0200	0.0030	0.1500	
	6980	0.0400	0.0060	0.1500	
	10260	0.0600	0.0100	0.1667	
	16350	0.1000	0.0160	0.1600	
	25000	0.1590	0.0250	0.1572	
GC2	1460	0.0050	0.0010	0.2000	
	4130	0.0200	0.0040	0.2000	
	7760	0.0400	0.0070	0.1750	
	11570	0.0600	0.0110	0.1833	
	17520	0.1000	0.0180	0.1800	
	25010	0.1510	0.0260	0.1722	
GC3	1400	0.0050	0.0010	0.2000	
	4130	0.0200	0.0040	0.2000	
	7390	0.0400	0.0070	0.1750	
	10740	0.0600	0.0110	0.1833	
	17230	0.1000	0.0180	0.1800	
	25300	0.1540	0.0270	0.1753	

Table A-22. Compressive strength records and calculations of the GOM group

	F(lbs)	Area(mm²)	Strength(MPa)
GOM1	69200	8107.32	37.94
GOM2	75480	8107.32	41.39
GOM3	69450	8107.32	38.08
		Average	39.14

Table A-23. Young's modulus records and calculations of the GOM group

	0.005	0.005 Force	End	End Force	Stress	Strain	E
GOM1	0.0050	940	0.1660	25300	13.36	0.000792323	16857.27
GOM2	0.0050	1100	0.1620	25000	13.10	0.000772638	16960.33
GOM3	0.0050	1090	0.1610	25050	13.14	0.000767717	17111.90
						Average	16976.50

Table A-24. Poisson's ratio records and calculations of the GOM group

	Force	Long. DSPL	Tran. DSPL	Poisson's ratio	Average
GOM1	940	0.0050	0.0000	0.0000	0.15553
	3460	0.0200	0.0025	0.1250	
	6690	0.0400	0.0050	0.1250	
	10120	0.0600	0.0075	0.1250	
	16070	0.1000	0.0125	0.1250	
	25300	0.1660	0.0240	0.1446	
GOM2	1100	0.0050	0.0010	0.2000	
	3470	0.0200	0.0030	0.1500	
	6820	0.0400	0.0070	0.1750	
	10310	0.0600	0.0100	0.1667	
	16380	0.1000	0.0160	0.1600	
	25000	0.1620	0.0250	0.1543	
GOM3	1090	0.0050	0.0010	0.2000	
	3810	0.0200	0.0040	0.2000	
	7000	0.0400	0.0070	0.1750	
	10530	0.0600	0.0100	0.1667	
	16420	0.1000	0.0160	0.1600	
	25050	0.1610	0.0270	0.1677	

Table A-25. Compressive strength records and calculations of the GOC group

	F(lbs)	Area(mm²)	Strength(MPa)
GOC1	67570	8107.32	37.05
GOC2	70040	8107.32	38.40
GOC3	70880	8107.32	38.86
		Average	38.10

Table A-26. Young's modulus records and calculations of the GOC group

	0.005	0.005 Force	End	End Force	Stress	Strain	E
GOC1	0.0050	1060	0.1590	25020	13.14	0.000757874	17334.13
GOC2	0.0050	970	0.1600	25190	13.28	0.000762795	17409.18
GOC3	0.0050	1330	0.1580	25280	13.13	0.000752953	17440.14
						Average	17394.49

Table A-27. Poisson's ratio records and calculations of the GOC group

	Force	Long. DSPL	Tran. DSPL	Poisson's ratio	Average
GOC1	1060	0.0050	0.0010	0.2000	0.17611
	3690	0.0200	0.0040	0.2000	
	6990	0.0400	0.0080	0.2000	
	10390	0.0600	0.0120	0.2000	
	16630	0.1000	0.0180	0.1800	
	25020	0.1590	0.0280	0.1761	
GOC2	1190	0.0050	0.0010	0.2000	
	2210	0.0200	0.0300	1.5000	
	3210	0.0400	0.0070	0.1750	
	7610	0.0600	0.0110	0.1833	
	11090	0.1000	0.0180	0.1800	
	14430	0.1600	0.0280	0.1750	
GOC3	1310	0.0050	0.0001	0.0200	
	2280	0.0200	0.0040	0.2000	
	3180	0.0400	0.0070	0.1750	
	4120	0.0600	0.0110	0.1833	
	7810	0.1000	0.0180	0.1800	
	11270	0.1580	0.0280	0.1772	

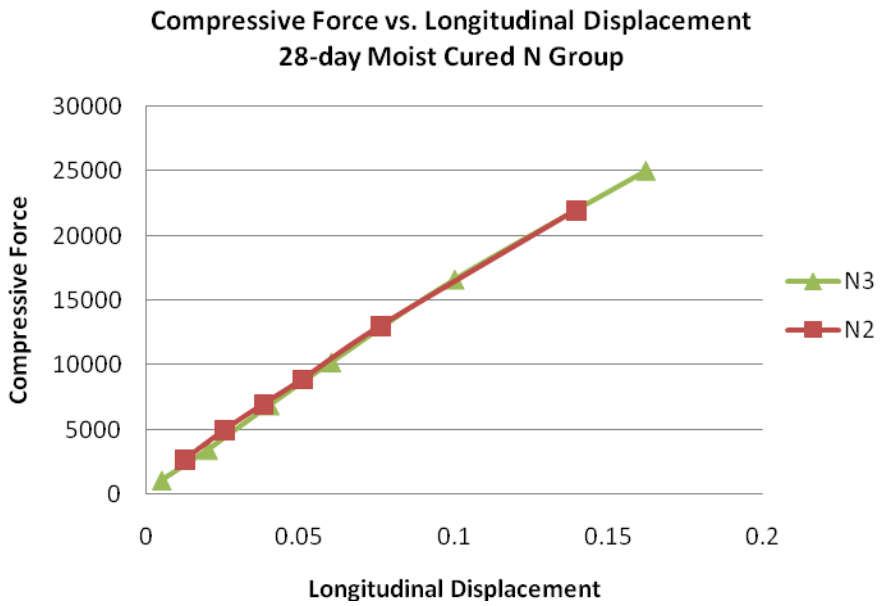

Figure A-1. Compressive force vs. longitudinal displacement of the N group

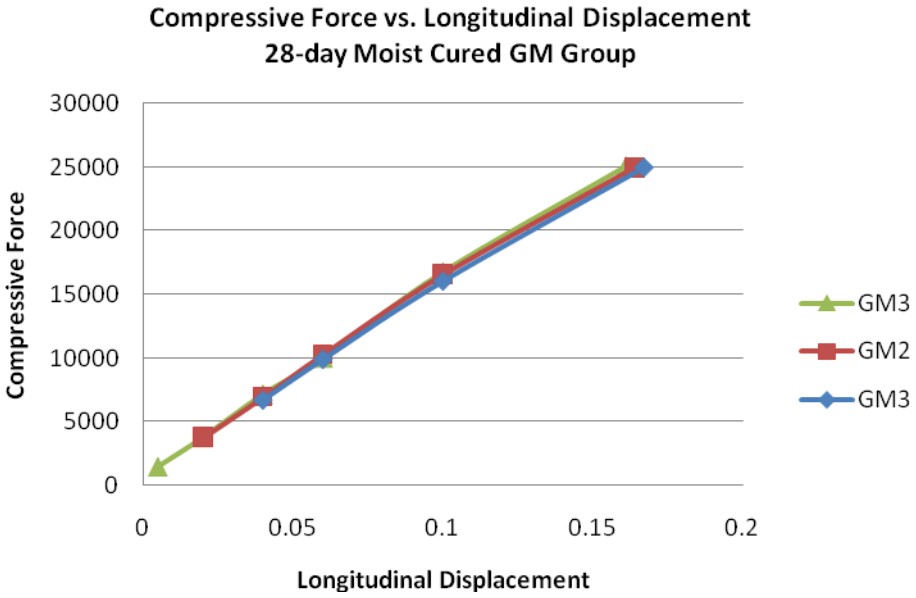

Figure A-2. Compressive force vs. longitudinal displacement of the GM group

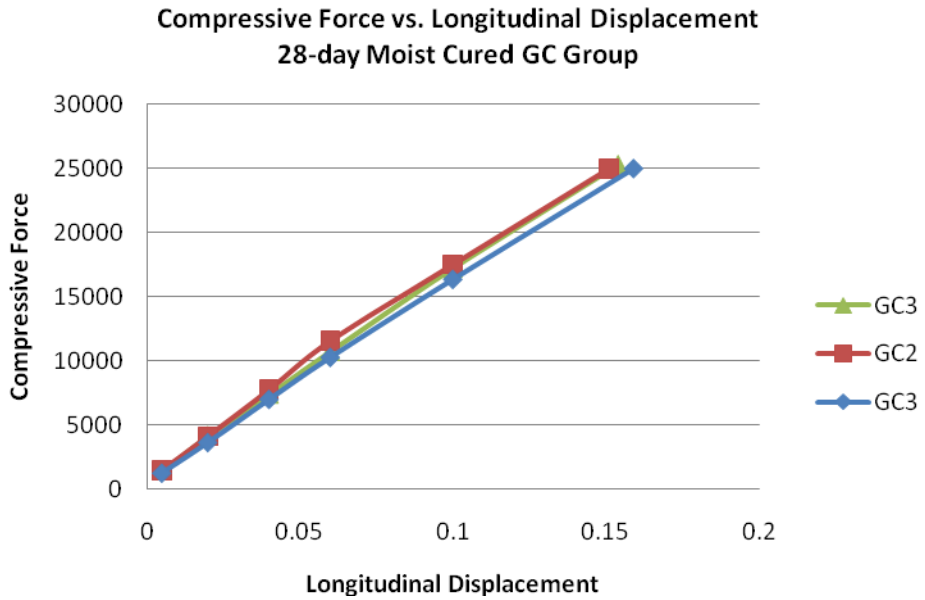

Figure A-3. Compressive force vs. longitudinal displacement of the GC group

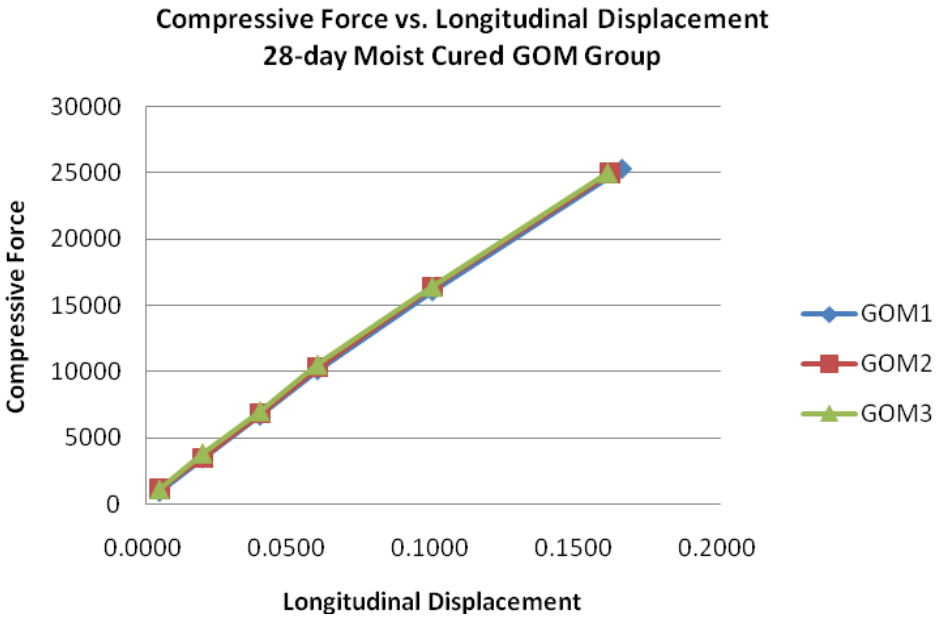

Figure A-4. Compressive force vs. longitudinal displacement of the GOM group

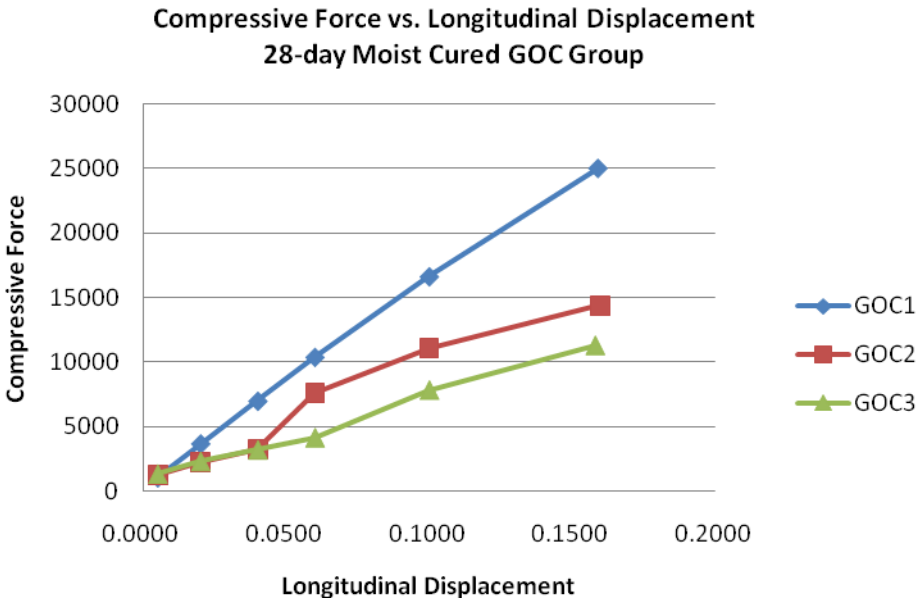

Figure A-5. Compressive force vs. longitudinal displacement of the GOC group

A.4 TEST RESULTS AND CALCULATIONS OF FREEZING & THAWING TEST

Table A-28. The weight records of the N group

Weight	Weight Records (g)			Relative Weight (g)		
Date	N1	N2	N3	N1	N2	N3
Jul.17	3837.3	3801.5	3804.4	0	0	0
Aug. 07	3830	3797.7	3799.1	-7.3	-3.8	-5.3
Aug. 23	3824.5	3794.3	3795	-12.8	-7.2	-9.4
Sept. 9	3822.5	3791.1	3793.2	-14.8	-10.4	-11.2
Sept. 19	3818.8	3786.2	3787.5	-18.5	-15.3	-16.9
Sept. 30	3814.7	3785.2	3784.4	-22.6	-16.3	-20
Oct. 10	3812.1	3783.8	3780.5	-25.2	-17.7	-23.9
Oct. 21	3809.6	3782.1	3778.2	-27.7	-19.4	-26.2
Nov. 04	3808.3	3775	3772	-29	-26.5	-32.4
Nov. 18	3805.6	3773.5	3769.6	-31.7	-28	-34.8
Dec. 02	3804.3	3768.2	3765.6	-33	-33.3	-38.8
Jan. 20	3802.9	3764.9	3763.8	-34.4	-36.6	-40.6
Jan. 27	3803.5	3764.5	3764.6	-33.8	-37	-39.8

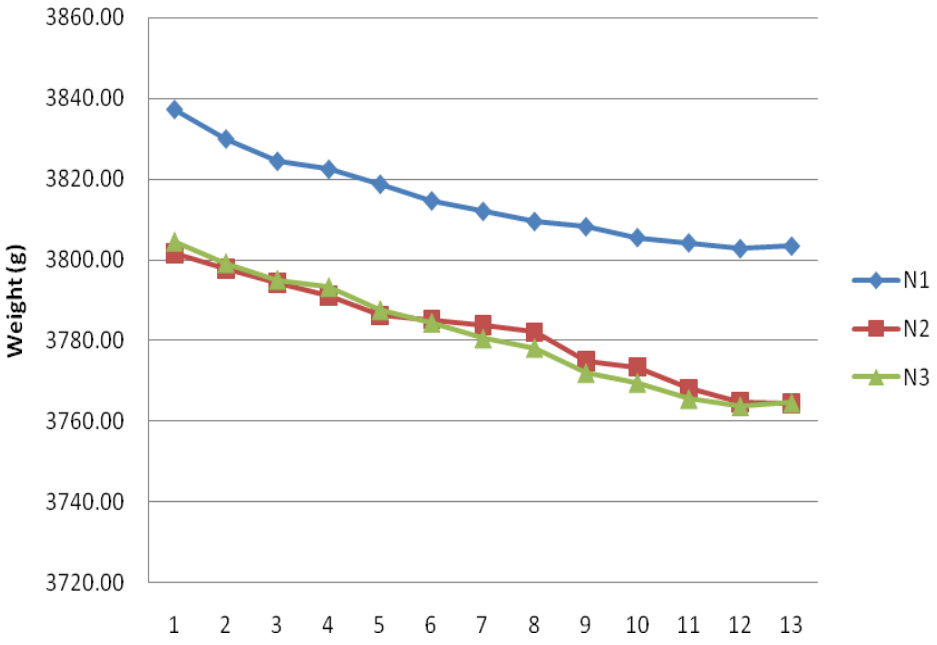

Figure A-6. The weight records of the N group

Table A-29. The weight records of the GM group

Weight	Weight Records (g)			Relative Weight (g)		
Date	GM1	GM2	GM3	GM1	GM2	GM3
Jul.17	3865.7	3841	3840.4	0	0	0
Aug. 07	3858.2	3830.4	3831.9	-7.5	-10.6	-8.5
Aug. 23	3852.5	3822.9	3824.7	-13.2	-18.1	-15.7
Sept. 9	3849.8	3817.8	3819.8	-15.9	-23.2	-20.6
Sept. 19	3843.5	3812.6	3814.8	-22.2	-28.4	-25.6
Sept. 30	3839.2	3809.5	3809.8	-26.5	-31.5	-30.6
Oct. 10	3836.3	3807.1	3807.2	-29.4	-33.9	-33.2
Oct. 21	3835.1	3805.2	3804.6	-30.6	-35.8	-35.8
Nov. 04	3829.9	3801.7	3801.8	-35.8	-39.3	-38.6
Nov. 18	3826.5	3800.9	3799.7	-39.2	-40.1	-40.7
Dec. 02	3825	3794.8	3796.6	-40.7	-46.2	-43.8
Jan. 20	3821.2	3793.3	3793.2	-44.5	-47.7	-47.2
Jan. 27	3820.3	3792.3	3794.6	-45.4	-48.7	-45.8

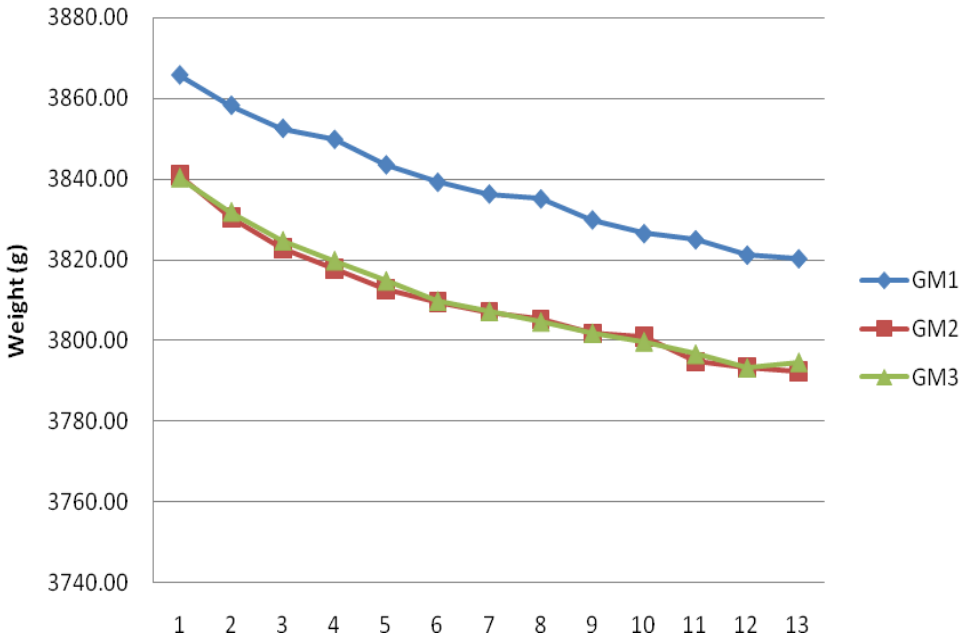

Figure A-7. The weight records of the GM group

Table A-30. The weight records of the GC group

Weight	Weight Records (g)			Relative Weight (g)		
Date	GC1	GC2	GC3	GC1	GC2	GC3
Jul.17	3849.4	3884.7	3837.4	0	0	0
Aug. 07	3850.1	3889.6	3841.4	0.7	4.9	4
Aug. 23	3854.4	3893.7	3846.2	5	9	8.8
Sept. 9	3858.6	3895.1	3849.8	9.2	10.4	12.4
Sept. 19	3858.6	3896.3	3850.2	9.2	11.6	12.8
Sept. 30	3860.6	3896.7	3851.6	11.2	12	14.2
Oct. 10	3858.5	3895.7	3851.5	9.1	11	14.1
Oct. 21	3857.2	3892.3	3852.4	7.8	7.6	15
Nov. 04	3850.4	3892.1	3851.1	1	7.4	13.7
Nov. 18	3839.5	3892	3848.2	-9.9	7.3	10.8
Dec. 02	3835.9	3890.7	3847	-13.5	6	9.6
Jan. 20	3831.9	3890.4	3847.7	-17.5	5.7	10.3
Jan. 27	3826.6	3888.3	3848.1	-22.8	3.6	10.7

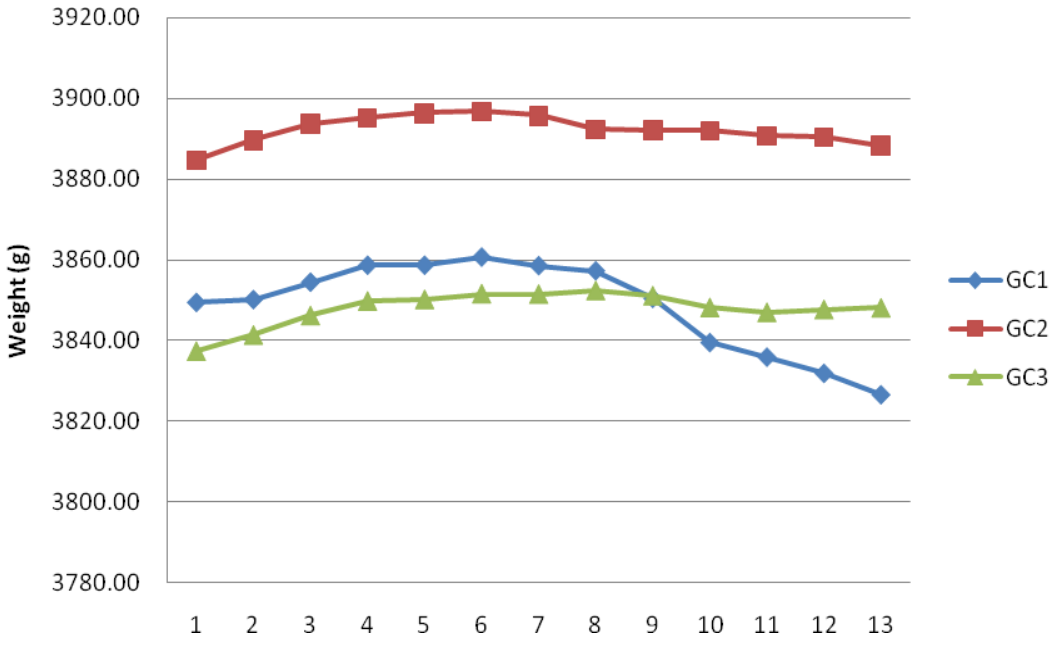

Figure A-8. The weight records of the GC group

Table A-31. The weight records of the GOM group

Weight	Weight Records (g)			Relative Weight (g)		
Date	GOM1	GOM2	GOM3	GOM1	GOM2	GOM3
Jul.17	3842.6	3868	3839.9	0	0	0
Aug. 07	3838.9	3863.4	3834.2	-3.7	-4.6	-5.7
Aug. 23	3834.8	3861.9	3829.8	-7.8	-6.1	-10.1
Sept. 9	3832.3	3861.6	3826.8	-10.3	-6.4	-13.1
Sept. 19	3828.1	3860.1	3822.1	-14.5	-7.9	-17.8
Sept. 30	3824.2	3855.6	3820.6	-18.4	-12.4	-19.3
Oct. 10	3821.8	3855.2	3817.3	-20.8	-12.8	-22.6
Oct. 21	3817.8	3855.1	3813.7	-24.8	-12.9	-26.2
Nov. 04	3812.7	3853.3	3807.9	-29.9	-14.7	-32
Nov. 18	3809	3852.5	3803.8	-33.6	-15.5	-36.1
Dec. 02	3808.9	3845.7	3798.2	-33.7	-22.3	-41.7
Jan. 20	3808.1	3842.7	3794.1	-34.5	-25.3	-45.8
Jan. 27	3807.3	3841.9	3794	-35.3	-26.1	-45.9

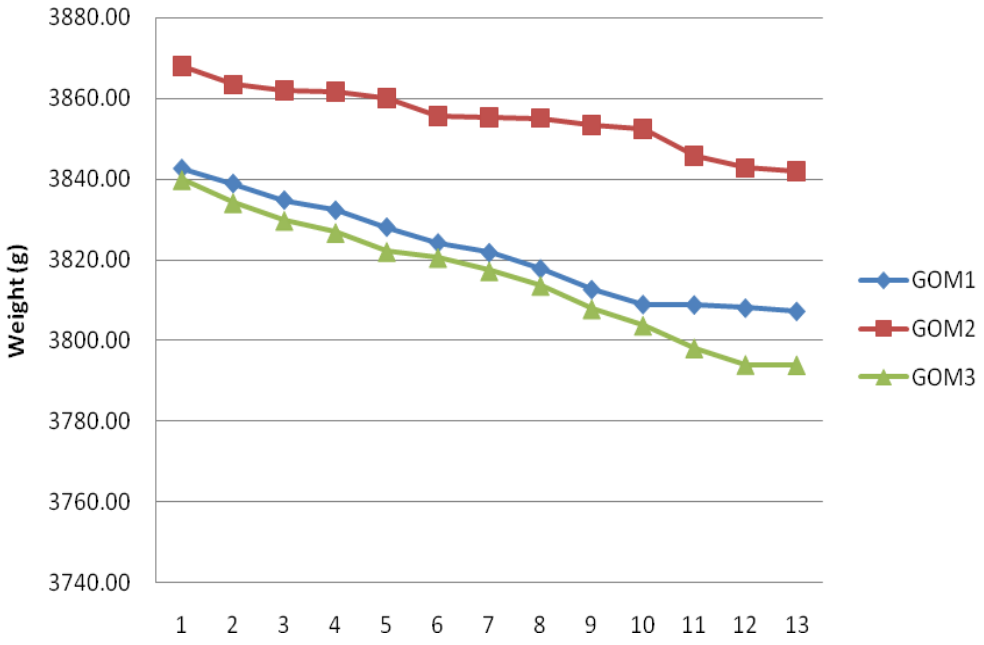

Figure A-9. The weight records of the GOM group

Table A-32. The weight records of the GOC group

Weight	Weight Records (g)			Relative Weight (g)		
Date	GOC1	GOC2	GOC3	GOC1	GOC2	GOC3
Jul.17	3857.7	3874.8	3870.6	0	0	0
Aug. 07	3860	3876.5	3871.5	2.3	1.7	0.9
Aug. 23	3862.5	3876	3873.3	4.8	1.2	2.7
Sept. 9	3864.5	3876.1	3873.6	6.8	1.3	3
Sept. 19	3864.1	3871.1	3870.9	6.4	-3.7	0.3
Sept. 30	3859.7	3866.3	3866.8	2	-8.5	-3.8
Oct. 10	3851	3860.1	3862.6	-6.7	-14.7	-8
Oct. 21	3845.6	3855.7	3862.5	-12.1	-19.1	-8.1
Nov. 04	3836.9	3849.5	3858.9	-20.8	-25.3	-11.7
Nov. 18	3834.2	3845.1	3853.6	-23.5	-29.7	-17
Dec. 02	3828	3840.9	3853	-29.7	-33.9	-17.6
Jan. 20	3826.9	3838.2	3852.9	-30.8	-36.6	-17.7
Jan. 27	3827.4	3836.5	3853.3	-30.3	-38.3	-17.3

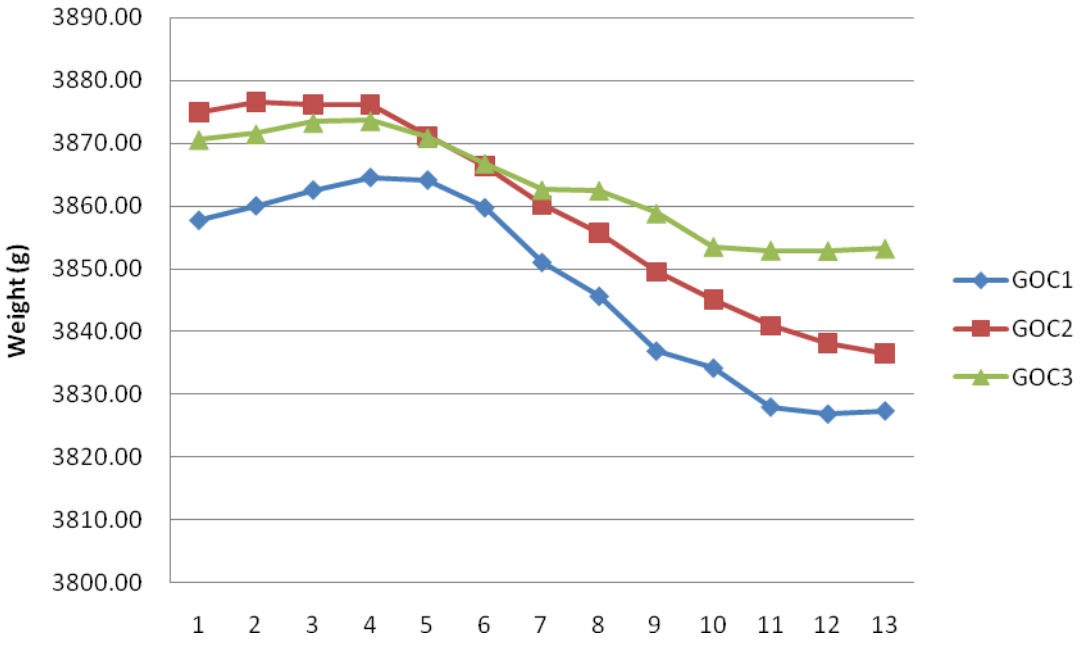

Figure A-10. The weight records of the GOC group

Table A-33. The length records of the N group

Length	Length Records (mm)			Relative Length (mm)		
Date	N1	N2	N3	N1	N2	N3
Jul.17	360.03	361.77	360.04	0.00	0.00	0.00
Aug. 07	359.97	361.62	359.96	-0.06	-0.15	-0.08
Aug. 23	359.87	361.56	359.87	-0.16	-0.21	-0.17
Sept. 9	359.94	361.61	359.99	-0.09	-0.16	-0.05
Sept. 19	359.89	361.60	359.88	-0.14	-0.17	-0.16
Sept. 30	359.84	361.58	359.90	-0.19	-0.19	-0.14
Oct. 10	359.86	361.60	359.87	-0.17	-0.17	-0.17
Oct. 21	359.82	361.55	359.86	-0.21	-0.22	-0.18
Nov. 04	359.87	361.54	359.85	-0.16	-0.23	-0.19
Nov. 18	359.82	361.54	359.88	-0.21	-0.23	-0.16
Dec. 02	359.82	361.54	359.88	-0.21	-0.23	-0.16
Jan. 20	359.87	361.55	359.88	-0.16	-0.22	-0.16
Jan. 27	359.88	361.55	359.87	-0.15	-0.22	-0.17

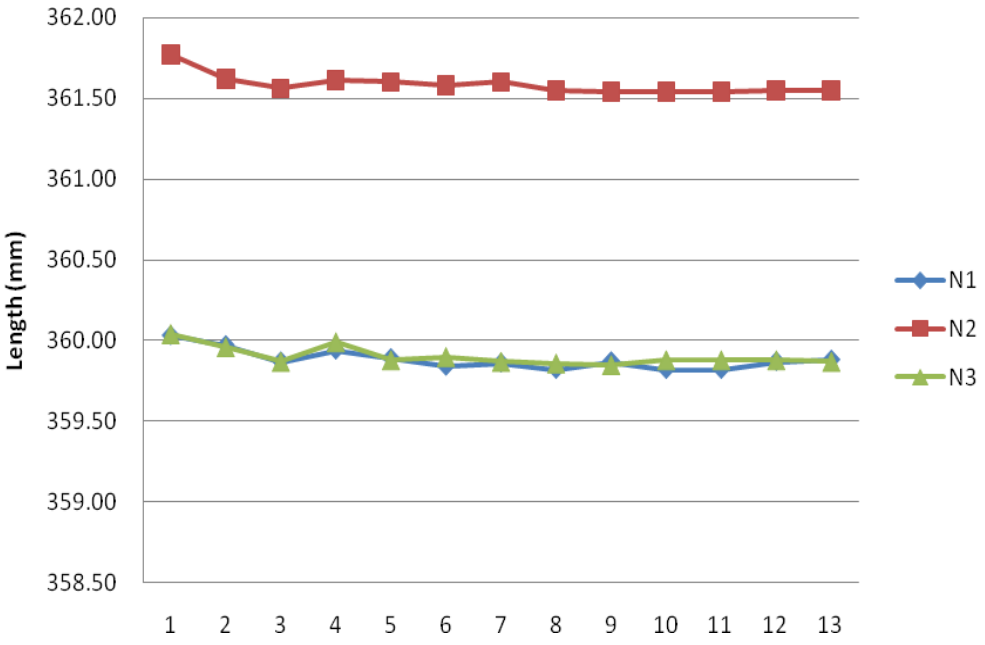

Figure A-11. The length records of the N group

Table A-34. The length records of the GM group

Length	Length Records (mm)			Relative Length (mm)		
Date	GM1	GM2	GM3	GM1	GM2	GM3
Jul.17	361.17	359.23	358.84	0.00	0.00	0.00
Aug. 07	361.04	359.14	358.72	-0.13	-0.09	-0.12
Aug. 23	361.03	359.13	358.69	-0.14	-0.10	-0.15
Sept. 9	361.06	359.15	358.77	-0.11	-0.08	-0.07
Sept. 19	360.98	359.11	358.69	-0.19	-0.12	-0.15
Sept. 30	360.99	359.06	358.64	-0.18	-0.17	-0.20
Oct. 10	360.97	359.05	358.63	-0.20	-0.18	-0.21
Oct. 21	360.98	359.02	358.66	-0.19	-0.21	-0.18
Nov. 04	360.90	359.03	358.63	-0.27	-0.20	-0.21
Nov. 18	360.92	359.04	358.63	-0.25	-0.19	-0.21
Dec. 02	360.92	359.04	358.63	-0.25	-0.19	-0.21
Jan. 20	360.98	359.01	358.69	-0.19	-0.22	-0.15
Jan. 27	360.93	359.03	358.61	-0.24	-0.20	-0.23

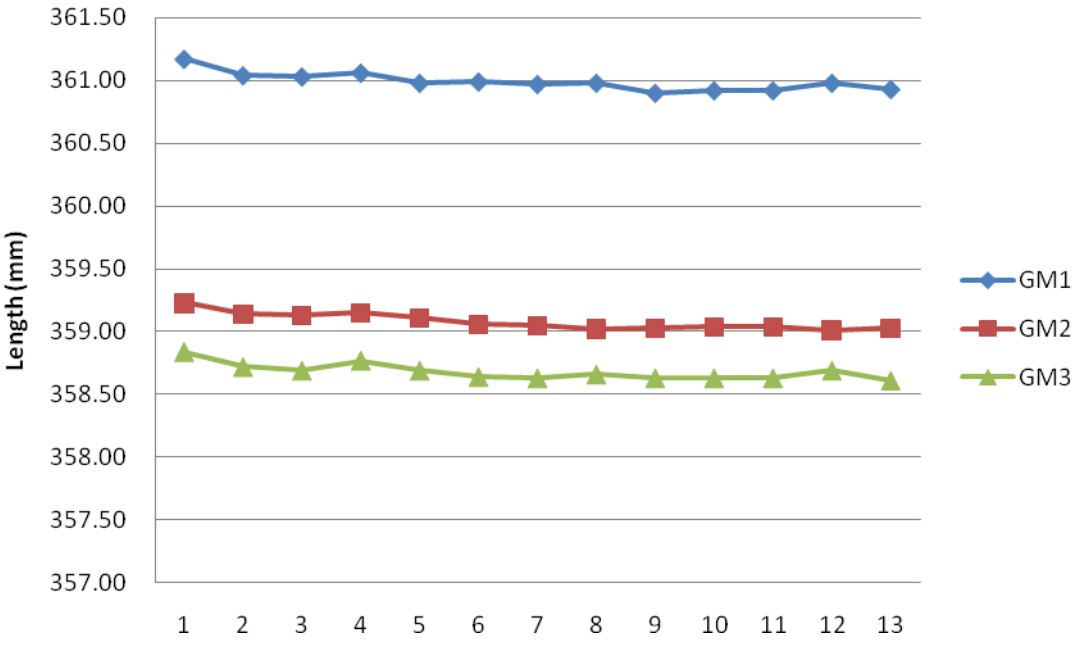

Figure A-12. The length records of the GM group

Table A-35. The length records of the GC group

Length	Length Records (mm)			Relative Length (mm)		
Date	GC1	GC2	GC3	GC1	GC2	GC3
Jul.17	359.58	357.96	358.58	0.00	0.00	0.00
Aug. 07	359.66	358.08	358.68	0.08	0.12	0.10
Aug. 23	359.81	358.33	358.83	0.23	0.37	0.25
Sept. 9	360.02	358.42	358.98	0.44	0.46	0.40
Sept. 19	360.03	358.47	359.01	0.45	0.51	0.43
Sept. 30	360.01	358.46	359.06	0.43	0.50	0.48
Oct. 10	360.02	358.51	359.02	0.44	0.55	0.44
Oct. 21	359.98	358.51	359.02	0.40	0.55	0.44
Nov. 04	359.99	358.51	359.06	0.41	0.55	0.48
Nov. 18	360.02	358.49	359.08	0.44	0.53	0.50
Dec. 02	360.02	358.49	359.08	0.44	0.53	0.50
Jan. 20	360.03	358.58	359.19	0.45	0.62	0.61
Jan. 27	360.03	358.55	359.19	0.45	0.59	0.61

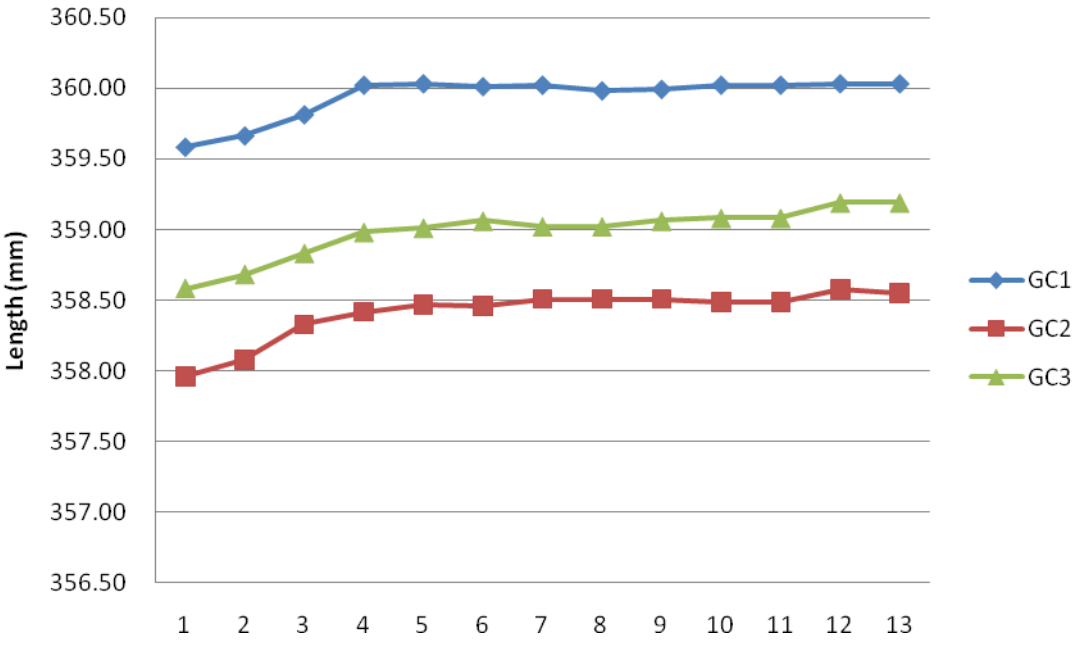

Figure A-13. The length records of the GC group

Table A-36. The length records of the GOM group

Length	Length Records (mm)			Relative Length (mm)		
Date	GOM1	GOM2	GOM3	GOM1	GOM2	GOM3
Jul.17	360.89	360.97	360.95	0.00	0.00	0.00
Aug. 07	360.82	360.91	360.85	-0.07	-0.06	-0.10
Aug. 23	360.77	360.94	361.03	-0.12	-0.03	0.08
Sept. 9	360.84	360.99	360.90	-0.05	0.02	-0.05
Sept. 19	360.82	360.93	360.86	-0.07	-0.04	-0.09
Sept. 30	360.80	360.95	360.85	-0.09	-0.02	-0.10
Oct. 10	360.79	360.96	360.83	-0.10	-0.01	-0.12
Oct. 21	360.73	360.92	360.76	-0.16	-0.05	-0.19
Nov. 04	360.71	360.92	360.75	-0.18	-0.05	-0.20
Nov. 18	360.74	360.92	360.75	-0.15	-0.05	-0.20
Dec. 02	360.78	360.92	360.75	-0.11	-0.05	-0.20
Jan. 20	360.81	360.95	360.77	-0.08	-0.02	-0.18
Jan. 27	360.82	360.97	360.78	-0.07	0.00	-0.17

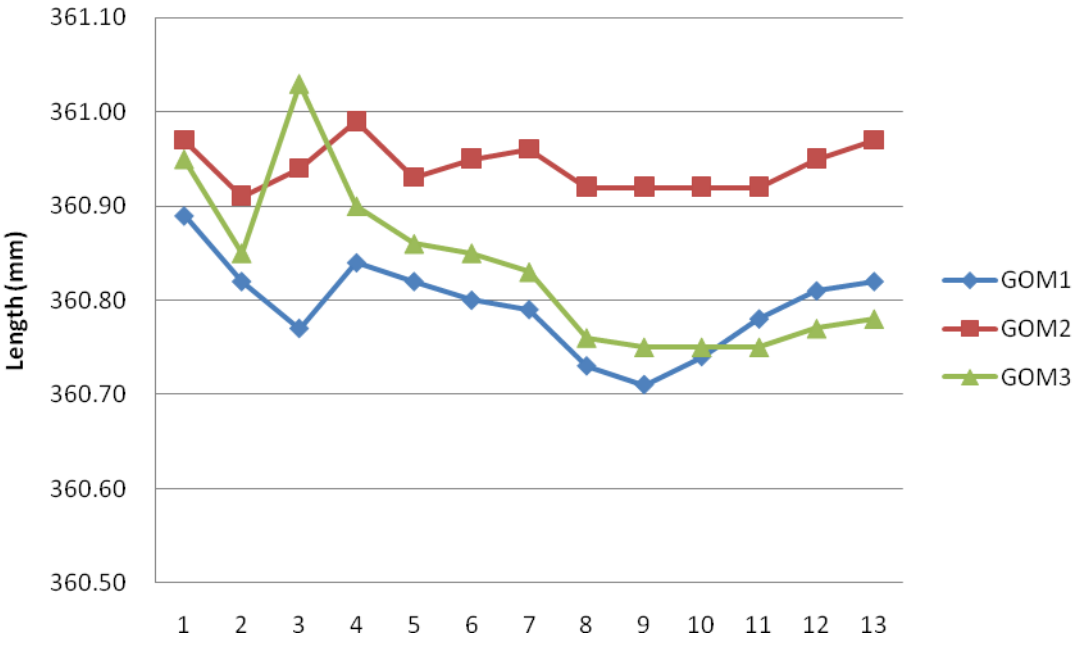

Figure A-14. The length records of the GOM group

Table A-37. The length records of the GOC group

Length	Length Records (mm)			Relative Length (mm)		
Date	GOC1	GOC2	GOC3	GOC1	GOC2	GOC3
Jul.17	358.97	359.73	362.42	0.00	0.00	0.00
Aug. 07	358.90	359.64	362.34	-0.07	-0.09	-0.08
Aug. 23	359.02	359.66	362.43	0.05	-0.07	0.01
Sept. 9	359.12	359.76	362.51	0.15	0.03	0.09
Sept. 19	359.12	359.73	362.49	0.15	0.00	0.07
Sept. 30	359.18	359.76	362.54	0.21	0.03	0.12
Oct. 10	359.05	359.70	362.50	0.08	-0.03	0.08
Oct. 21	359.07	359.63	362.50	0.10	-0.10	0.08
Nov. 04	359.05	359.67	362.46	0.08	-0.06	0.04
Nov. 18	359.02	359.65	362.44	0.05	-0.08	0.02
Dec. 02	359.02	359.65	362.44	0.05	-0.08	0.02
Jan. 20	359.06	359.69	362.50	0.09	-0.04	0.08
Jan. 27	359.06	359.66	362.53	0.09	-0.07	0.11

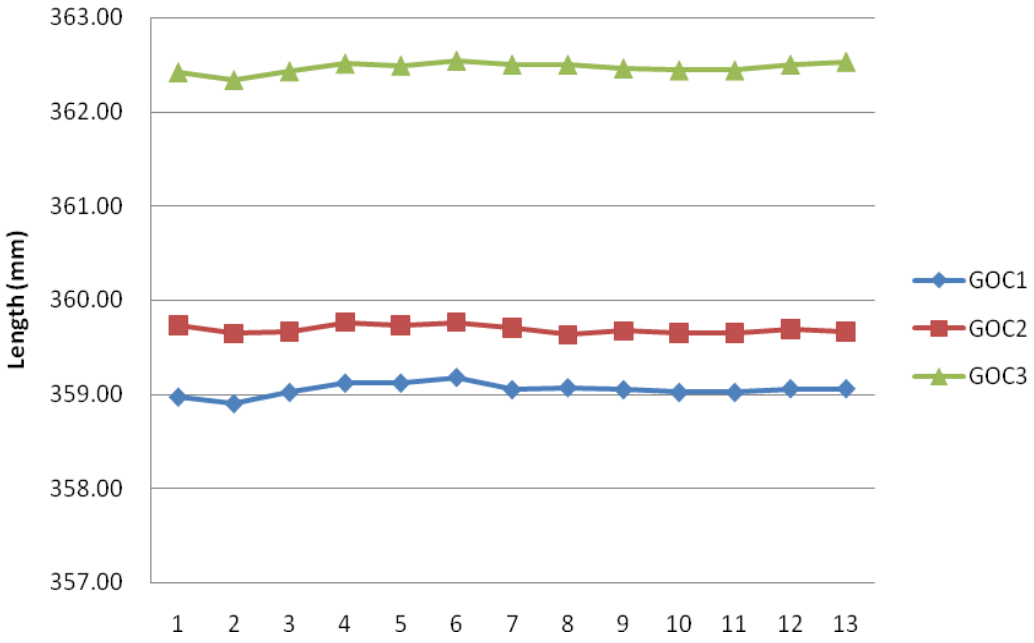

Figure A-15. The length records of the GOC group

Table A-38. The average weight change percentage of each groups

Weight	N	GM	GC	GOM	GOC
Jul. 17	0	0	0	0	0
Aug. 07	-0.143%	-0.230%	0.083%	-0.121%	0.042%
Aug. 23	-0.257%	-0.407%	0.197%	-0.208%	0.075%
Sept. 9	-0.318%	-0.517%	0.277%	-0.258%	0.096%
Sept. 19	-0.443%	-0.660%	0.290%	-0.348%	0.026%
Sept. 30	-0.514%	-0.767%	0.323%	-0.434%	-0.089%
Oct. 10	-0.584%	-0.836%	0.296%	-0.487%	-0.253%
Oct. 21	-0.640%	-0.885%	0.263%	-0.554%	-0.339%
Nov. 04	-0.768%	-0.985%	0.191%	-0.664%	-0.498%
Nov. 18	-0.826%	-1.039%	0.071%	-0.738%	-0.605%
Dec. 02	-0.919%	-1.132%	0.018%	-0.847%	-0.700%
Jan. 20	-0.975%	-1.207%	-0.013%	-0.915%	-0.733%
Jan. 27	-0.967%	-1.212%	-0.074%	-0.930%	-0.740%

Table A-39. The average length change percentage of each groups

Length	N	GM	GC	GOM	GOC
Jul. 17	0	0	0	0	0
Aug. 07	-0.027%	-0.031%	0.028%	-0.021%	-0.022%
Aug. 23	-0.050%	-0.036%	0.079%	-0.006%	-0.001%
Sept. 9	-0.028%	-0.024%	0.121%	-0.007%	0.025%
Sept. 19	-0.043%	-0.043%	0.129%	-0.018%	0.020%
Sept. 30	-0.048%	-0.051%	0.131%	-0.019%	0.033%
Oct. 10	-0.047%	-0.055%	0.133%	-0.021%	0.012%
Oct. 21	-0.056%	-0.054%	0.129%	-0.037%	0.007%
Nov. 04	-0.054%	-0.063%	0.134%	-0.040%	0.006%
Nov. 18	-0.055%	-0.060%	0.137%	-0.037%	-0.001%
Dec. 02	-0.055%	-0.060%	0.137%	-0.033%	-0.001%
Jan. 20	-0.050%	-0.052%	0.156%	-0.026%	0.012%
Jan. 27	-0.050%	-0.062%	0.153%	-0.022%	0.012%

A.5 TEST RESULTS AND CALCULATIONS OF CORROSION TEST

Table A-40. The corrosion test records of the N group

N				
		Force	Area (in²)	Stress (psi)
28 days	N1	24810	4	6202.50
	N2	25230	4	6307.50
	N3	25120	4	6280.00
	Average			6263.33
Corrosion 1 month	N1	23560	4	5890.00
	N2	26960	4	6740.00
	N3	28040	4	7010.00
	Average			6546.67
Corrosion 3 month	N1	20690	4	5172.50
	N2	24960	4	6240.00
	N3	21900	4	5475.00
	Average			5629.17
Corrosion 5 month	N1	19630	4	4907.50
	N2	21240	4	5310.00
	N3	17750	4	4437.50
	Average			4885.00

Table A-41. The corrosion test records of the GM group

GM					
28 days		Force	Area(in²)	Stress	
	GM1	23480	4	5870.00	psi
	GM2	24170	4	6042.50	psi
	GM3	25820	4	6455.00	psi
	Average			6122.50	-2.25%
Corrosion for 1 month	GM1	24210	4	6052.50	psi
	GM2	25900	4	6475.00	psi
	GM3	25680	4	6420.00	psi
	Average			6315.83	-3.53%
Corrosion for 3 months	GM1	21510	4	5377.50	psi
	GM2	21610	4	5402.50	psi
	GM3	20190	4	5047.50	psi
	Average			5275.83	-6.28%
Corrosion for 5 months	GM1	17320	4	4330.00	psi
	GM2	17960	4	4490.00	psi
	GM3	17650	4	4412.50	psi
	Average			4410.83	-9.71%

Table A-42. The corrosion test records of the N group

GC					
28 days		Force	Area(in²)	Stress	
	GC1	27480	4	6870.00	psi
	GC2	24720	4	6180.00	psi
	GC3	27140	4	6785.00	psi
	Average			6827.50	9.01%
Corrosion for 1 month	GC1	28010	4	7002.50	psi
	GC2	24920	4	6230.00	psi
	GC3	27200	4	6800.00	psi
	Average			6677.50	2.00%
Corrosion for 3 months	GC1	23850	4	5962.50	psi
	GC2	21920	4	5480.00	psi
	GC3	20690	4	5172.50	psi
	Average			5538.33	-1.61%
Corrosion for 5 months	GC1	22510	4	5627.50	psi
	GC2	20680	4	5170.00	psi
	GC3	21960	4	5490.00	psi
	Average			5429.17	11.14%

Table A-43. The corrosion test records of the N group

GOM					
		Force	Area(in²)	Stress	
28 days	GOM1	27770	4	6942.50	psi
	GOM2	25840	4	6460.00	psi
	GOM3	25500	4	6375.00	psi
	average			6592.50	5.26%
Corrosion for 1 month	GOM1	24740	4	6185.00	psi
	GOM2	21800	4	5450.00	psi
	GOM3	24590	4	6147.50	psi
	Average			6166.25	-5.81%
Corrosion for 3 months	GOM1	23900	4	5975.00	psi
	GOM2	24130	4	6032.50	psi
	GOM3	23710	4	5927.50	psi
	Average			5951.25	5.72%
Corrosion for 5 months	GOM1	20490	4	5122.50	psi
	GOM2	17860	4	4465.00	psi
	GOM3	19110	4	4777.50	psi
	Average			4950.00	1.33%

Table A-44. The corrosion test records of the N group

GOC					
		Force	Area(in²)	Stress	
28 days	GOC1	25940	4	6485.00	psi
	GOC2	23700	4	5925.00	psi
	GOC3	25170	4	6292.50	psi
	Average			6234.17	-0.47%
Corrosion for 1 month	GOC1	22920	4	5730.00	psi
	GOC2	27260	4	6815.00	psi
	GOC3	26660	4	6665.00	psi
	Average			6403.33	-2.19%
Corrosion for 3 months	GOC1	20430	4	5107.50	psi
	GOC2	22540	4	5635.00	psi
	GOC3	23690	4	5922.50	psi
	Average			5555.00	-1.32%
Corrosion for 5 months	GOC1	17290	4	4322.50	psi
	GOC2	19120	4	4780.00	psi
	GOC3	20270	4	5067.50	psi
	Average			4723.33	-3.31%

APPENDIX B

B.1 DETAILS OF GRAPHENE NANOPLATELETS

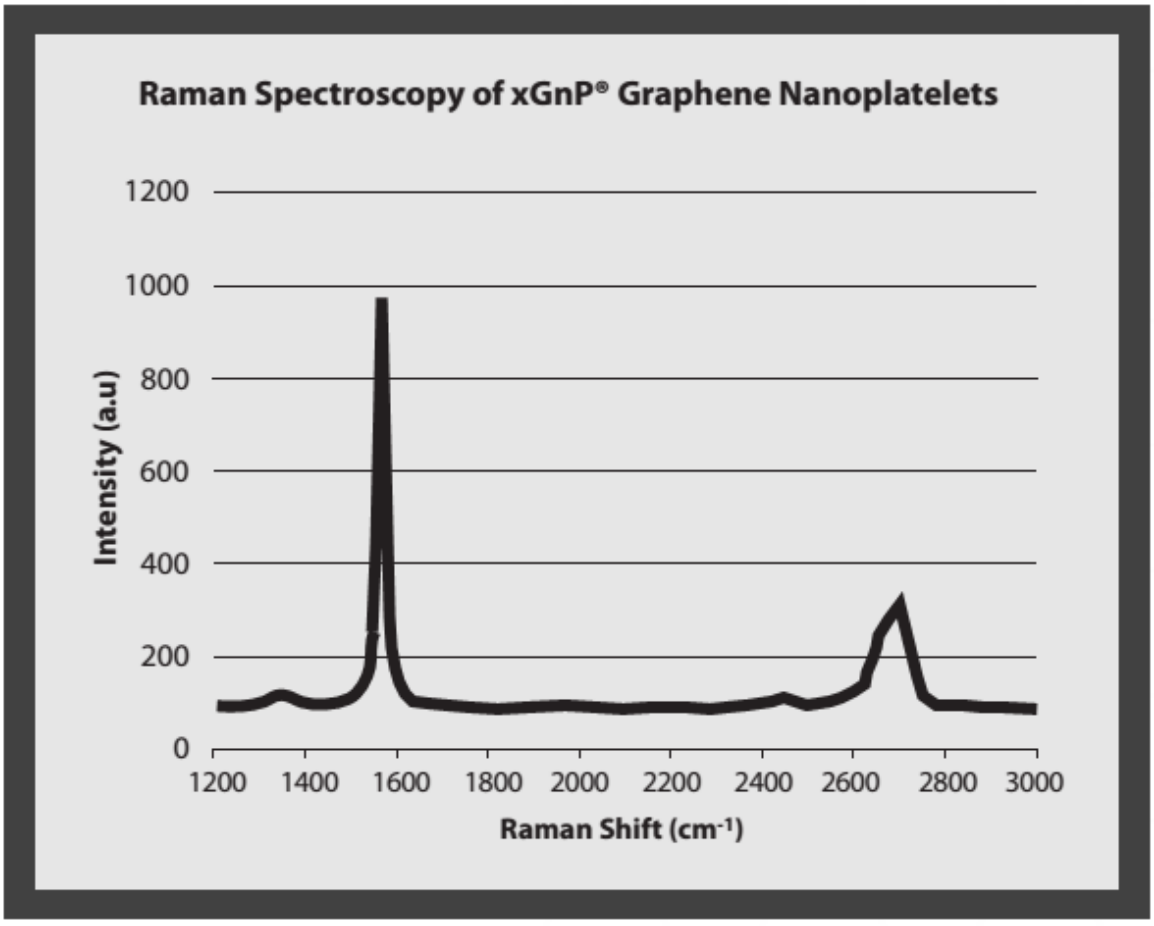

Figure B-16. Raman spectroscopy of xGnP® grade M graphene nanoplatelets (XG Sciences, 2013)

Table B-45. Characteristics of xGnP® grade M graphene nanoplatelets (XG Sciences, 2013)

	Parallel to Surface	Perpendicular to Surface
Density (g/c^3)	2.2	
Carbon Content (%)	>99.5	
Thermal Conductivity (W/mK)	3,000	6
Thermal Expansion (CTE) (m/m/°K)	$4 - 6 \times 10^{-6}$	$0.5 - 1.0 \times 10^{-6}$
Tensile Modulus (GPa)	1,000	N/A
Tensile Strength (GPa)	5	N/A
Electrical Conductivity (S/m)	10^7	10^2

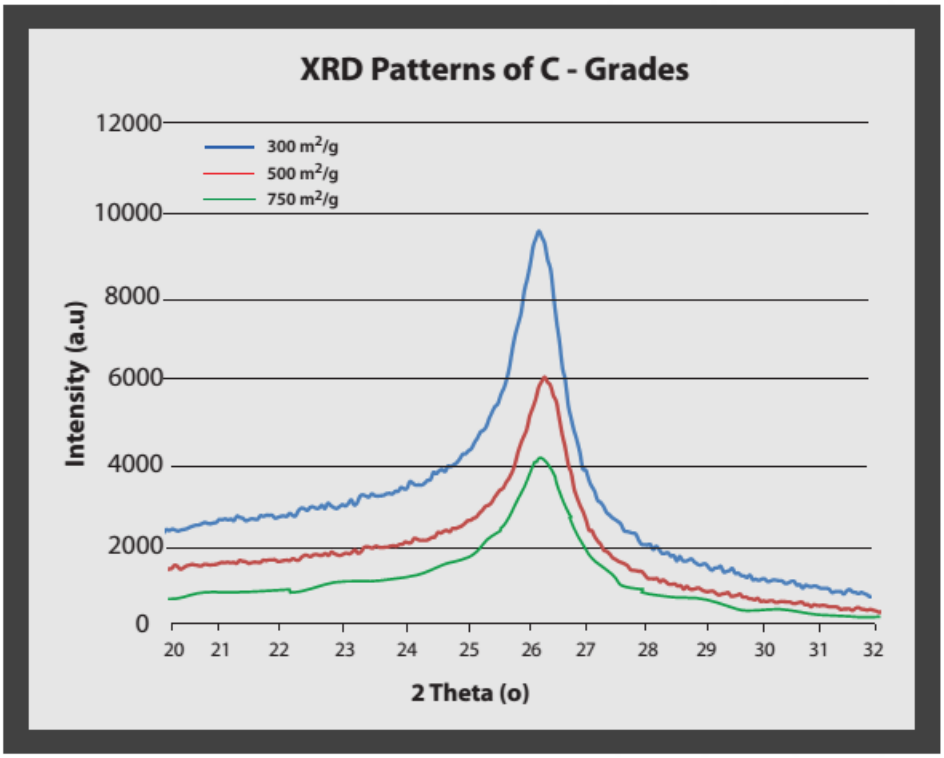

Figure B-17. XRD patterns of xGnP® grade C graphene nanoplatelets (XG Sciences, 2013)

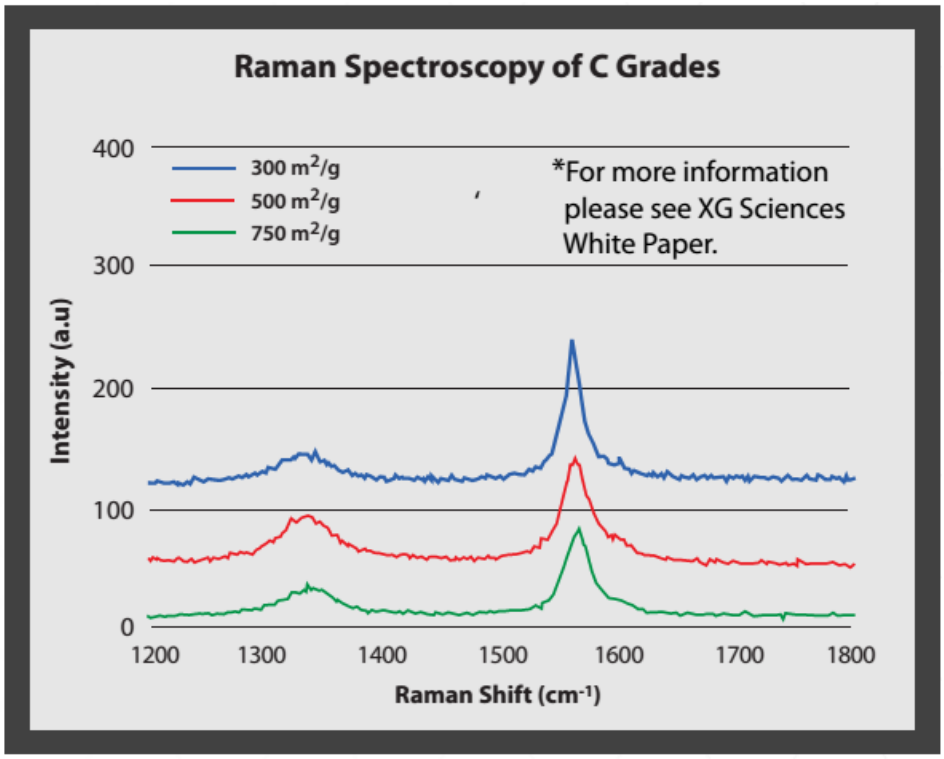

Figure B-18. Raman spectroscopy of xGnP® grade C graphene nanoplatelets (XG Sciences, 2013)

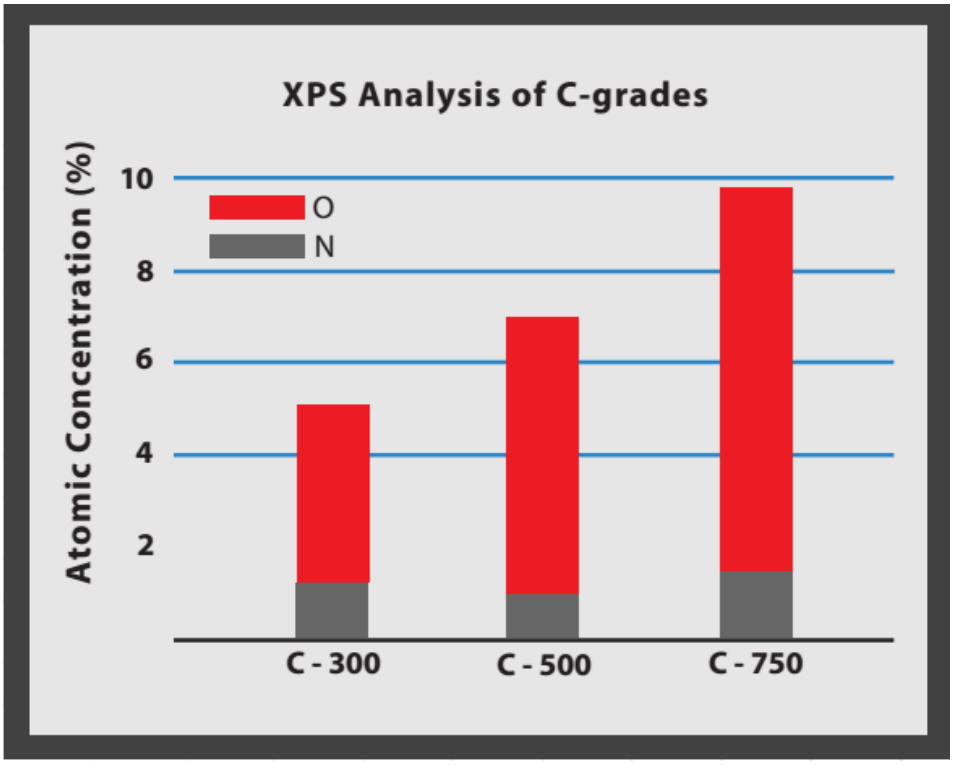

Figure B-19. XPS analysis of xGnP® grade C graphene nanoplatelets (XG Sciences, 2013)

B.2 RAMAN SPECTROSCOPY DATA

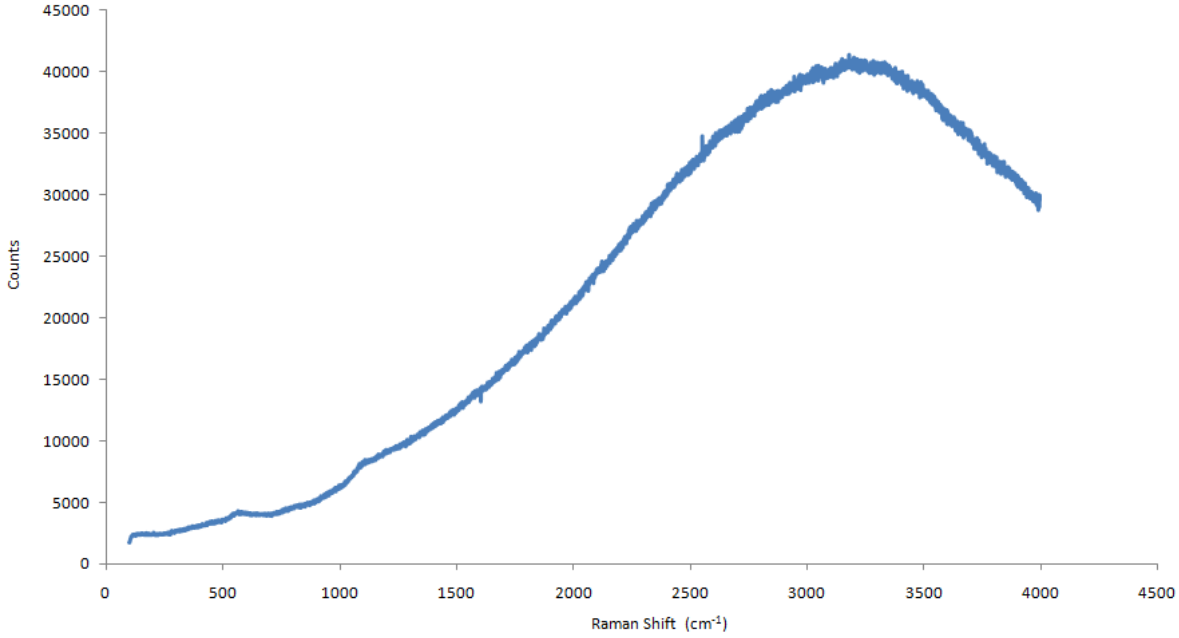

Figure B-20. Raman spectroscopy of water on glass slide obtained by Renishaw inVia

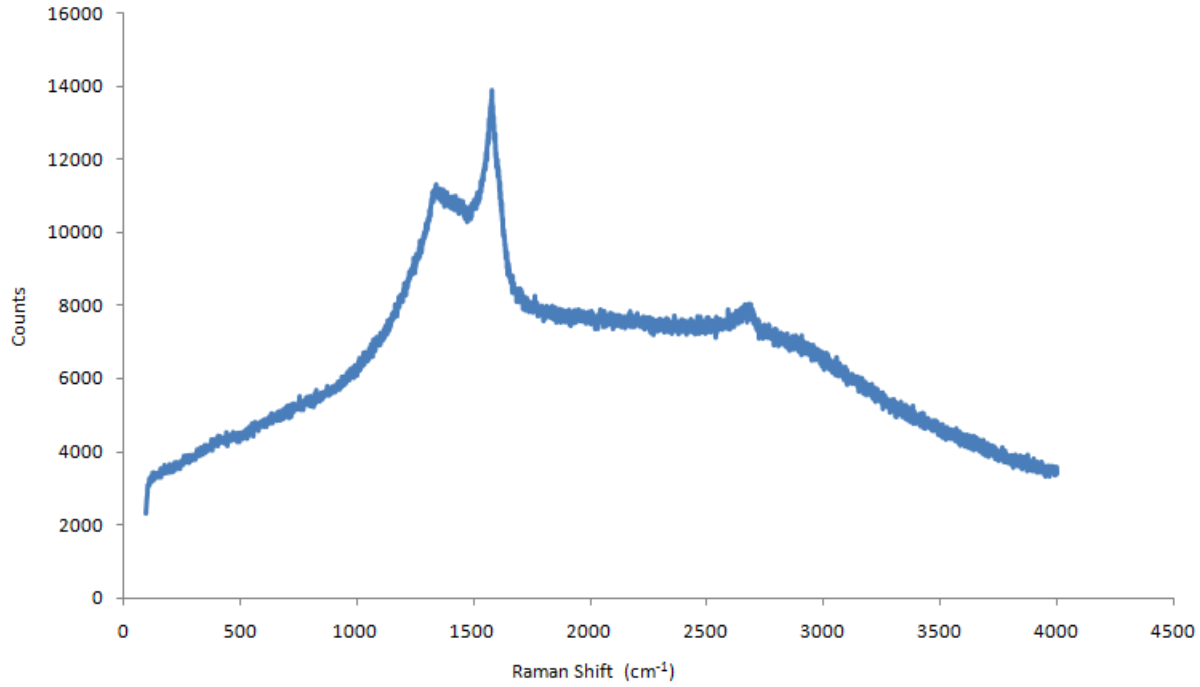

Figure B-21. Raman spectroscopy of water with GM obtained by Renishaw inVia

B.3 RAMAN SPECTROSCOPY DATA

Table B-46. Sand sieve data

Sieves Size(mm)	Sieve Weight(g)	Sieve Material Weight (g)	Retained Weight(g)	Cumulative Retained Weight(g)	Cumulative Retained Percentage	Cumulative Passing Percentage
4.75	515.5	515.5	0	0	0.0%	100.0%
2.36	432.1	436.2	4.1	4.1	0.4%	99.6%
1.18	427.6	653.8	226.2	230.3	23.0%	77.0%
0.6	398.2	690.7	292.5	522.8	52.3%	47.7%
0.3	359	677	318	840.8	84.1%	15.9%
0.15	352.1	470.3	118.2	959	95.9%	4.1%
Pan	524.7	565.7	41	1000	100.0%	0.0%
					Fineness Modulus	2.557

BIBLIOGRAPHY

Abu Al-Rub, Rashid K, Tyson, Bryan M, Yazdanbakhsh, Ardavan, & Grasley, Zachary. (2012). Mechanical Properties of Nanocomposite Cement Incorporating Surface-Treated and Untreated Carbon Nanotubes and Carbon Nanofibers. *Journal of Nanomechanics and Micromechanics, 2*(1), 1 - 6. doi: 10.1061/(ASCE)NM.2153-5477.0000041

Alkhateb, Hunain, Al-Ostaz, Ahmed, Cheng, Alexander H. D., & Li, Xiaobing. (2013). Materials Genome for Graphene-Cement Nanocomposites. *Journal of Nanomechanics and Micromechanics, 3*(3), 67-77. doi: 10.1061/(asce)nm.2153-5477.0000055

ASTM Standard C192/C192M-07, 2007. *"Making and Curing Concrete Test Specimens in the Laboratory"*. ASTM International, West Conshohocken, PA, 2007, doi: 10.1520/C0192_C0192M-07, www.astm.org.

ASTM Standard C33-03, 2003. *" Specification for Concrete Aggregates"*. ASTM International, West Conshohocken, PA, 2003, doi: 10.1520/C0033-03, www.astm.org.

ASTM Standard C469/C469M-10, 2010. *"Static Modulus of Elasticity and Poisson' s Ratio of Concrete in Compression"*. ASTM International, West Conshohocken, PA, 2010, doi: 10.1520/C0469_C0469M-10, www.astm.org.

ASTM Standard C666/C666M-03, 2003. *"Resistance of Concrete to Rapid Freezing and Thawing*. ASTM International, West Conshohocken, PA, 2003, doi: 10.1520/C0666_C0666M-03R08, www.astm.org.

Bogner, A., Jouneau, P. H., Thollet, G., Basset, D., & Gauthier, C. (2007). A history of scanning electron microscopy developments: towards "wet-STEM" imaging. *Micron, 38*(4), 390-401. doi: 10.1016/j.micron.2006.06.008

Brown, Theodore E, LeMay, H. Eugene, Bursten, Bruce E., Murphy, Catherine, & Woodward, Patrick. (2010). *Chemistry : The Central Science* (12th ed.): Prentice Hall PTR.

Cai, H., & Liu, X. (1998). Freeze-thaw durability of concrete: Ice formation process in pores. *Cement and Concrete Research, 28*(9). doi: 10.1016/S0008-8846(98)00103-3

Chaipanich, Arnon, Nochaiya, Thanongsak, Wongkeo, Watcharapong, & Torkittikul, Pincha. (2010). Compressive strength and microstructure of carbon nanotubes–fly ash cement

composites. *Materials Science and Engineering: A, 527*(4-5), 1063-1067. doi: 10.1016/j.msea.2009.09.039

Chan, Lai Yin, & Andrawes, Bassem. (2009). Characterization of the uncertainties in the constitutive behavior of carbon nanotube/cement composites. *Science and Technology of Advanced Materials, 10*(4), 045007. doi: 10.1088/1468-6996/10/4/045007

Chen, Jianlong, & Lei, Honggang. (2003). *Mechanism of Corrosion of Ammonia Nitrate Attack of Concrete Structure*. Paper presented at the National Academic Conference of Building Evaluation, Reinforcement and Reconstruction, China.

Chen, Wen, Du, Rong-Gui, Ye, Chen-Qing, Zhu, Yan-Feng, & Lin, Chang-Jian. (2010). Study on the corrosion behavior of reinforcing steel in simulated concrete pore solutions using in situ Raman spectroscopy assisted by electrochemical techniques. *Electrochimica Acta, 55*(20), 5677-5682. doi: 10.1016/j.electacta.2010.05.003

Chollet, M., & Horgnies, M. (2011). Analyses of the surfaces of concrete by Raman and FT-IR spectroscopies: comparative study of hardened samples after demoulding and after organic post-treatment. *Surface and Interface Analysis, 43*(3), 714-725. doi: 10.1002/sia.3548

Cote, Laura J., Kim, Jaemyung, Tung, Vincent C., Luo, Jiayan, Kim, Franklin, & Huang, Jiaxing. (2010). Graphene oxide as surfactant sheets. *Pure and Applied Chemistry, 83*(1). doi: 10.1351/pac-con-10-10-25

Cwirzen, A., Habermehl-Cwirzen, K., Nasibulin, A. G., Kaupinen, E. I., Mudimela, P. R., & Penttala, V. (2009). SEM/AFM studies of cementitious binder modified by MWCNT and nano-sized Fe needles. *Materials Characterization, 60*(7), 735-740. doi: 10.1016/j.matchar.2008.11.001

Datsyuk, V., Kalyva, M., Papagelis, K., Parthenios, J., Tasis, D., Siokou, A., . . . Galiotis, C. (2008). Chemical oxidation of multiwalled carbon nanotubes. *Carbon, 46*(6), 833-840. doi: 10.1016/j.carbon.2008.02.012

Dresselhaus, M. S., Jorio, A., Hofmann, M., Dresselhaus, G., & Saito, R. (2010). Perspectives on carbon nanotubes and graphene Raman spectroscopy. *Nano Letters, 10*(3), 751-758. doi: 10.1021/nl904286r

Dreyer, D. R., Park, S., Bielawski, C. W., & Ruoff, R. S. (2010). The chemistry of graphene oxide. *Chem Soc Rev, 39*(1), 228-240. doi: 10.1039/b917103g

Elsen, J. (2006). Microscopy of historic mortars—a review. *Cement and Concrete Research, 36*(8), 1416-1424. doi: 10.1016/j.cemconres.2005.12.006

Fanina, E. A., & Lopanov, A. N. (2009). Electric conductivity and aggregation of anthracite and graphite particles in concretes. *Solid Fuel Chemistry, 43*(1), 38-42. doi: 10.3103/s0361521909010091

Ferrari, A. C., Meyer, J. C., Scardaci, V., Casiraghi, C., Lazzeri, M., Mauri, F., . . . Geim, A. K. (2006). Raman Spectrum of Graphene and Graphene Layers. *Physical Review Letters, 97*(18). doi: 10.1103/PhysRevLett.97.187401

Fu, Xuli, & Chung, D.D.L. (1998). Submicron-diameter-carbon-filament cement-matrix composites. *Carbon, 36*(4), 459–462. doi: 10.1016/S0008-6223(98)90017-3

Gao, Di, Sturm, Mariel, & Mo, Y. L. (2011). Electrical resistance of carbon-nanofiber concrete. *Smart Materials and Structures, 20*(4), 049501. doi: 10.1088/0964-1726/20/4/049501

Geim, A. K, & Novoselov, K. S. (2007). The rise of graphene. *Nature Materials, 6*, 183-191. doi: 10.1038/nmat1849

Goncalves, G., Cruz, S. M., Ramalho, A., Gracio, J., & Marques, P. A. (2012). Graphene oxide versus functionalized carbon nanotubes as a reinforcing agent in a PMMA/HA bone cement. *Nanoscale, 4*(9), 2937-2945. doi: 10.1039/c2nr30303e

Hou, Zuofu, Li, Zhuoqiu, & Wang, Jianjun. (2007). Electrical conductivity of the carbon fiber conductive concrete. *Journal of Wuhan University of Technology-Mater. Sci. Ed., 22*(2), 346-349. doi: 10.1007/s11595-005-2346-x

Janotka, I, & Krajèi, L.è. (2000). Resistance to freezing and thawing of mortar specimens made from sulphoaluminate–belite cement. *Bulletin of Materials Science, 23*(6), 521-527. doi: 10.1007/BF02903894

Kjellsen, Knut O, & Jennings, Hamlin M. (1996). Observations of microcracking in cement paste upon drying and rewetting by environmental scanning electron microscopy. *Advanced Cement Based Materials, 3*(1), 14 - 19. doi: 10.1016/S1065-7355(96)90065-6

Konsta-Gdoutos, Maria S., Metaxa, Zoi S., & Shah, Surendra P. (2010). Highly dispersed carbon nanotube reinforced cement based materials. *Cement and Concrete Research, 40*(7), 1052-1059. doi: 10.1016/j.cemconres.2010.02.015

Kumar, Sanjeev, Kolay, Prabir, Malla, Sunil, & Mishra, Sanjay. (2012). Effect of Multiwalled Carbon Nanotubes on Mechanical Strength of Cement Paste. *Journal of Materials in Civil Engineering, 24*(1), 84 - 91. doi: 10.1061/(ASCE)MT.1943-5533.0000350

Lomboy, Gilson, Sundararajan, Sriram, Wang, Kejin, & Subramaniam, Shankar. (2011). A test method for determining adhesion forces and Hamaker constants of cementitious materials using atomic force microscopy. *Cement and Concrete Research, 41*(11), 1157-1166. doi: 10.1016/j.cemconres.2011.07.004

Lv, Shenghua, Ma, Yujuan, Qiu, Chaochao, Sun, Ting, Liu, Jingjing, & Zhou, Qingfang. (2013). Effect of graphene oxide nanosheets of microstructure and mechanical properties of cement composites. *Construction and Building Materials, 49*, 121-127. doi: 10.1016/j.conbuildmat.2013.08.022

Malard, L. M., Pimenta, M. A., Dresselhaus, G., & Dresselhaus, M. S. (2009). Raman spectroscopy in graphene. *Physics Reports, 473*(5-6), 51-87. doi: 10.1016/j.physrep.2009.02.003

Mao, Shun, Pu, Haihui, & Chen, Junhong. (2012). Graphene oxide and its reduction: modeling and experimental progress. *RSC Advances, 2*(7), 2643. doi: 10.1039/c2ra00663d

Marchand, J., Pigeon, Miche, & Setzer, M. (1996). Freeze-Thaw Durability of Concrete.

Mesbah, H. A., Yahia, A., & Khayat, K. H. (2011). Electrical conductivity method to assess static stability of self-consolidating concrete. *Cement and Concrete Research, 41*(5), 451-458. doi: 10.1016/j.cemconres.2011.01.004

Monteiro, Paulo J.M. , & Mehta, P. . (2005). *Concrete: Microstructure, Properties, and Materials*: McGraw-Hill.

Neubauer, C M, Bergstrom, T B, Sujata, K; Xi, Y, Garboczi, E J, & Jennings, H M. (1997). Drying shrinkage of cement paste as measured in an environmental scanning electron microscope and comparison with microstructural models. *Journal of Materials Science, 32*(24), 6415 - 6427. doi: 10.1023/A:1018682404655

Neubauer, C. M, & Jennings, H. M. (1996). The role of the environmental scanning electron microscope in the investigation of cement-based materials. *Scanning, 18*(7), 515 - 521. doi: 10.1002/sca.1996.4950180708

Pešková, Šárka, Machovič, Vladimír, & Procházka, Petr. (2011). Raman Spectroscopy Structural Study of Fired Concrete. *Ceramics-Silikáty, 55*(4), 410 - 417.

Petersen Institute of NanoScience and Engineering (PINSE) (2014). Raman Microscope. Retrieved from http://www.nano.pitt.edu/node/248

Petersen Institute of NanoScience and Engineering (PINSE) (2014). Scanning Electron Microscope (SEM). Retrieved from http://www.nano.pitt.edu/node/238

Petersen Institute of NanoScience and Engineering (PINSE) (2014). Scanning Probe Microscopy (SPM). Retrieved from http://www.nano.pitt.edu/node/241

Powers, T. C. (1945). A Working Hypothesis for Further Studies of Frost Resistance. *Journal of the American Concrete Institute, 16*, 272-220.

Rosca, Iosif Daniel, Watari, Fumio, Uo, Motohiro, & Akasaka, Tsukasa. (2005). Oxidation of multiwalled carbon nanotubes by nitric acid. *Carbon, 43*(15), 3124-3131. doi: 10.1016/j.carbon.2005.06.019

Sakulich, Aaron Richard, & Li, Victor C. (2011). Nanoscale characterization of engineered cementitious composites (ECC). *Cement and Concrete Research, 41*(2), 169-175. doi: 10.1016/j.cemconres.2010.11.001

Schneider, U, & Chen, S.-W. (1998). The Chemomechanical Effect and the Mechanochemical Effect on High-Performance Concrete Subjected to Stress Corrosion. *Cement and Concrete Research, 28*(4), 509 - 522. doi: 10.1016/S0008-8846(98)00015-5

Schneider, U, & Chen, S -W. (1998). Modeling and empirical formulas for chemical corrosion and stress corrosion of cementitious materials. *Materials and Structures, 31*(10), 662 - 668. doi: 10.1007/BF02480442

Schneider, U., & Chen, S. W. (2005). Deterioration of high-performance concrete subjected to attack by the combination of ammonium nitrate solution and flexure stress. *Cement and Concrete Research, 35*(9), 1705-1713. doi: 10.1016/j.cemconres.2004.11.011

Sedaghat, Ahmadreza, Ram, Manoj K., Zayed, A., Kamal, Rajeev, & Shanahan, Natallia. (2014). Investigation of Physical Properties of Graphene-Cement Composite for Structural Applications. *Open Journal of Composite Materials, 04*(01), 12-21. doi: 10.4236/ojcm.2014.41002

Shang, H. S., & Yi, T. H. (2013). Freeze-thaw durability of air-entrained concrete. *ScientificWorldJournal, 2013*, 650791. doi: 10.1155/2013/650791

Si, Yongchao, & Samulski, Edward T. (2008). Synthesis of water soluble graphene. *Nano letters, 8*(6), 1679 - 1682. doi: 10.1021/nl080604h

Siddique, Rafat, & Khan, Mohammad Iqbal. (2011). *Supplementary cementing materials* doi:10.1007/978-3-642-17866-5

Singh, A. P., Mishra, M., Chandra, A., & Dhawan, S. K. (2011). Graphene oxide/ferrofluid/cement composites for electromagnetic interference shielding application. *Nanotechnology, 22*(46), 465701. doi: 10.1088/0957-4484/22/46/465701

Šmilauer, Vít, Hlaváček, Petr, & Padevět, Pavel. (2012). Micromechanical Analysis of Cement Paste with Carbon Nanotubes. *Acta Polytechnica, 52*(6), 22 - 28.

Swamy, R. N. (1992). The Alkali-silica reaction in concrete.

Tan, Susheng, Sherman, Jr, Robert L, & Ford, Warren T. (2004). Nanoscale compression of polymer microspheres by atomic force microscopy. *Langmuir : the ACS journal of surfaces and colloids, 20*(17), 7015-7020. doi: 10.1021/la049597c

Tyson, Bryan M., Abu Al-Rub, Rashid K., Yazdanbakhsh, Ardavan, & Grasley, Zachary. (2011). Carbon Nanotubes and Carbon Nanofibers for Enhancing the Mechanical Properties of Nanocomposite Cementitious Materials. *Journal of Materials in Civil Engineering, 23*(7), 1028-1035. doi: 10.1061/(asce)mt.1943-5533.0000266

Vaidya, Saiprasad, & Allouche, Erez N. (2011). Strain sensing of carbon fiber reinforced geopolymer concrete. *Materials and Structures, 44*(8), 1467-1475. doi: 10.1617/s11527-011-9711-3

Wu, Shaopeng, Mo, Liantong, Shui, Zhonghe, & Chen, Zheng. (2005). Investigation of the conductivity of asphalt concrete containing conductive fillers. *Carbon, 43*(7), 1358-1363. doi: 10.1016/j.carbon.2004.12.033

XG Sciences, Inc (2013). Technical Data Sheet: xGnP® Grade C Product Characteristics. Retrieved from http://xgsciences.com/wp-content/uploads/2012/10/10-15-13_xGnP-C_Data-Sheet.pdf

XG Sciences, Inc (2013). Technical Data Sheet: xGnP® Grade M Product Characteristics. Retrieved from http://xgsciences.com/wp-content/uploads/2012/10/10-15-13_xGnP-M_Data-Sheet.pdf

Zhang, shiping, Deng, Min, & Tang, Mingshu. (2008). Advance in Research on Damagement of Concrete Due to Freeze-thaw Cycles. *Journal of Materials Science & Engineering, 26*(6), 990 - 994.

Zhu, C. Z., Guo, S. J., Fang, Y. X., & Dong, S. J. (2010). Reducing sugar: new functional molecules for the green synthesis of graphene nanosheets. *ACS nano, 4*(4), 2429 - 2437. doi: 10.1021/nn1002387

Zoubir, Arnaud. (2012). *Raman imaging: techniques and applications* Vol. 168. A. Zoubir (Ed.) (pp. 387). doi:10.1007/978-3-642-28252-2